Zeitschrift: IABSE reports of the working commissions = Rapports des commissions de travail AIPC = IVBH Berichte der Arbeitskommissionen

Band: 13 (1973)

Rubrik: Theme I: Theorization of structural behaviour with a view to defining resistance and ultimate deformability

I

Plastic H-Columns Under Repeated Biaxial Loading

Colonnes plastiques à profiles H soumises à des charges répétées biaxiales

Plastische Stützen mit H-Querschnitt unter wiederholter zweiaxiger Belastung

W.F. CHEN
Associate Professor
Department of Civil Engineering
Fritz Engineering Laboratory
Lehigh University
Bethlehem, Pennsylvania
USA

INTRODUCTION: Moment-curvature-thrust relationships are of prime importance in any analysis of structural behavior. For a biaxially loaded steel H-column, the appropriate set of loadings are bending moments M_x and M_y, axial force P and warping moment M_{xy}. The corresponding set of deformations are bending curvatures, φ_x and φ_y, axial strain ϵ_o and warping curvature φ_{xy}. This may be demonstrated clearly by considering a simple physical model as shown in Fig. 1. The biaxial load is seen to be decomposed into four components. The first three are statically equivalent to an axial force 4P and two bending moments M_x and M_y about two principal axis of the H-section. However, these three equivalent systems do not produce the biaxial load 4P. It is necessary to consider a fourth system which produces zero axial force and zero bending moment resultants on the section. This fourth system termed warping moment, M_{xy}, causes the column to warp or twist.

For the most part, plastic analysis and design of biaxially loaded columns have in the past been directed toward the study of proportional, monotonically increasing loading to failure [1]. This type of loading is not entirely realistic for many applications, however. Herein a study is made of the relationships between moments and curvatures for a relatively short steel column subject to repeated and reversed compression combined with biaxial bending moments.

The term relatively "short" steel columns referred to here means that the effect of lateral deflections on the magnitudes of bending moment is negligible. Furthermore, effects of local buckling are not included in the analysis.

STRESS-STRAIN RELATIONSHIPS INCLUDING HYSTERESIS: The stress-strain relationship is assumed to be tri-linear as shown in Fig. 2. The curve is composed of three regimes: elastic; plastic; and strain hardening. The plastic unloading behavior is idealized as shown in the figure. If the material is unloaded from the plastic regime, the material exhibits no Bauschinger effect. However, if the material is unloaded from the strain hardening regime, some Bauschinger effects are exhibited. This strain hardening, plastic unloading rule and Bauschinger effect are interpreted clearly by the kinematic model of the parallelogram BD'B'D and the straight line AA' (Fig. 2). Elastic loading or plastic unloading within the line AA' does not change the condition at all (Fig. 2a). Plastic loading along lines DB or D'B' changes the position of line AA' only (Fig. 2b). Strain hardening along lines BC or B'C' translates the position of the parallelogram BD'B'D in parallel to the lines BC and B'C' (Fig. 2c). In this case, the elastic line AA' coincides with the line BD'. Positions of the lines BC and B'C' do not change for any loading history.

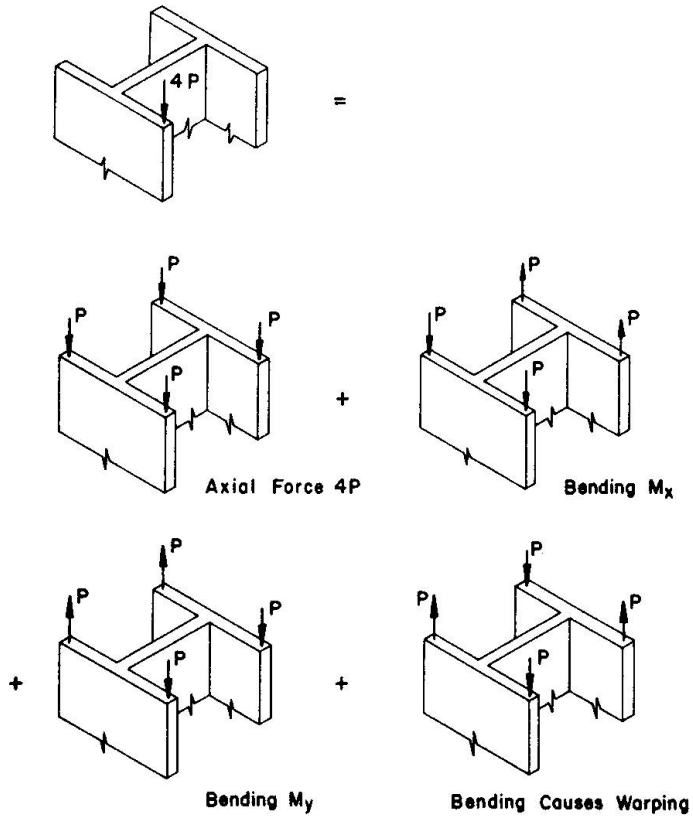

Fig. 1 Decomposition of a Biaxial Loading

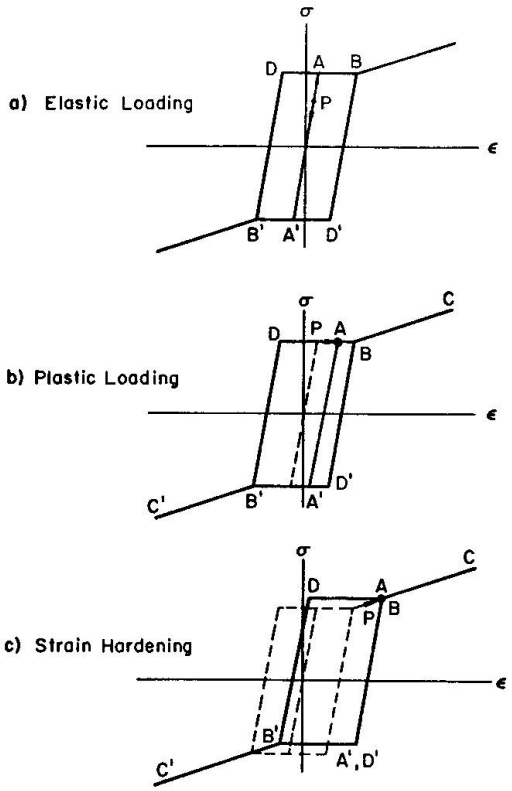

Fig. 2 Stress-Strain Model

MATHEMATICAL FORMULATION: Since only normal stress and normal strain are considered, deformation quantities related to normal strain are taken as generalized strains of the H-section. This results in the following relationship between the generalized strain $\{\delta\}$ and the strain, ϵ:

$$\{\delta\} = \begin{Bmatrix} \epsilon_o \\ \varphi_x \\ \varphi_y \\ \varphi_{xy} \end{Bmatrix} = \begin{Bmatrix} \frac{1}{A}\int dA \\ \frac{1}{A}\int \frac{\partial \epsilon}{\partial y}\, dA \\ \frac{1}{A}\int \frac{\partial \epsilon}{\partial x}\, dA \\ \frac{1}{A}\int \frac{\partial^2 \epsilon}{\partial x\, \partial y}\, dA \end{Bmatrix} \qquad \begin{matrix} \text{strain at centroid} \\ \text{curvature about x-axis} \\ \text{curvature about y-axis} \\ \text{warping curvature about the centroid} \end{matrix} \qquad (1)$$

Strain distribution is assumed to be linear in x and y coordinate.

$$\epsilon = \epsilon_o + x\,\varphi_y + y\,\varphi_x + xy\,\varphi_{xy} \qquad (2)$$

The corresponding resultant forces or generalized stresses are determined from the rate of internal energy dissipation

$$\dot{D}_I = \int \sigma\, \dot{\epsilon}\, dA = \dot{\epsilon}_o \int \sigma\, dA + \dot{\varphi}_x \int \sigma y\, dA + \dot{\varphi}_y \int \sigma x\, dA + \dot{\varphi}_{xy} \int \sigma xy\, dA \qquad (3)$$

This results in the following relationship between the generalized stress $\{f\}$ and the stress, σ:

$$\{f\} = \begin{Bmatrix} P \\ M_x \\ M_y \\ M_{xy} \end{Bmatrix} = \begin{Bmatrix} \int \sigma\, dA \\ \int \sigma y\, dA \\ \int \sigma x\, dA \\ \int \sigma xy\, dA \end{Bmatrix} \qquad \begin{matrix} \text{axial thrust} \\ \text{bending moment about x-axis} \\ \text{bending moment about y-axis} \\ \text{warping moment about the centroid} \end{matrix} \qquad (4)$$

Because plastic behavior is load path dependent and usually requires step-by-step calculations that follows the history of loading. For this reason, it has proven useful to establish an analytical relationship of the generalized stress-strain or moment-curvature relation in terms of the incremental changes of $\{df\}$ and $\{d\delta\}$. This leads to the linear relationship between these quantities

$$\{df\} = [K]\{d\delta\} \tag{5}$$

The matrix $[K]$ is defined as the tangent stiffness matrix as it represents the tangent of the generalized stress-strain curve as well as the stiffness of the cross section. A detailed description on the analytical derivation of this equation is given in Ref. 2.

METHOD OF SOLUTION: The numerical solution of Eq. 5 can be obtained by the tangent stiffness method. Details of the method have been given in Ref. 3 for a relatively short column and in Ref. 4 for the case of a long column: A brief description of the tangent stiffness method will be given herein.

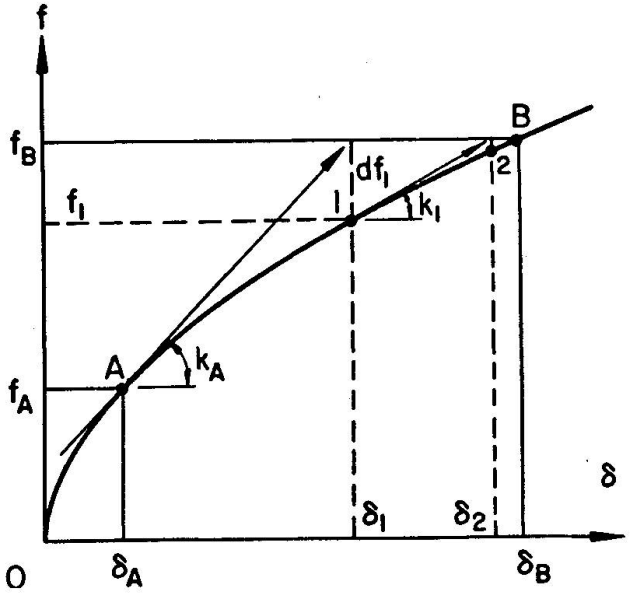

Fig. 3 Tangent Stiffness Method

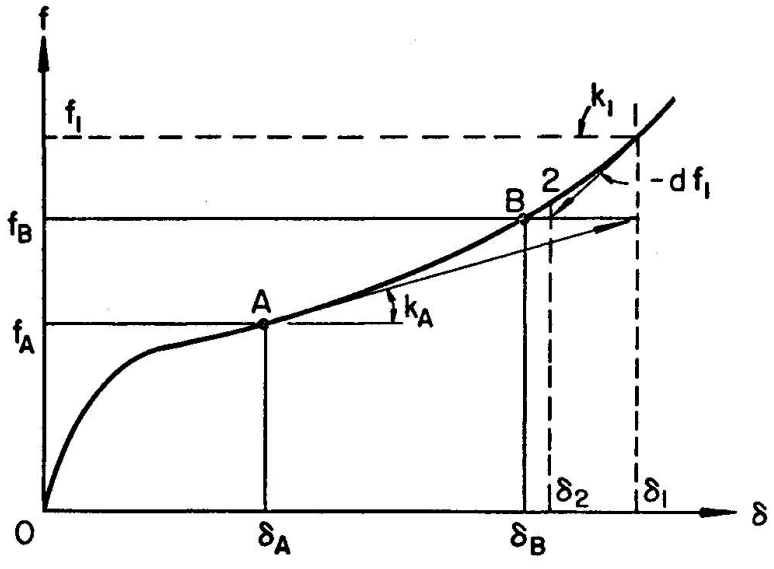

Fig. 4 Tangent Stiffness Method with Strain Hardening

Consider a generalized stress or a force vector f, a generalized strain or a deformation vector δ and their relationship is shown in Fig. 3. The column segment has experienced loadings along the path OA. At point A, the current force vector f_A, deformation vector δ_A and the stiffness matrix K_A are assumed to be known, the problem is to find the corresponding deformation vector δ_B when the force vector is increased from f_A to f_B

Since the deformation increment $d\delta$ can be calculated from the force increment df or $df = f_B - f_A$ using the tangent stiffness K_A at the current state A, or $d\delta_1 = K_A^{-1} df$. The first approximate value of total deformation is obtained by $\delta_1 = \delta_A + d\delta_1$. From this approximate deformation δ_1, the total strain distribution ϵ can be determined from Eq. 2 and hence the corresponding state of stress can be determined. Integration of the stress over the entire cross section gives the new internal force vector f_1 using Eq. 4. This new state is expressed by the point 1 in Fig. 3. The new tangent stiffness K_1 at point 1 corresponding to the state f_1 and δ_1 can now be computed. The new internal force vector f_1 is now not in equilibrium with the externally applied force vector f_B. The first unbalanced force vector df_1 is computed from $df_1 = f_B - f_1$.

The next step is to find a correction deformation vector $d\delta_2$ which will be added to δ_1 in order to eliminate the unbalance force f_1. Vector $d\delta_2 = K_1^{-1} df_1$. Repeating the same procedure for point 2 again, the second internal force vector f_2 and the unbalanced force vector $df_2 = f_B - f_2$ are obtained. Repeating the

same procedure as at point 2 until the unbalanced force df_n at point n becomes zero or is within a prescribed tolerance limit, the final deformation vector is then obtained by $\delta_B \approx \delta_n$.

During the procedure, the unbalance force vector df may be negative as shown in Fig. 4. This happens when there is some strain hardening in the material. In such a case, tangent stiffness rather then elastic unloading stiffness should be used in the computations because this negative force vector is an imaginary unloading.

In most cases, a few cycles of iteration are found to be sufficient to obtain an accurate solution. Even with a large incremental force or a rather accurate calculation of large deformation on a plastic plateau the solution will generally converge within just a few more cycles of iteration.

HYSTERESIS DIAGRAMS: The moment-curvature diagrams for a column segment contain considerable information about the behavior of a biaxially loaded long column. In addition to providing the essential relationship between forces and deformations for a long column solution, the diagrams make it possible to determine the energy input to the segment through integration of the work done by the external forces.

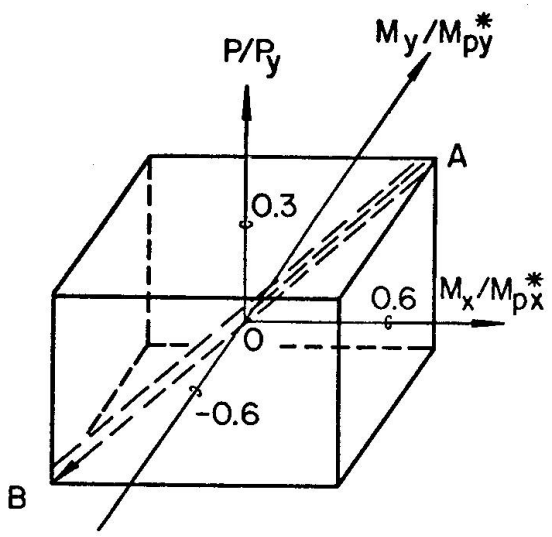

Fig. 5 Repeated and Reversed Proportional Loading

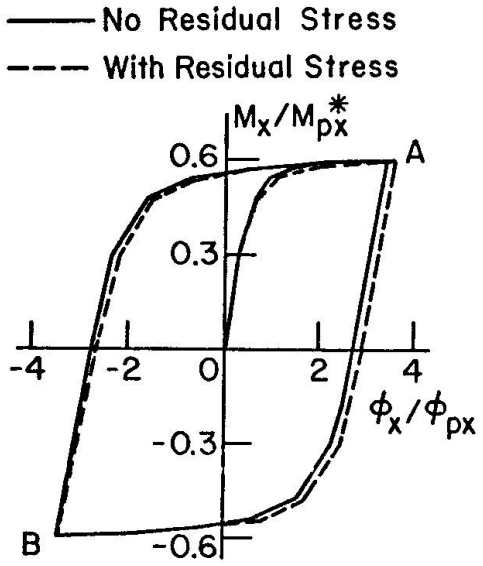

Fig. 6 Moment-Curvature Hysteresis Diagram

Figure 5 shows a proportional loading case with the loads (P, M_x, M_y) being repeated and reversed proportionally between 99% (point A) and -99% (point B) of the values $(0.3, 0.6, 0.6)$ of the full plastic limit state $(P_y, M^*_{px}, M^*_{py})$. Linear strain hardening and linear residual stress distributions are considered but the warping deformation φ_{xy} is assumed to be completely restrained, the corresponding warping moment M_{xy} required for such a restraint is therefore considered as a reaction. Its magnitude is found to be the same at points A and B. The presence of residual stress is seen to have some effects on the moment-curvature curves as shown by the typical example of M_x vs. φ_x curve in Fig. 6, but the effect of material strain hardening on the curves is found to be not significant.

The typical moment-curvature hysteresis loop shown in Fig. 6 is composed of three portions: initial loading portion (0 → A), unloading (A → B), and reloading portion (B → A). For each portion, a function similar to a Ramberg-Osgood type of function may be used for curve-fitting. As an example, Fig. 7 shows a typical example of the close curve-fitting for the M_x vs. φ_x curve discussed in Fig. 6. The Ramberg-Osgood function for the initial loading portion is shown on the top of the figure. The functions for the unloading portion and reloading portion are identical in shape to the function shown, but enlarged by a factor of two and shifting the origin.

RESPONSE TO REPEATED AND REVERSED LOADING: Response of section under repeated and reversed loadings is of major importance in the low-cycle fatigue and shakedown analysis. In these analyses, estimation of energy dissipation during the loading cycle plays an important role.

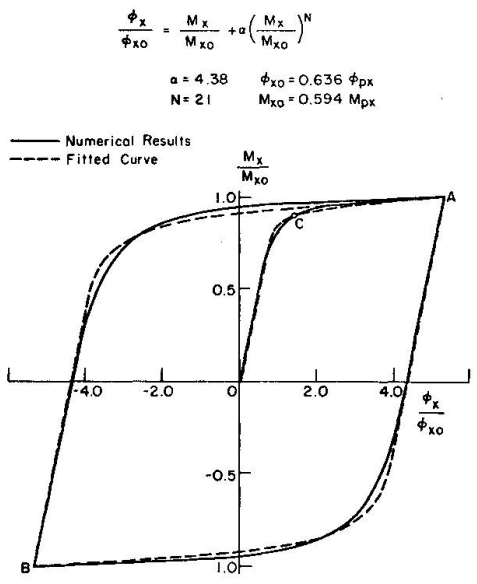

Fig. 7 Curve-Fitting by Ramberg-Osgood Type of Function

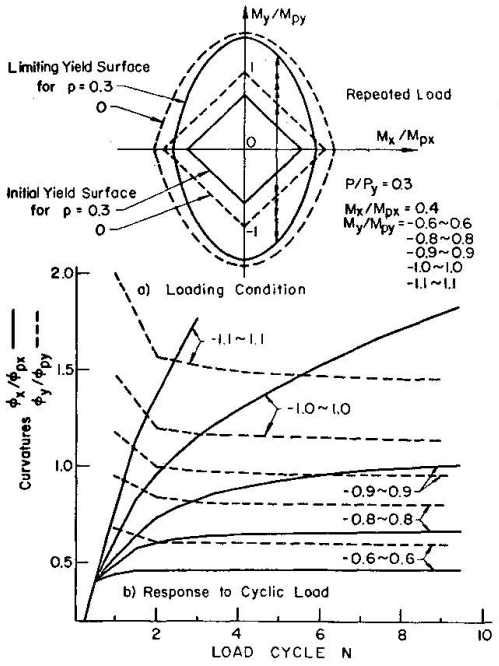

Fig. 8 Repeated and Reversed Non-Proportional Loading

Figure 8 shows the load M_y fluctuating between some limits while the other two loads are kept constant ($P/P_y = 0.3$, $M_x/M_{px} = 0.4$). The half amplitude of the limits for the moment M_y/M_{py} is 0.6, 0.8, 0.9, 1.0 and 1.1 (M_{px} and M_{py} denote initial yield values). Since the elastic region is bounded by $-0.3 \leq M_y/M_{py} \leq 0.3$, plastic deformations are produced in all cases. Numerical results are illustrated in Fig. 8. In all cases, curvature φ_y decreases with loading cycles and tends to converge to a certain limit value. The deformations ϵ_o and φ_x and the energy dissipation are found to increase monotonically with the loading cycles for large amplitudes but tend to converge for small amplitudes ($M_y/M_{py} < 1.0$).

SUBSEQUENT YIELD SURFACES: Since the loading condition is kept constant during the repetition of loadings, shakedown is possible only when the subsequent yield surface is transformed so that the loading points will eventually move within the yield surface.

Figure 9 shows subsequent yield surfaces due to loadings $P/P_y = 0$, $M_x/M_{px} = 0.4$ and M_y/M_{py} between 0.8 and -0.8. The dotted lines are the initial yield surface and the limiting yield surface. A load point inside and outside of the yield surface represent elastic and elastic-plastic states of stress, respectively. No load point can move outside the limiting surface.

After the first loading (point A), the yield surface translates so that the load point A is now on the subsequent yield surface. There are two interesting points: (1) The opposite side of point A moves towards the origin (Bauschinger Effect); (2) The subsequent yield surface has a corner at the loading point. After the second loading (point B), the subsequent yield surface changes again and both points A and B are now inside the surface. Thus the repetition of loading between A and B proceeds all in elastic regime and further plastic deformation has ceased, or the section has shaken down.

Figure 10 shows changes of the subsequent yield surface due to repeated and reversed loading $P/P_y = 0.3$, $M_x/M_{px} = 0.4$ and M_y/M_{py} between 1.1 and -1.1. The repeated loading M_y is applied between the points A and B. When the amplitude

of M_y is small (M_y/M_{py} = 0.8, Fig. 9) the subsequent yield surface tends to change so that the column segment shakes down. When the amplitude is large (M_y/M_{py} = 1.1, Fig. 10), the tendency of shakedown is not observed.

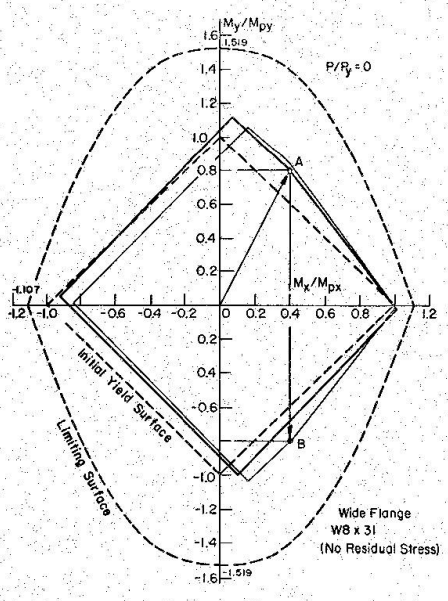

Fig. 9 Subsequent Yield Surface

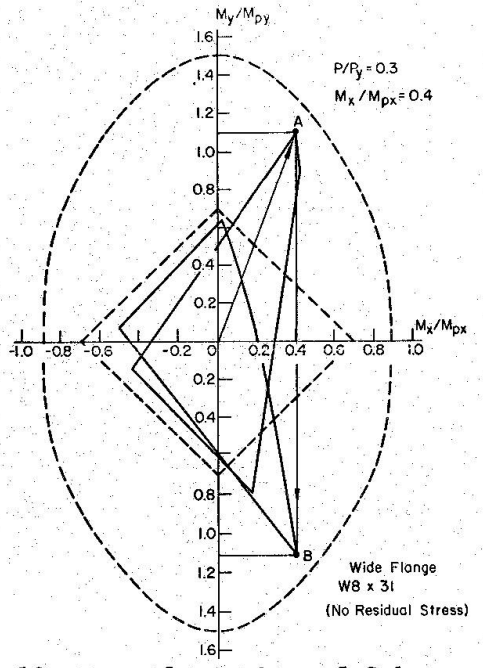

Fig. 10 Transformation of Subsequent Yield Surface

CONCLUSIONS: Based upon the formulation (Eq. 5), a computer program was developed to provide numerical results. It is found that (1) The method is extremely powerful and efficient for computer solutions of moment-curvature hysteresis loops; (2) The mathematical representation of a hysteresis moment-curvature curve using the Ramberg-Osgood relationship is highly satisfactory; and (3) The response of a column segment subjected to repeated and reversed biaxial loading and the concepts of a shakedown analysis can be interpreted from the viewpoint of transformation of the subsequent yield surfaces in the generalized stress space.

ACKNOWLEDGMENTS: The research reported here was supported by the National Science Foundation under Grant GK-35886 to Lehigh University.

REFERENCES:

1. Chen, W. F. and Santathadaporn, S., "Review of Column Behavior under Biaxial Loading", Journal of the Structural Division, ASCE, Vol. 94, No. ST12, Proc. paper 6316, December 1968, pp. 2999-3021.

2. Chen, W. F. and Atsuta, T., "Inelastic Response of Column Segments under Biaxial Loads", Journal of the Structural Division, ASCE, Vol. 99, 1973, (in press).

3. Santathadaporn, S. and Chen, W. F., "Tangent Stiffness Method for Biaxial Bending", Journal of the Structural Division, ASCE, Vol. 98, No. ST1, Proc. paper 8637, January 1972, pp. 153-163.

4. Santathadaporn, S. and Chen, W. F., "Analysis of Biaxially Loaded H-Columns", Journal of the Structural Division, ASCE, Vol. 99, ST3, March 1973, pp. 491-509.

SUMMARY

A study is made of the relationships between moments and curvatures for a relatively short steel H-column subject to repeated and reversed compression combined with biaxial bending moments. Plastic unloading, residual stresses, strain hardening and Bauschinger effect of the material are considered in the analysis. Moment-curvature curves corresponding to several repeated and reversed loading paths are presented.

RESUME

Dans ce rapport on étudie les relations moment-courbure pour une colonne à larges ailes en acier relativement courte, soumise à des efforts de compression répétés et alternés, combinés avec des moments de flexion biaxiaux. Le déchargement plastique, les tensions résiduelles, l'écrouissage et l'effet Bauschinger du matériau sont considérés dans l'analyse. On présente aussi certains diagrammes moment-courbure correspondant à plusieurs types de charges répétées et alternées.

ZUSAMMENFASSUNG

Es wird eine Untersuchung der Beziehung zwischen Moment und Krümmung einer relativ gedrungenen Stahlstütze mit H-Querschnitt unter wiederholter und wechselnder Last, kombiniert mit Biegemomenten in beiden Richtungen vorgelegt. Plastische Entlastung, bleibende Spannungen und der Bauschinger-Effekt werden in der Berechnung berücksichtigt, und Momenten-Krümmungs-Kurven entsprechend wiederholter und wechselnder Belastungen gezeigt.

Leere Seite
Blank page
Page vide

I

A Study of Cyclic Plasticity

Une étude sur la plasticité en régime cyclique

Eine Studie über zyklische Plastizität

N.C. LIND
Solid Mechanics Division
University of Waterloo
Ontario, Canada

Z. MRÓZ
Inst. of Fundamental Technical Research
Polish Academy of Sciences
Warszawa, Poland

1. INTRODUCTION

The plastic behaviour of structures under monotonic loading is usually predicted with sufficient accuracy by simple theories of plasticity such as flow rules associated with a single yield surface. For varying loads, however, these theories do not represent the complex plastic behaviour with sufficient fidelity. The theory of plasticity must be modified by introducing a suitable set of internal state parameters that enter into the yield condition and the constitutive relations. The mathematical structure can become quite complicated, as has been demonstrated [1], and there is a particular need for simpler material models that reflect the most essential aspects of plastic behaviour for a reasonably wide class of problems but have sufficient simplicity and accuracy for practical design. It is the aim of this paper to discuss a simplified theory of cyclic plasticity suitable for solving boundary value problems of small deformation behaviour of structures under cyclic proportional loading. We present a stress-strain relationship suitable for cyclic proportional stressing employing the Masing [2] hardening rule and two scalar state parameters (equivalent stress, or equivalent strain, at the last two reversals) and show that a wide class of problems of cyclic loading can be solved for this representation. For line or surface structures the formulation is readily transformed in terms of generalized stresses and strains.

2. STRESS STRAIN RELATIONS

Consider a material with the uniaxial hardening curve

$$\sigma = f(\epsilon) \tag{1}$$

relating stress σ and strain ϵ by a monotonic odd function f, with a reverse loading curve given by the "Masing transformation" of Eq. 1, viz.

$$\left.\begin{aligned} \sigma - \sigma^{-} &= 2f(\tfrac{1}{2}[\epsilon - \epsilon^{-}]), \dot{\epsilon} > 0 \\ \sigma - \sigma^{+} &= 2f(\tfrac{1}{2}[\epsilon - \epsilon^{+}]), \dot{\epsilon} < 0 \end{aligned}\right\} . \tag{2}$$

Here, $(\epsilon^{-}, \sigma^{-})$ and $(\epsilon^{+}, \sigma^{+})$ are the points of strain and stress respectively at the applicable sign reversal of stress rate (or equivalently, strain rate).

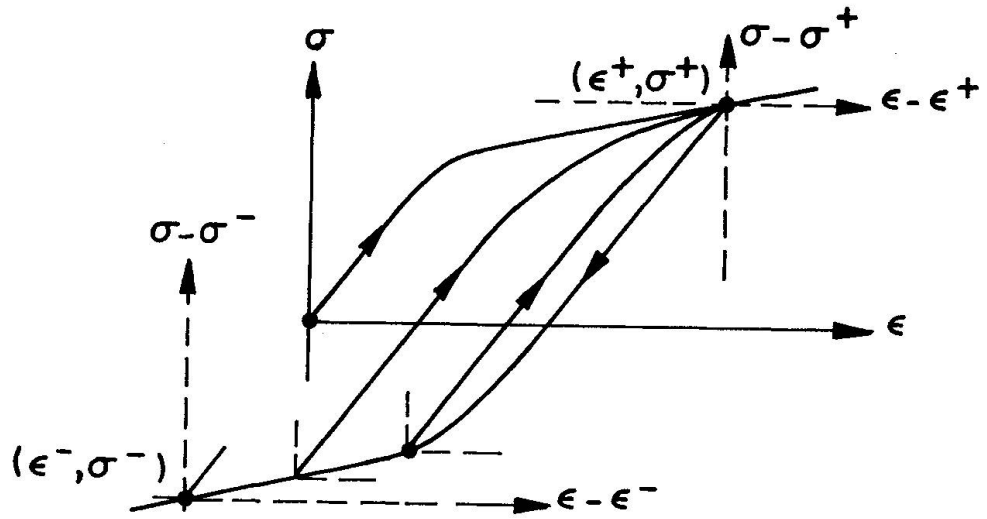

FIG. 1. Uniaxial stress-strain curve and steady-state hystersis loops

In cyclic proportional deformation these four parameters are constant after the first cycle. Point (ϵ^-, σ^-) satisfies Eq. 2b, so that two scalars are sufficient to characterize the stress strain cycle. Although this model is highly idealized since it gives a steady loop after just one cycle, it does provide a useful basis for design or for more accurate analysis of cyclic creep or relaxation phenomena.

We generalize this description to three-dimensional stress states, assuming that the principal stresses are proportional and remain constant in direction. Define a suitable equivalent strain function

$$\epsilon = \epsilon(\epsilon_1, \epsilon_2, \epsilon_3), \tag{3}$$

symmetric in the indices and specializing to $\epsilon = \epsilon_1$ if $\epsilon_2 = \epsilon_3 = 0$; if we calculate the strain rate $\dot{\epsilon}$ from this equation, the constitutive relations for three-dimensional states can be written formally as Eqs 1 and 2, with σ and ϵ now denoting vectors ($\sigma = \sigma_i$, i = 1, 2, 3 etc.) and f denoting a vector function. These constitutive relations are piecewise finite, and for cyclic loading characterized completely by the functions f_i, and two "end" points of the stress path σ_i^+ and σ_i^- (or, equivalently, ϵ_i^- and ϵ_i^+). This extends the Masing relationship (between Eq. 1 and 2) to cyclic proportional triaxial deformation.

3. SELF MAPPING OF BOUNDARY VALUE PROBLEMS

Consider the following class P(1,1) of boundary value problems (of geometrically linear elastostatics):

$$\begin{aligned} &A\sigma + X = 0, \quad B\delta = \epsilon, \quad \sigma = F(\epsilon) \quad \text{in} \quad V; \\ &N\sigma = T \quad \text{in} \quad \partial V' \subset \partial V; \\ &M\delta = D \quad \text{in} \quad \partial V - \partial V'; \end{aligned} \tag{4}$$

where A, B, N and M are linear (differential) operations; V is the region, bounded by ∂V, occupied by the body in the unstressed state; δ, ϵ, and σ are vector-valued point functions in V (representing displacement, strain and stress respectively); and X, T, and D are prescribed functions (representing body force, surface traction and prescribed displacement respectively). Let a progression $P^o(\lambda)$ of boundary values in class P(1,1) be defined by

$$[X,T,D] = [\lambda X^o, \lambda T^o, \lambda D^o], \tag{5}$$

where X^o, T^o, D^o are constant. Assume that a unique solution exists, viz. the progression

$$[\delta,\varepsilon,\sigma] = [\delta^o(\lambda),\varepsilon^o(\lambda),\sigma^o(\lambda)]. \tag{6}$$

Now consider the related class $P(\frac{1}{2},\frac{1}{2})$ of boundary values obtained by replacing the constitutive relation $\sigma = F(\varepsilon)$ in Eq. 4 with

$$\sigma/2 = F(\varepsilon/2), \tag{7}$$

and let a new progression $P(\mu)$ of boundary value problems be defined by

$$[X,T,D] = [2\mu X^o, 2\mu T^o, 2\mu D^o]. \tag{8}$$

Then, $P(\mu)$ has the solution

$$[\delta,\varepsilon,\sigma] = [2\delta^o(\mu), 2\varepsilon^o(\mu), 2\sigma^o(\mu)], \tag{9}$$

as is easily verified.

Now, let Eq. 5, with λ increasing from 0 to λ^+ represent the loading cycle for a body governed by Eq. 4 with constitutive relation F as in Eq. 1; the ensuing displacements, strains and stresses are given by Eq. 6. When the load factor reverses, the corresponding values are given as

$$[\delta^+,\varepsilon^+,\sigma^+] \equiv [\delta^o(\lambda^+),\varepsilon^o(\lambda^+), {}^o(\lambda^+)] \tag{10}$$

If we make the substitutions

$$\delta - \delta^+ \to \delta, \sigma - \sigma^+ \to , \varepsilon - \varepsilon^+ \to \varepsilon, \tag{11}$$

the boundary value problem progression for increments of stress, strain and displacement for the unloading cycle with λ decreasing from λ^+ to λ^- is generated by Eq. 8 with μ representing $\lambda - \lambda^+$. Eq. 9 gives the solution. The unloading path for all points of the body is determined by the corresponding points on the loading path. We conclude: If a material under cyclic proportional triaxial deformation follows the Masing relationship, the stresses, strains and deformations at all points in a body made of this material, subjected to cyclic proportional loading, will also follow a Masing relationship.

4. SIMPLE MATERIALS

A convenient approximation to the uniaxial hardening curve is the power law

$$\sigma = c\varepsilon^{(1/n)} \equiv c(\operatorname{sign}\varepsilon)|\varepsilon|^{1/n} \tag{12}$$

where c and n are positive material constants. The exponent in parenthesis is a convenient symbolic notation which reduces to an ordinary exponent if n is an odd integer.

We may generalize this to complex stress states as follows. Denote the principal shearing stresses and corresponding strains respectively by

$$\tau_i = \tfrac{1}{2}|\sigma_j - \sigma_k| \quad ; \quad \gamma_i = \tfrac{2}{3}|\varepsilon_j - \varepsilon_k| \tag{13}$$

where i,j,k is any permutation of 1,2,3.

Define the plastic potential as

$$W = \frac{2^n c}{n+1}[\tau_1^{(n+1)} + \tau_2^{(n+1)} + \tau_3^{(n+1)}] \quad ; \tag{14}$$

Using Eq. 13 this gives the strains

$$\varepsilon_1 = \frac{c}{2}[(\sigma_1 - \sigma_2)^{(n)} - (\sigma_3 - \sigma_1)^{(n)}] \tag{15}$$

and the analogous expressions by cyclic permutation.

Assume that for a certain value of $\tau_3 = \tau_{3A} = \frac{1}{2}(\sigma_{1A} - \sigma_{2A})$ the further stress path corresponds to a change of sign of $\dot{\tau}_3$ from positive to negative while $\dot{\tau}_2$ and $\dot{\tau}_1$ remain positive. Then instead of Eq. 14 the stress potential takes the form

$$W = \frac{2^n c}{n+1} [\tau_1^{(n+1)} + \tau_2^{(n+1)} + (\tau_3 - \tau_{3A})^{(n+1)}] \tag{16}$$

yielding readily the stress-strain relations for the new path.

Alternatively we may derive a simplified hardening model already discussed by Mróz [2]. The state of hardening is assumed to be described with sufficient accuracy in terms of a set of surfaces of constant hardening moduli $K = \partial\sigma_f/\partial\varepsilon$, where σ_f denotes the component of the stress increment along the normal to the yield surface and $\varepsilon = (d\varepsilon_{ij} d\varepsilon_{ij})^{\frac{1}{2}}$ denotes the absolute value of the plastic strain increment. Since these surfaces cannot intersect, the active surfaces are assumed to translate with the stress point and become tangential along the stress path. For a piecewise linear yield condition this model results in finite stress-strain relations valid in particular sub-domains of stress space similar to the model described above. Fig. 2 show the translation for two radial stress paths.

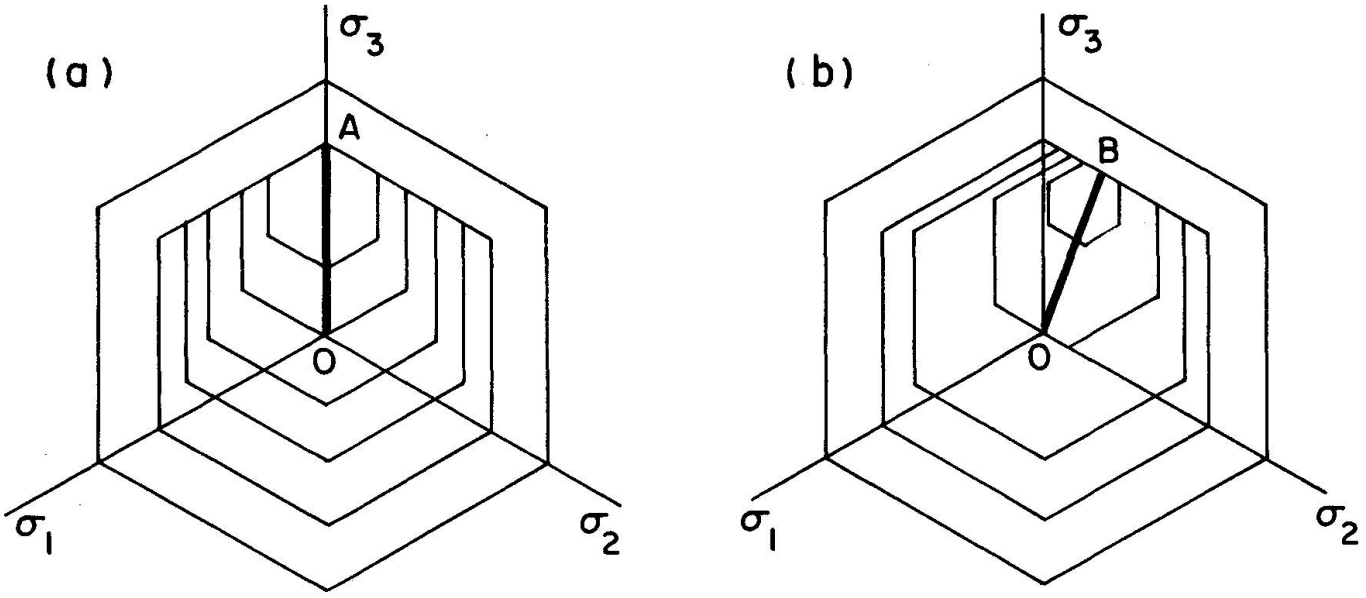

FIG. 2. Fields of hardening moduli after plastic loading
(a) along OA (b) along OB

The postulated materials have piecewise finite stress-strain relations that are homogeneous functions of order n. The materials may be called simple, incrementally hyperelastic of order n [4]. For loading increment $\Delta\lambda$, the corresponding stress increment is everywhere proportional to $\Delta\lambda$ and the corresponding strain and deformation increments are proportional to $\Delta\lambda^{(n)}$. If $[\delta^\circ, \varepsilon^\circ, \sigma^\circ]$ solves $[X^\circ, T^\circ, D^\circ]$, then $[\lambda^{(n)}\delta^\circ, \lambda^{(n)}\varepsilon^\circ, \lambda\sigma^\circ]$ is the solution field for $[\lambda X^\circ, \lambda T^\circ, \lambda^{(n)} D^\circ]$. Thus, the entire solution for a cyclic loading (either traction-controlled: $D^\circ = 0$ or displacement-controlled: $X^\circ, T^\circ \equiv 0, 0$) can be derived from a single equilibrium solution. This solution can be obtained for many structures of practical interest, using a variety of numerical methods. We note, in particular

that the unloaded state is stress free under cyclic proportional loading.

5. EXAMPLE: THICK-WALLED CYLINDER

Consider a long thick-walled tube of internal and external radii a and b, subjected to internal pressure p varying between the prescribed limits p^+ and p^-. A simple, closed form cyclic solution can be obtained when only plastic strains satisfying Eq. 15 are accounted for. Since the strain normal to the plane of deformation vanishes, we have

$$\epsilon_\theta + \epsilon_r = \frac{u}{r} + \frac{du}{dr} = 0 , \quad u = \frac{A}{r} \tag{17}$$

where u denotes the radial displacement and ϵ_θ, ϵ_r are principal strains in the

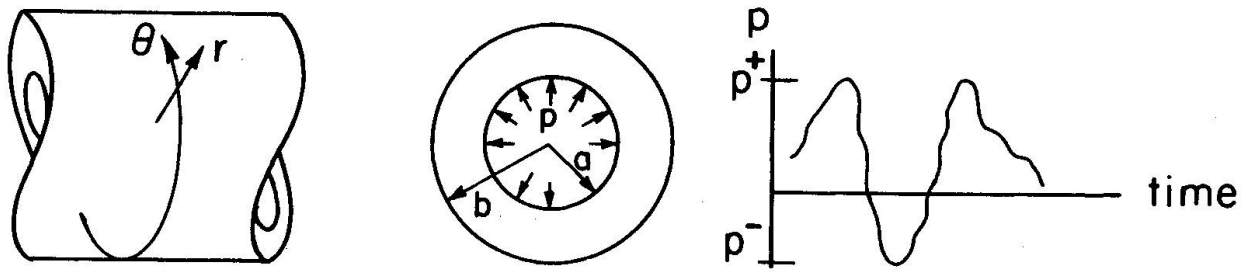

FIG. 3. Thick walled cylinder under cyclic pressure

plane (r,θ) ; A denotes an integration constant. From Eq. 15 we have

$$\epsilon_\theta = C'(\sigma_\theta - \sigma_r)^n, \quad \epsilon_r = -C'(\sigma_\theta - \sigma_r)^n, \tag{18}$$

where $C' = c(1 + 2^{-n})/2$. The inverse relations take the form

$$\sigma_\theta - \sigma_r = C(\epsilon_\theta)^{1/n} = C(\tfrac{A}{r}2)^{1/n} , \tag{19}$$

where $C = (C')^{-n}$. Using the equilibrium equation

$$\frac{d\sigma_r}{dr} + \frac{\sigma_r - \sigma_\theta}{r} = 0 \tag{20}$$

the stress state within the tube is determined in the form

$$(\sigma_r;\sigma_\theta) = \frac{p}{(\frac{b}{a})^{2/n} - 1} \left[(\frac{b}{r})^{2/n} - 1;\ 1 - (1 - 2/n)(\frac{b}{r})^{2/n}\right] \tag{21}$$

where the boundary conditions $\sigma_r = -p$ for $r = a$ and $\sigma_r = 0$ for $r = b$ have been satisfied. The displacement field is given by

$$u = \frac{2^n p^n b^2}{C^n n^n [(\frac{b}{a})^{2/n} - 1]} \frac{1}{r} . \tag{22}$$

Consider now the unloading program. Denote by $\Delta p = p - p^+$, $\Delta u = u - u^+$ $\Delta\epsilon_r = \epsilon_r - \epsilon_r^+$, $\Delta\epsilon_\theta = -\epsilon_\theta^+$. Instead of Eq. 19 we now have

$$\Delta\sigma_\theta - \Delta\sigma_r = 2C\left(\frac{\Delta\epsilon_\theta}{2}\right)^{1/n} = D(\Delta\epsilon_\theta)^{1/n} = D\left(\frac{\Delta A}{r}\right)^{1/n}, \tag{23}$$

where $D = 2^{\left(\frac{n-1}{n}\right)} C$. The equilibrium equations now provide expressions for stresses identical to Eq.21 with p replaced by Δp. The radial displacement for any p satisfying $p^- \leq p < p^+$ equals

$$u_2 = \frac{b^2 p^n}{C^n n^n \left[\left(\frac{b}{a}\right)^{2/n} - 1\right]} (2^n - 2) \tag{24}$$

Since the stress state does not depend on constants D or C, upon removal of the pressure both stresses vanish. Thus, no residual stresses are created for zero pressure in the steady state. For further repetition of pressure between p^+ and p^-, the displacement and stress fields are described by Eqs. 21 and 24.

6. CONCLUSION

Plastic analysis of practical structures under variable loading, however difficult in general, is tractable for cyclic proportional loading when the plastic behaviour of the material can be adequately described by a Masing-type relationship with an incremental power-law, and when one solution to the corresponding static nonlinear elastic boundary value problem can be produced. An example is given herein; other examples (circular and annular plates, etc.)have been presented by the authors elsewhere [4]. Experimental verification of the practical validity of such analysis is currently underway.

BIBLIOGRAPHY

[1] Z. Mróz, "A Description of Workhardening of Metals with Application to Variable Loading", Proc. Symp. on Plasticity, Warsaw, 1972.

[2] Z. Mróz, "On the Theory of Steady Plastic Cycles in Structures", Proc. First Int. Conf. Struct. Mech. in Reactor Tech., Berlin, 1971.

[3] N.C. Lind, "Exremum principles for Certain Hyperelastic Materials", International Journal of Non-Linear Mechanics (in press).

[4] Z. Mróz and N.C. Lind, "Simplified Theories of Cyclic Plasticity", ASCE meeting preprint 1841. Report No. 20, Solid Mechanics Division, University of Waterloo, June 1972.

SUMMARY

Piecewise finite representations of material behaviour are proposed for practical analysis of plastic metal behaviour under cyclic loading.

RESUME

Quelques représentations constitutives finies du matériau sont présentées pour l'analyse pratique du comportement plastique des structures sous charges cycliques.

ZUSAMMENFASSUNG

Stückweise endliche Modelle für das Stoffverhalten werden zur praktischen Berechnung zyklisch beanspruchter plastifizierender Metallkonstruktionen vorgeschlagen.

Method of Analysis for Cyclically Loaded R.C. Plane Frames Including Changes in Geometry and Non-Elastic Behavior of Elements under Combined Normal Force and Bending

Méthode d'analyse de cadres plans en b.a. chargés cycliquement, comprenant les variations de géométrie et le comportement non-élastique d'éléments soumis à effort normal et à flexion composés

Untersuchungsmethode für zyklisch belastete ebene Stahlbeton-Rahmen einschliesslich der Geometrie-Änderungen und des nicht-elastischen Verhaltens von Elementen unter zusammengesetzten Axial- und Biegungskräften

Marco MENEGOTTO Paolo Emilio PINTO
Istituto di Scienza e Tecnica delle Costruzioni
Università di Roma, Italia

INTRODUCTION. The advances gained by structural analysis, coupled with the availability of large capacity computers, could lead to the idea that today the "exact" solution of any structural problem exists, and its obtainment is only a matter of assembling in a program the appropriate ingredients, all of them already well established.

This is not the case for reinforced concrete structures in non linear range: neither the constitutive laws of the materials nor the behavior of the structural elements can be said to be conveniently clarified. The method that will be briefly exposed in the following (°) includes most of the ingredients necessary to be defined as "general", but nevertheless its classification as "exact" is justified only within certain simplifying hypotheses that are listed below without comment:

- the constitutive laws of the materials are independent of time
- the contribution of concrete in tension is disregarded
- linear distribution of strain along the depht of section is assumed, excluding bond slip during all the loading history, and local buckling of steel bars
- properties of the materials are assumed not to deteriorate after repeated stressing, while Bauschinger effect on steel is considered
- actions of shear stresses are disregarded

GENERAL DESCRIPTION OF THE METHOD. The procedure follows an incremental way. Each step requires solution of the set of equilibrium equations:

$$|K|_s \{\Delta S\}=\{\Delta P\} \qquad (1)$$

The vectors $\{\Delta S\}$ and $\{\Delta P\}$ contain the increments of nodal displacements and external loads: both have $3n$ (n=number of nodes) dimension and are referred to a global coordinate system x,y .

(°) A more extended illustration is contained in ref.|11|

The geometrical and mechanical behavior of the structure in the course of each step is described by the stiffness matrix $|K|_s$, which is the result of the assembly of the stiffness matrices $|K|$ determined for every individual member in which the structure has been discretized.

The essence of the method lies evidently on the calculation of matrix $|K|_s$ for each step. The procedure requires an iteration, which ends when two coincidental successive solutions $\{\Delta S\}$ are obtained for the same $\{\Delta P\}$ from Eqs. (1).

Two causes of non-linearity are contained in $|K|_s$: behavior of materials and variations in the geometry of the structure. They can be analized separately, and so will they be presented.

NON LINEARITY DUE TO INELASTIC BEHAVIOR OF THE ELEMENTS.

Constitutive laws of the materials. The calculation of the stresses σ for given ε is performed in two separate subroutines so that any particular law can be inserted simply; figs.1 and 2 show the laws presently adopted.

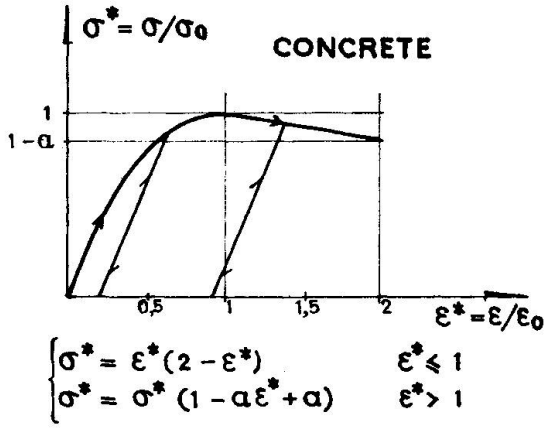

FIG.1

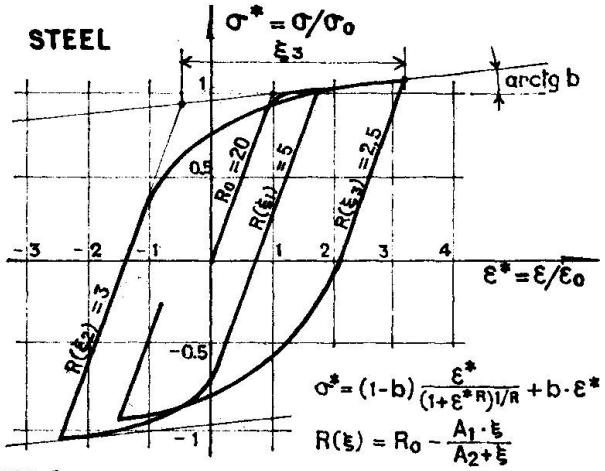

FIG.2

The diagram in fig.1 reproduces the well known Hognestad formula, extended to general stress paths with straight unloading or reloading lines, parallel to the initial tangent. The law for the steel is described in detail elsewhere |7|. It can reproduce with good approximation the behavior of different types of steel: the constant b defines the slope of the hardworking line; the exponent R, which varies after every inversion, affects the curvature of the diagram, to represent the Bauschinger effect.

Stiffness matrix of an element. A matrix $|K_n|$ defines the relationship between the three nodal force components (incremental), and the three nodal "deformations" $\{\Delta S_n\}$. This relationship is established in the intrinsic coordinate system m,n. Elements must be such, that 2° order effects within them are negligible (see fig.3).

First the flexibility matrix of the element is determined. The columns of the three-by-three $|K_n|^{-1}$ contain the increments of nodal deformations versus the increments of the components of $\{\Delta F_n\}$. The coefficients are calculated by numerical integration along the length of

the element, applying separately the three components of $\{\Delta F_n\}$ but considering the deformability due to their simultaneous application. The matrix $|K_n|^{-1}$ is a linearization of a non-linear step: its coefficients are the exact ones, only if at the end of the step the values of the nodal increments $\{\Delta F_n\}$ result to be equal to those applied in calculating the matrix itself.

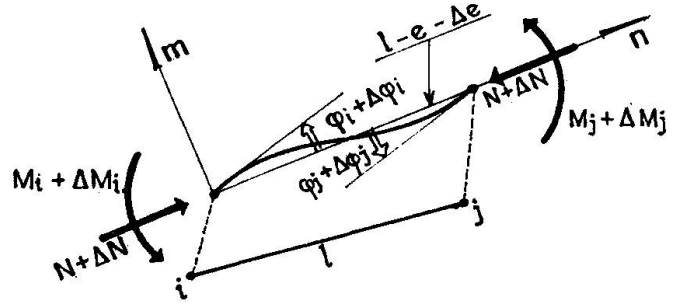

$$\{\Delta Fn\} = \begin{bmatrix} \Delta N \\ \Delta M_i \\ \Delta M_j \end{bmatrix} \qquad \{\Delta Sn\} = \begin{bmatrix} \Delta e \\ \Delta \varphi_i \\ \Delta \varphi_j \end{bmatrix}$$

FIG.3

To perform the integration along the element, the current deformability of a suitable number of internal cross-sections must be determined, which is defined by the relationship: $\{\Delta\varepsilon\}=|E|\ \{\Delta\Sigma\}$ (see fig.4)

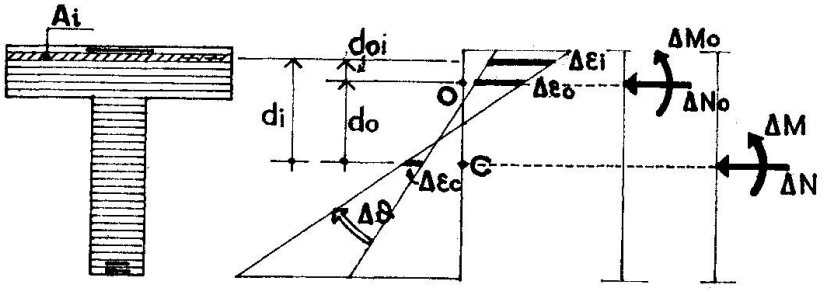

$$\{\Delta\varepsilon\} = \begin{Bmatrix} \Delta\varepsilon_c \\ \Delta\vartheta_c \end{Bmatrix} \qquad \{\Delta\Sigma\} = \begin{Bmatrix} \Delta N \\ \Delta M \end{Bmatrix}$$

$$\{\Delta\varepsilon_o\} = \begin{Bmatrix} \Delta\varepsilon_o \\ \Delta\vartheta_o \end{Bmatrix} \qquad \{\Delta\Sigma_o\} = \begin{Bmatrix} \Delta N_o \\ \Delta M_o \end{Bmatrix}$$

FIG.4

where matrix $|E|$ of the section is generally variable from step to step. The cross-section is subdivided into a number of concrete and steel areas: the path of every area in the space σ-ε must be recorded, because it determines the behavior of the area for the load history.

Provided that $\Delta\sigma_i$ and $\Delta\varepsilon_i$ are the actual stress and strain variations due to application of combined ΔM and ΔN on the i-th concrete or steel area, its secant modulus E_i for the current step will be defined: $E_i = \frac{\Delta\sigma_i}{\Delta\varepsilon_i}$. Thus, the cross-section can be treated as if composed by elastic parts with varied moduli. The following relations can be written, referring to the current homogenized cross-section centroid O:

$$\begin{vmatrix} \Delta\varepsilon_o \\ \Delta\vartheta_o \end{vmatrix} = \begin{vmatrix} \frac{1}{\Sigma A_i E_i} & 0 \\ 0 & \frac{1}{\Sigma A_i E_i d_{oi}^2} \end{vmatrix} \cdot \begin{vmatrix} \Delta N_o \\ \Delta M_o \end{vmatrix} \qquad (2)$$

which, transferring the vectors $\{\Delta\varepsilon_o\}, \{\Delta\Sigma_o\}$ to the fixed geometric center C, become:

$$\begin{vmatrix} \Delta\varepsilon_c \\ \Delta\vartheta_c \end{vmatrix} = \begin{vmatrix} \left(\frac{1}{A}+\frac{S}{A^2J}\right) & -\frac{S}{AJ} \\ -\frac{S}{AJ} & -\frac{1}{J} \end{vmatrix} \cdot \begin{vmatrix} \Delta N \\ \Delta M \end{vmatrix} \qquad \begin{aligned} A &= \Sigma A_i E_i \\ S &= \Sigma A_i E_i d_i \\ J &= \Sigma A_i E_i d_i^2 - \frac{S^2}{A} \end{aligned} \qquad (3)$$

During the step, a "general" iteration is performed to obtain the solution of equations (1). Within each cycle of it, for each element every cross-section is given a vector$\{\Delta\Sigma\}$, corresponding to the proposed $\{\Delta F_n\}$, and, by "internal" iterations, relations (3) are solved, yielding matrix $|E|$. Thus, the general iteration proceeds dealing always whith deformabilities updated with actual state and history of stress.

It may be noted that matrices $|E|$ are symmetrical. The same property consequently extends to all $|K_n|^{-1}$, $|K|$ and to $|K|_s$ matrices.

NON LINEARITY DUE TO CHANGES IN GEOMETRY. Finite deflections of elastic plane frames have been the object of recent extensive studies [8] [10], [13] so that only a brief account of the relations employed will be reported.

Prior to their assembly into the overall matrix $|K|_s$, matrices $|K_n|$ of individual elements must be trasferred from the local system m,n to a global system x,y. When the displacements of the elements during the load history cannot be neglected, the transformation from m,n to x,y is non linear. The technique of linearization adopted is the approximation of a first order differential expansion with finite increments.

In order to pass from the intrinsic to the global system, an intermediate coordinate system u,v is employed.

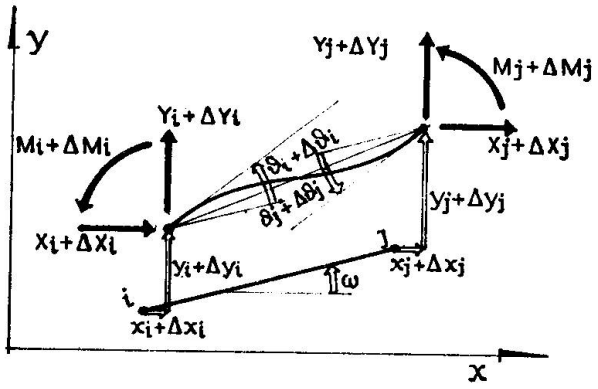

$$\{\Delta Fx\} = [\Delta X_i \ \Delta Y_i \ \Delta M_i \ \Delta X_j \ \Delta Y_j \ \Delta M_j]^T$$

FIG.5 $$\{\Delta Sx\} = [\Delta x_i \ \Delta y_i \ \Delta\vartheta_i \ \Delta x_j \ \Delta y_j \ \Delta\vartheta_j]^T$$

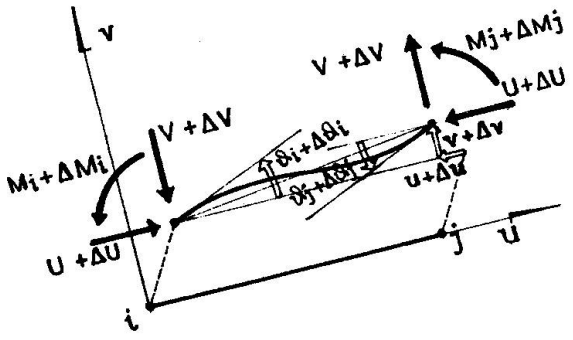

$$\{\Delta Fu\} = [\Delta U \ \Delta V \ \Delta M_i \ \Delta M_j]^T$$

FIG.6 $$\{\Delta Su\} = [\Delta u \ \Delta v \ \Delta\vartheta_i \ \Delta\vartheta_j]^T$$

For finite displacements, the relationships between the components of the vectors$\{S_u\}$ and$\{S_n\}$ are:

$$e = l-\sqrt{(l-u)^2+v^2} \qquad \phi_i = \theta_i - arctg\frac{v}{l-u} \qquad \phi j = \theta_j - arctg\frac{v}{l-u} \tag{4}$$

By differentiation, the preceding relations can be given the linear form: $\{\Delta S_n\}=|A|\ \{\Delta S_u\}$, with increments in place of differentials.

The relationship between the vectors of nodal forces in the two systems is: $\{F_u\}=|A|'\{F_n\}$; and, by diffentiating:

$$\{\Delta F_u\} = |A|'\{\Delta F_n\} + |D|\ \{\Delta S_u\} \tag{5}$$

The matrices $|A|$ and $|D|$ have the expressions:

$$|A| = \begin{vmatrix} \frac{l-u}{l-e} & \frac{-v}{l-e} & 0 & 0 \\ \frac{-v}{(l-e)^2} & \frac{-(l-u)}{(l-e)^2} & 1 & 0 \\ \frac{-v}{(l-e)^2} & \frac{-(l-u)}{(l-e)^2} & 0 & 1 \end{vmatrix}$$

$$|D| = \begin{vmatrix} d_{11}\ d_{12} & 0 & 0 \\ d_{22} & 0 & 0 \\ (symm) & 0 & 0 \\ & 0 & \end{vmatrix} \begin{vmatrix} d_{11}=\frac{1}{(l-e)^4} & |v^2(l-u)\cdot U+\{2(l-u)^2+v^2\}vV| \\ d_{12}=\frac{1}{(l-e)^4} & |-v^3U+(l-u)^3V| \\ d_{22}=\frac{1}{(l-e)^4} & |(l-u)\{(l-u)^2+v^2\}U-v(l-u)^2V| \end{vmatrix} \qquad (6)$$

Both matrices contain in their coefficients the components of the displacements accumulated in the previous history; the "geometric"matrix $|D|$ contains also the accumulated force components U and V.

The transformation of displacements and forces from u,v to x,y is accomplished by a matrix with constant coefficients $|T|$, defining the initial position of the element (through its angle ω with x axis).

Making substitutions, the stiffness relation $|K_n|\ \{\Delta S_n\}=\{\Delta F_n\}$ becomes: $|K|\ \{\Delta S_x\}=\{\Delta F_x\}$, with:

$$|K| = (|T|'\ |A|'\ |K_n|\ |A|\ |T|)+|T|'\ |D|\ |T| \qquad (7)$$

The matrix $|K|$contains in $|K_n|$the linearization of the mechanical behavior, and in $|A|$and $|D|$the linearization of the kinematical behavior. It has to be noted a difference between the two criteria of linearization. The matrix $|K_n|$has a "secant" character, in what its coefficients are checked with the situation at the end of each step. Taking into account possible inversions of strain variations in the areolas from step to step, this matrix could not be expressed as "tangent". As much as $|K_n|$is concerned, the lenght of the step would be only limited by the possibility of missing strain inversions during the step itself.

The matrices $|A|$and $|D|$on the other hand, by the way they have been obtained, are "tangent initial" since their coefficients are calculated with the values of variables at the beginning of each step. Therefore the lenght of the step has to be commensured to the importance of the effects of changes in geometry.

EXAMPLE. It has been chosen as example a frame tested by Ferguson and Breen (Ref.|5|). Here the frame has been subdivided in 12 elements and the loading paths of 3960 concrete and 264 steel areas were recorded. The constants adopted for the materials were (kg/cm^2): concrete: σ_o= 280, initial modulus E=250000, $\sigma(3{,}8‰)=0{,}85\cdot\sigma_o$; steel: σ_o=3850, in E= 2050000, b=0.02, R_o=20. In fig. 7 experimental and theoretical curves are compared: the agreement is excellent. The curve(c) shows the first-order non elastic analysis of the same problem.Ultimate stress diagrams of two cross-sections appear in fig.9, while fig.8 shows the calculated deflected shape in case (b).

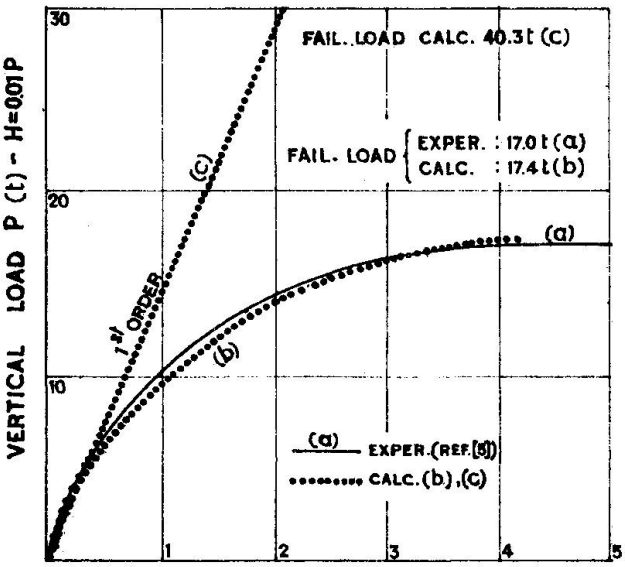

FIG.7 DEFLECTION - NODE 5 (cm)

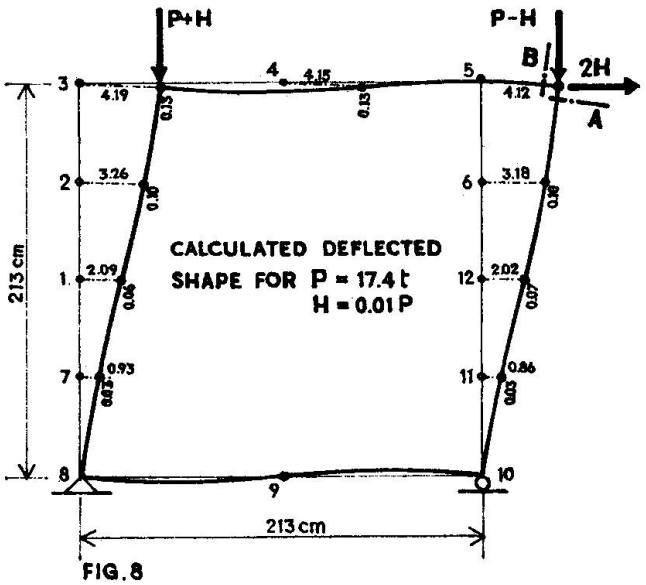

FIG.8

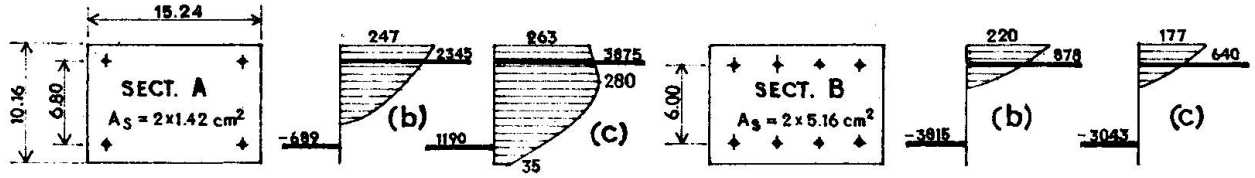

FIG.9 STRESS DIAGRAMS AT FAILURE (CALC.) Kg/cm²

The same frame has been submitted to two cyclical horizontal loadings,(case *d*): *P*=0, case *e*): *P*=6t). The influence of *P* is relevant both in(2*H*-δ)and(*M*-θ)diagrams. Case *e*) has higher moments but overall plasticization is very low and the frame fails for instability.The collapse in case *d*)is due to attainment of limit strains on concrete.

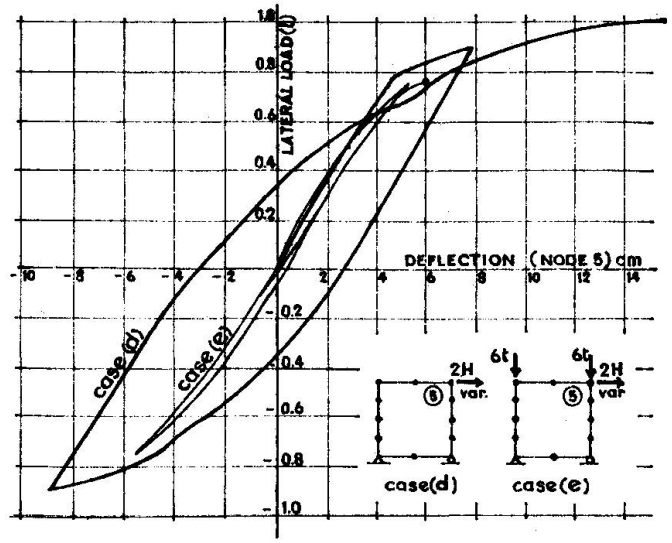

FIG.10 - HOR. LOAD - DEFLECTION (NODE 5)

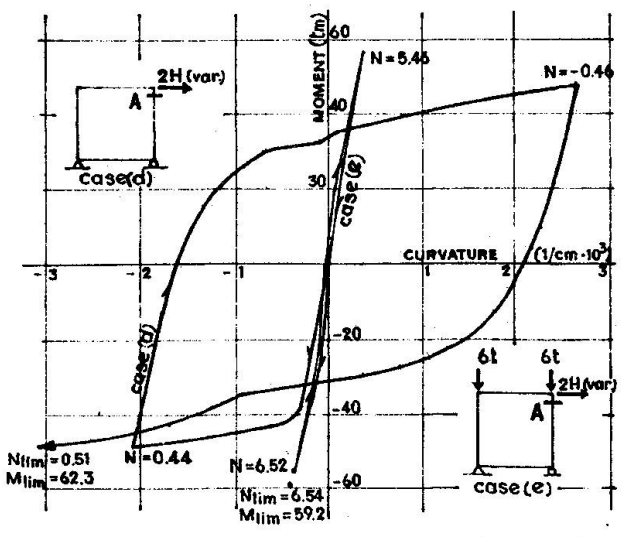

FIG.11 - MOMENT - CURVATURE (SECT. A)

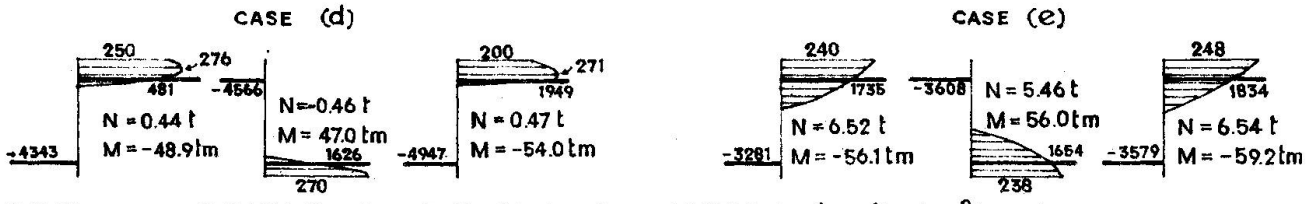

FIG. 12 HISTORY OF STRESSES ON SECTION A (kg/cm^2)

REFERENCES

|1| BERTERO, V. V., BRESLER, B. - Seismic Behavior of Reinforced Concrete Framed Structures. "IV World Conf. on Earth. Eng." - Chile, 1969.

|2| BLAAUWENDRAAD, IR, J. - Realistic Analysis of Reinforced Concrete Framed Structures - "Heron vol. 18, 1972, n°4".

|3| CRANSTON, W. B. - A computer Method for Inelastic Analysis of Plane Frames. "C. C. A. Tech. Rep." TRA 386, 1965.

|4| DE DONATO, O., MAIER, M., - Mathematical Programming Methods for the Inelastic Analysis of Reinforced Concrete Frames Allowing for Limited Rotation Capacity. "Int. Journ. Num. Meth. Eng." Vol. 4, 1972.

|5| FERGUSON, P. M., BREEN J. E., - Investigation of the Long Concrete Column in a Frame Subject to Lateral Loads. Symposium on Reinforced Concrete Columns - ACI publ. SP. 13.

|6| FERRY BORGES, J., ARANTES E OLIVEIRA, E. R. - Non linear Analysis of Reinforced Concrete Structures. "Mémoires A. I. P. C.", vol. 23, 1963.

|7| GIUFFRE', A., PINTO, P. E., - Il Comportamento del Cemento Armato per Sollecitazioni Cicliche di Forte Intensità. "Giornale del Genio Civile", Maggio 1970.

|8| JENNINGS, A. - Frame Analysis Including Change of Geometry. "Journ. of Struct. Div.", ASCE, vol. 94, March. 1968.

|9| MACCHI, G. - Methodes de calcul des structures hyperstatiques. "C. E. B. Bulletin" n. 53, 1964.

|10| MALLET, R. H., MARCAL, P. V. - Finite Element Analysis of Nonlinear Structures. "Journ. of Struct. Div.", ASCE, vol. 94, Sept. 1968.

|11| MENEGOTTO, M., PINTO, P. E. - Method of Analysis for Cyclically Loaded R. C. Frames Including Changes in Geometry and Non-elastic Behavior of Elements under Combined Normal Force and Bending - Ist. Scienza e Tecnica d. Costruzioni - Univ. of Rome - Rep. n°32, Oct. 1972.

|12| PARK, R., KENT, D. C., SAMPSON, R. A. - Reinforced Concrete Members with Cyclic Loading", "Jnl. of Struct. Div.", ASCE, vol. 98 , July 1972.

|13| POWELL, G. H. - Theory of Nonlinear Elastic Structures. "Journ. of Struct. Div.", ASCE, vol. 95, Dec. 1969.

SUMMARY

The procedure is based on the stiffness method in incremental way, and has been programmed for computer. The solution is obtained by the calculation of a lineari-

zed stiffness matrix for every increment. The element matrices derive from an analysis of the behavior of several internal cross-sections: these are discretized into concrete and steel areolae, for each of which the loading path is recorded, following any non-holonomic constitutive law. Geometric effects are included in the overall matrix by adjusting the projection of elements displacements and forces at every step.

RESUME

Le procédé se base sur la méthode des déformations appliquée par incréments, et a été programmé pour ordinateur. La solution s'obtient en calculant une matrice de rigidité linéarisée à chaque incrément. Les matrices des éléments dérivent de l'analyse du comportement d'un certain nombre de sections: celles-ci sont discretisées en aréoles de béton et d'acier, dont l'histoire de charge est mémorisée, suivant une loi constitutive quelquonque. Les effets géometriques sont inclus dans la matrice d'ensemble, par le réglage de la projection des déplacements et des forces des éléments à chaque pas.

ZUSAMMENFASSUNG

Das Verfahren stützt sich auf die Steifigkeitsmethode auf inkrementalem Wege und wurde auf dem Computer programmiert. Die Lösung ergibt sich durch Berechnung einer linearisierten Steifigkeitsmatrix für jeden Zuwachs. Die Elementmatrizen folgen aus der Analyse des Verhaltens einer bestimmten Anzahl innerer Querschnitte: diese sind in Beton- und Stahlareolen diskretisiert, deren Belastung nach einem konstitutiven Gesetz aufgezeichnet wurde. Die geometrischen Aenderungen sind in der Gesamtmatrix durch Anpassung der Projektion der Elementverschiebungen und -kräfte bei jedem Schritt inbegriffen.

I

Theoretical Prediction of the Load-Deflexion Relationship of Steel Members and Frames

Prédiction théorique de la relation charge-déformation d'éléments en acier et de cadres

Theoretische Voraussage der Last-Deformations-Beziehung von Stahlteilen und Rahmen

Ben KATO
Professor of
Structural Engineering

Hiroshi AKIYAMA
Associate Professor of
Structural Engineering

University of Tokyo, Japan

1. INTRODUCTION

Failure modes of steel members and frames subject to repeated and reversed loading can be classified into three categories,that is,low-stress high-cycle fatigue,high-stress low-cycle fatigue and failure due to instability by the accumulation of deformation. For aerodynamic excitation associated with wind turbulence,it is usual to design the structures to resist elastically since the duration of it be substantially long and the response associated with resonance will tend to unlimited,accordingly high cycle fatigue problem may be paramount for such a situation. On the contrary,the duration of the earthquake ground motion is very short and the expected return period of the occurence of catastrophic earthquake is very long(say more than 100 years),though variable in different zones. For such a large but short term loading with very small expectation of occurence,it will be reasonable to allow the structures to undergo substantial plastic deformation provided that the human lives should not be lost by the collapse of the structures. So far as available experimental results and actual experiences of earthquake response indicated,it is very likely that the numbers of deformation response accompanying large plastic strain will be limited to the order of ten,thence low-cycle fatigue will not take place if severe buckle and stress concentration are carefully avoided.

In this discussion,it is assumed that all kinds of buckling are properly prevented until enough plastic deformation will develop. Under this condition, principal objective is forcussed to the prediction of the load-deformation relationship of members and frames under repeated and reserved loading,which forms the essential part of the dynamic response analysis of structures in inelastic region, and of the evaluation of the incremental collapse load(overturning by instability) of structures by earthquake. It commences with the description of the stress-strain characteristics of steel material under cyclic and reversed loading and then reports on a theoretical method for determining the moment-curvature and load-deflexion characteristics of steel members under monotonic loading. The explanation of a technique to construct the load-deflexion relationship for cyclic and reversed loading directly from the obtained monotonic loading curve will be succeeded. Finally, several experimental results of members and frames are compared with this theoretical prediction.

2. MATERIAL BEHAVIOR

Load-deformation(or σ-ϵ) relationship of a steel bar subject to alternative tension and compression in plastic region is shown in Fig.1(1). Let unloading point at i.cycle C_i and let the corresponding load point on the curve of i+1.cycle C_i'. Segment $C_i'C_{i+1}$ is transfered rightward horizontally until C_i' coincides with C_i. If this maneuver is worked out for i=1~n, a fictitious load-deformation curve is obtained. This fictitious curve is compared with the monotonic load-deformation curve of the same specimen in Fig.2. It can be seen both are almost identical. Based upon this finding,the curve for cyclic loading can be constructed from the monotonic load-deformation(or σ-ϵ)curve in a reverse order as is illustrated in Fig.3. The Baushinger effect cannot be included in this technique. Detailed discussion on material behavior including Baushinger effect will be done elswhere of this symposium(2).
Significant feature of the σ-ϵ relationship for cyclic and reversed loading is that the loop enlarges for every additional cycle. Obviously this phenomenon comes from the effect of strain-hardening.

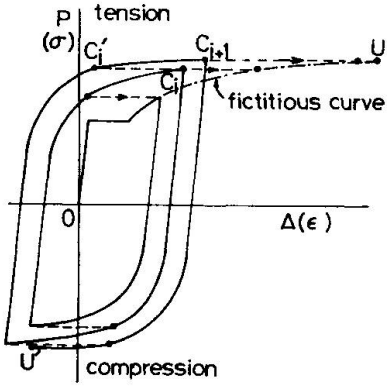

Fig.1 Stress-Strain Curve for Steel for Repeated Loading

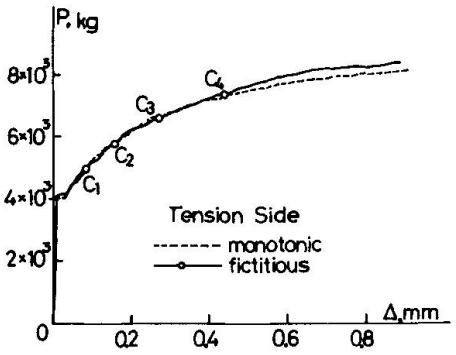

Fig.2 Comparison with Monotonic and Fictitious Curve

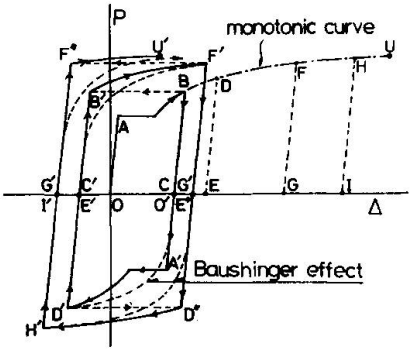

Fig.3 Construction of Cyclic Curve from Monotonic Curve

3.MOMENT-CURVATURE RELATIONSHIP

The load-deflexion characteristics of structural steel members are mainly dependent on the moment-curvature ($M-\Phi$)relationships of the sections since most of the deformation arises from strains associated with flexure.
Based on σ-ϵ relation shown in Fig.4, M-Φ relationship for H-shaped section is numerically calculated and depicted in Fig.5(3),(4). Dashed lines in the figure

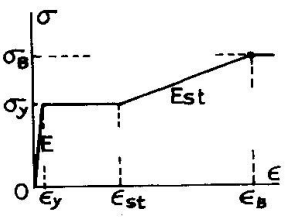

σ_y= 26.7 kg/mm²
σ_B= 42.0 " "
ϵ_{st}=1.27×10⁻²
ϵ_B=3.34×10⁻²
E =21,000 kg/mm²
Est=740 kg/mm²

Fig.4 σ-ϵ Relation

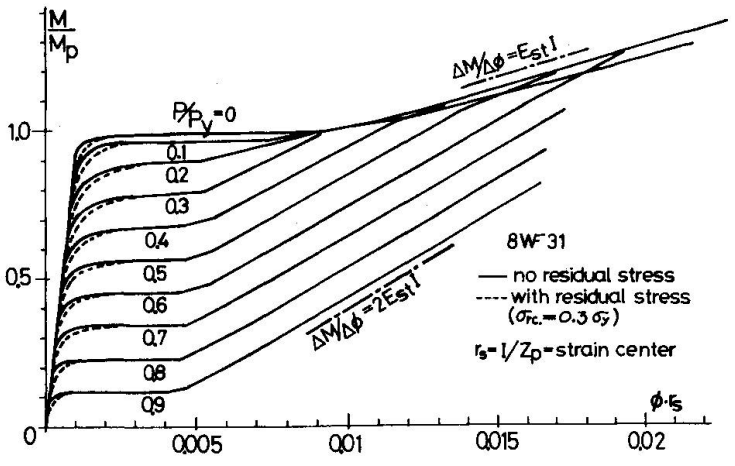

Fig.5 M-Φ Relation

show the effect of residual stress. It can be seen the effect of residual stress is negligible in the region of large curvature. For a member with substantial axial thrust($P \geqq 0.3P_y$),flexural rigidity in strain-hardening region is nearly twice the value of that for a member with no axial thrust(beam).

4.LOAD-DEFLEXION RELATIONSHIPS FOR MEMBERS AND FRAMES

4.1. Beams

When a member does not carry the axial compression,load-deflexion curve for monotonic loading can be readily obtained by the integration of the curvature obtained in chapter 3.

$$y = \iint \Phi(M)\, dx\, dx \qquad (1)$$

Since the calculation of $M-\Phi$ relation means a kind of geometrical transformation of $\sigma-\epsilon$ relationship,mechanical characteristics of $\sigma-\epsilon$ relation will remain unaltered in the expression of $M-\Phi$ relationship. Calculation of deflexion according to eq.(1) concerns the moment distribution along the member length only,and the relation between bending moment and applied force is linear,then the mechanical characteristics of $\sigma-\epsilon$ relation will remain unaltered in the load-deflexion relation again. From above observations,it can be assessed that load-deflexion curves for cyclic loading can be constructed from those for monotonic loading by the same technique as described for material behavior in chapter 2. Let OAU be the load-deflexion curve for monotonic loading in Fig.6,where U represents the maximum load attributed to local buckling or lateral torsional buckling or some other causes. The curve for repeated and reversed loading can be constructed from OAU as follows; The beam is first subjected to an increasing transverse load up to point B. The load is then removed at point C and re-applied in the opposite direction. For further reversed loading,the response of the beam is represented by O'A'D' which is identical to the virgin curve OAD. If the beam is unloaded again at point D',the moment will be removed at point E'. The reloading curve C'B'F' will be identical to CBF. This process is continued until point U' is reached which corresponds to the maximum load point U of the monotonic curve.

4.2.Beam-Column

Though calculation of the deflexion becomes rather complicated due to the existence of $P-\Delta$ effect, the inelastic behavior of beam-columns subject to monotonic lateral loads is fairly well understood. $P-\Delta$ effect may cause the instability of beam-columns.

When a beam-column is subjected to repeated and reversed lateral force H under constant axial compressive force P,this $P-\Delta$ moment induces the additional effect(3),which can be explained with reference to Fig.7. For simplicity of discussion,elastic component of the deformation is ignored. There is no lateral deflexion along the column until the bending moment at the base reaches the plastic moment M_{pc}. The corresponding lateral load is equal to M_{pc}/L. The response of the column for monotonic loading condition is given by OABDFU in Fig.8. If the lateral load is removed after the column has reached a deflexion Δ ,there will be a residual moment equal to $P\times\Delta$ at the base of the column. The horizontal force that is required to remove this moment is

$$H = -\frac{P\Delta}{L} \qquad (2)$$

This equation is represented by line a-a' in Fig.8. Any point on this line defines a residual moment free condition for a column. Instead of horizontal axis, this line should be used as the base line in the analysis for the subsequent cycles of load application. In the construction of cyclic curve for beam-columns, this is the only difference from the case of beams.
The process of constructing the cyclic curve is illustrated in Fig.8. Note that

the expansion of the loop is more pronounced than that for the case of beam. For both beams and beam-columns,it has been shown that the collupse point for cyclic loading can be predicted if the monotonic load-deflexion curves and their terminal points(U) are known.

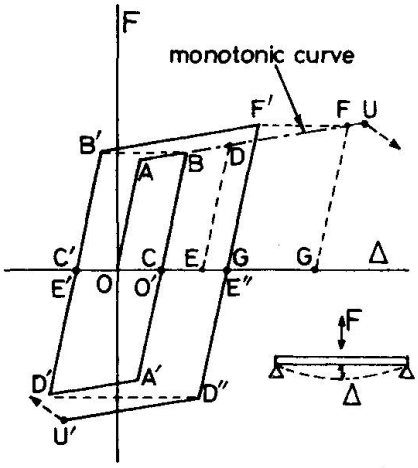

Fig.6 Construction of Cyclic Curve from Monotonic Curve of a Beam

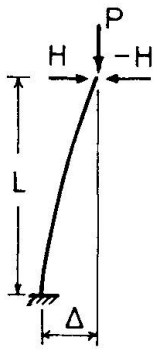

Fig.7 Cantilever Beam-Column

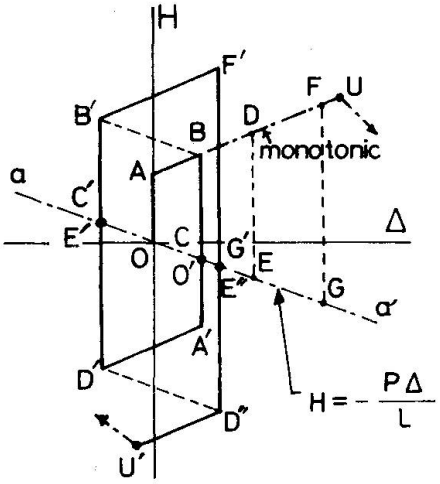

Fig.8 Construction of Cyclic Curve from Monotonic Curve of a Beam-Column

4.3. Frame

Examples of typical frame behavior subject to cyclic lateral loading are shown schematically in Fig.9*.
The behavior of frames which carry substantial vertical load is basically similar to that of beam-column, but the shape of loop varies with material property and loading condition. After attainment of full plastic moment,capacity of the member section increases further due to the strain-hardening of the material,so is the load carrying capacity of the member if it does not carry the axial compression. When this increasing rate overcomes the reducing rate due to P-Δ effect,slope in inelastic region is positive and the loop expands for every additional cycle(a1). When the increasing rate is smaller than the reducing rate due to P-Δ effect,slope in inelastic region is negative but the loop expands(a2). When there is no strain-hardening of the material,member shows elastic perfectly plastic behavior. In this case,slope is negative and the loop closes(a3). Finally when the moment capacity decreases in plastic region by local buckling or by some other causes,the slope is negative and loop diminishes(a4). The behavior of frames which carry very small vertical loads or no vertical loads is similar to that of beam,which is shown in (b) of this figure.

5.COMPARISON WITH TEST RESULTS

Available test results are compared with the prediction by the method described in the foregoing chapters in Fig.10. Except for the elastic-plastic transitive parts,for which Baushinger effect plays prominent role,theoretical predictions show satisfactory agreement with test results. Introduction of Baushinger effect and thus the modification of the curve must be made reflecting the knowledge obtained from the experimental investigation.

* · compare with Fig.21 of "Experimental Studies concerning Steel Structure,their Elements and Connections", Introductory Report of this Symposium (p.56),which seems to be incorrect.

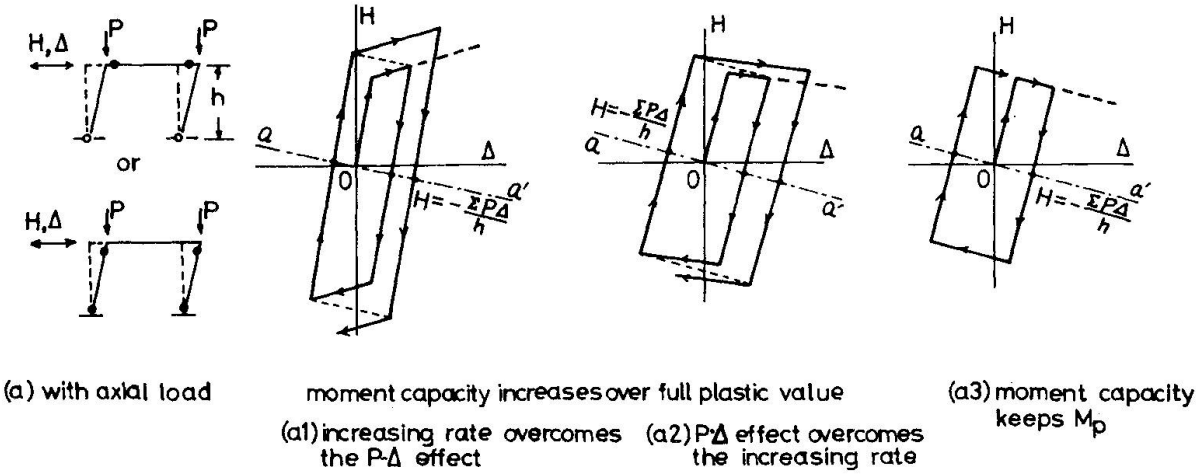

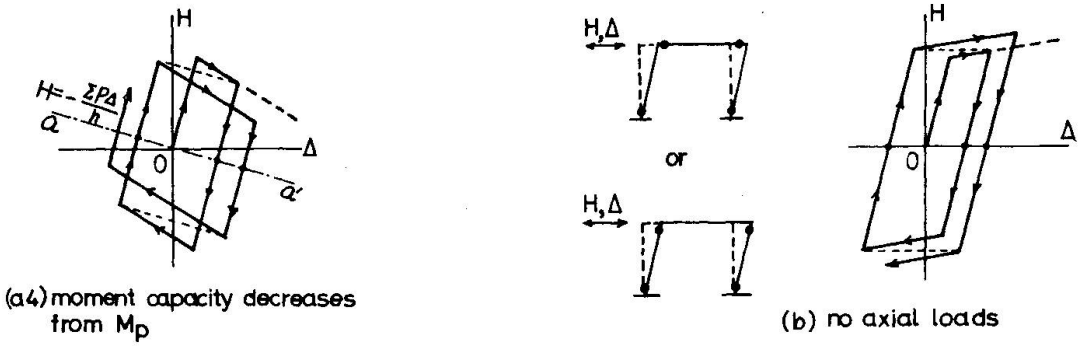

Fig.9 Various Types of Cyclic Behavior of Steel Frames

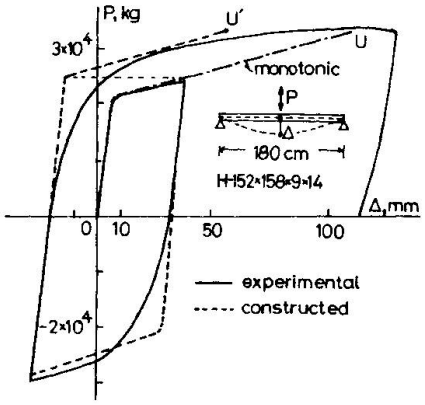

10.1 Beam(5)

Fig.10 Correlation between Test Results and Theoretical Predictions

Beam	
Beam-Column	Frame

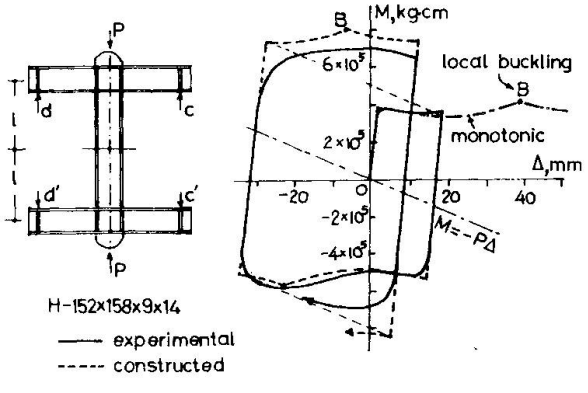

10.2 Beam-Column(3)

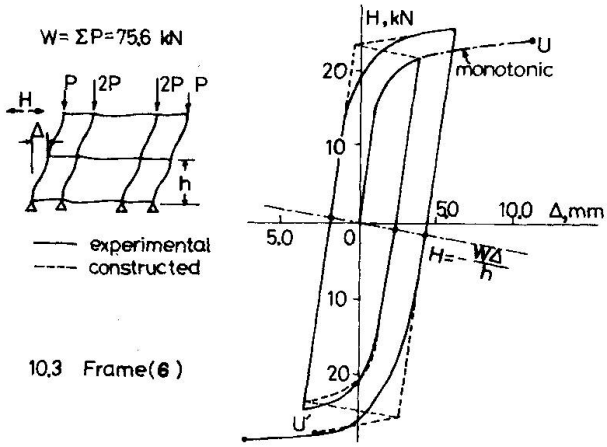

10.3 Frame(6)

6. CONCLUSION

1. Load-deflexion curves of steel members and frames subject to repeated and reversed loading have the property that the loop expands for every additional cycle provided that all kinds of buckling are properly prevented.
2. This phenomenon of expansion is associated with the property of strain-hardening of steel material and/or P-Δ effect of the structural system.
3. The cyclic behavior can be predicted theoretically from the monotonic loading curve if the loading conditions are well defined.
4. Baushinger effect is not taken into account in this theory. Introduction of Baushinger effect and thus the modification of the curve must be made reflecting the knowledge obtained from the experimental investigation.

7. REFERENCES

1. Kato,B.,Aoki,H. and Yamanouchi,H., Experimental Study on Structural Steel Subjected to Tensile and Compressive Cyclic Loads,Proc. of the 14th Japan Congress on Material Research,Japan Society of Material Science,May,1971.
2. Akiyama,H.,Yamanouchi,H. and Kato,B., Predictable Properties of Material under Incremental Cyclic Loading. Theme III,IABSE Symposium on Resistance and Ultimate Deformability of Structures acted on by well Defined Repeated Load, Lisboa,1973.
3. Kato,B. and Akiyama,H., Inelastic Bar Subjected to Thrust and Cyclic Bending, Proc.ASCE,ST1,January,1969.
4. Nishimura,S., Plastic Analysis of Plane Steel Frames, Dr.Eng.Thesis,University of Tokyo,Dec.1972(in Japanese).
5. Akiyama,H., Ultimate Strength of Steel Frames, Dr.Eng.Thesis,University of Tokyo,May,1967(in Japanese).
6. Kato,B.,Akiyama,H. and Nishimura,S., The Inelastic Behavior of the Steel Frame Subjected to the Horizontal Force,Proc. of The Symposium on Ultimate Strength of Structures and Their Components,16th National Symposium of IABSE,Japan Soc. for Promotion of Science,September,1971.

SUMMARY

Inelastic behavior of steel members and frames subject to repeated and reversed loading was analysed, and a technique to construct the load-deflexion relationship for cyclic loading directly from that for the monotonic loading condition was presented. The correlation between this theoretical prediction and the test results were shown to be satisfactory.

RESUME

On analyse dans ce rapport le comportement inélastique d'éléments et de cadres en acier soumis à des charges répétées et alternées et on présente une méthode permettant de déterminer la relation charge-déformation pour des charges cycliques directement à partir de celle obtenue pour des charges monotones. La concordance entre les résultats théoriques et les résultats des essais est satisfaisante.

ZUSAMMENFASSUNG

Das inelastische Verhalten von Stahlstäben und Rahmen unter wiederholter und wechselseitiger Belastung wurde untersucht und eine Methode zum Aufzeichnen der Last-Ausbiegungs-Abhängigkeit für zyklische Belastung, direkt ausgehend von der einseitigen, konstanten Belastung, angegeben. Es wurde gezeigt, dass der Unterschied zwischen dieser theoretischen Voraussage und den Versuchsresultaten innerhalb befriedigender Grenzen liegt.

I

Non-linear Analysis for K-Type Braced Steel Frames

Analyse non-linéaire des cadres en acier à structure en K

Nichtlineare Berechnung von Stahlrahmen mit K-Ausfachung

Akira WADA
Staff
Computer Division
Nikken Sekkei Ltd.

Fukuzo SUTO
Dr. Eng., Chief
Computer Division
Nikken Sekkei Ltd.
Japan

Morihisa FUJIMOTO
Dr. Eng., Professor
Tokyo Institute
of Technology

1. Introduction.

The architectural and civil engineering construction in Japan must be built up in the natural environments under frequently experienced great earthquakes and typhoons that visit our country at random or in autumn every year. Particularly in high storied buildings, since they are subjected to large repeated horizontal forces due to the earthquake and wind, there are several occasions that braces are set into frames as the structural elements against the external forces. (See Fig. 1)

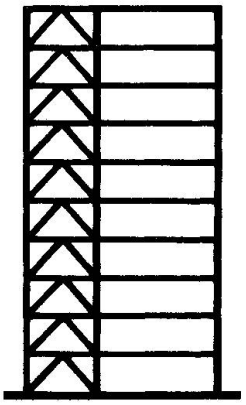

Fig.1 K-type braced frames

Since, however, the brace bears a large axial force, it is needed to secure the rigidity and ultimate strength, so that a large cross-sectional members must be used. As a result the slenderness ratio (L/r) becomes comparatively small in the order of 30~70, and consequently a brace on the compression side is apt to break down by plastic buckling.

In order to clarify the mechanical behavior of a structure having such characteristics analytically, this paper deals with a nonlinear analysis taking consideration of the nonlinearity due to the yield of materials and the nonlinearity based on the finite deformation theory unable to be neglected in the analysis of buckling, and thereby performs the analysis as mentioned below.

For the purpose, the behavior of compressive members with different slenderness ratio was first analyzed for repeated loadings, and after making various checkings of the results (omitted in this paper), the analysis of the behavior of 1 story 1 span frame provided with K-type braced as shown in Fig. 9 is made for the case in which a repeated horizontal force is applied.

Following is a review of selected recent studies conducted in our country on this topic. Yamada, Tsuji, and Takeda and Wakabayasi, Nonaka, Ogi, and Yamamoto studied the behavior of braces being subjected to repeated axial forces in the elasto-plastic range by using a small experimental model. On the other hand, Matsui, Mitani, and Tsumatori have studied the behavior of braces with various slenderness ratios in the state of buckling towards collapse state, taking propagation of plastic region in axial direction of material into consideration and using a numerical analysis of C-D-C method.

However, no exact analysis of braced frames has been reported yet , because it is extremely difficult to analyze the elasto-plastic behavior under the condition of repeated loading accompanied by such an instability phenomenon as buckling of braces.

2. Several assumptions taken for this analysis.

a. The residual stress and the deflection in the initial period due to welding etc. are not taken into account.

b. The member is assumed to be of such type that the beam theory is applicable. But, in order to approximate the curves of each member after deformation, the member is divided into 5~15 elements (Fig. 2 & 9).

c. In each element, only the bending deformation and the axial deformation is considered and the shearing deformation is neglected. As a result, the displacement functions used in this analysis are expressed by Eq. (1) (See Fig. 2).

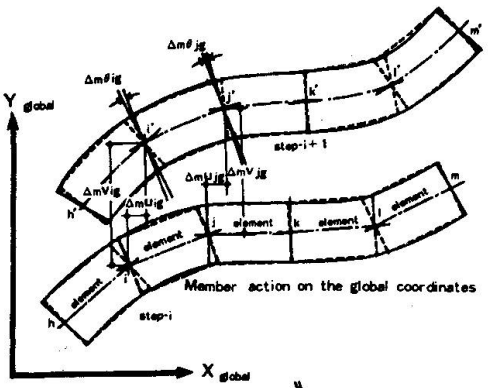

$$\begin{Bmatrix} \triangle u \\ \triangle v \\ \triangle \theta \end{Bmatrix} = \begin{bmatrix} 1 & x & 0 & 0 & 0 & 0 \\ 0 & 0 & 1 & x & x^2 & x^3 \\ 0 & 0 & 0 & 1 & 2x & 3x^2 \end{bmatrix} \cdot m\alpha \quad \ldots\ldots (1)$$

$$\text{where} \quad m\alpha = \{ m\alpha_1\ m\alpha_2\ m\alpha_3\ m\alpha_4\ m\alpha_5\ m\alpha_6 \}^T \quad \ldots\ldots (2)$$

The relation between incremental displacement $\triangle mu$ and $m\alpha$ of element m is expressed by Eq. (3) by substituting coordinates $x=\pm c/2$ at both ends i and j of the element into Eq. (1). (c : length of element)

$$\triangle mu = mT \cdot m\alpha \qquad \text{namely,}\ m\alpha = mT^{-1} \cdot \triangle mu \quad \ldots (3)$$

$$\text{where} \quad \triangle mu = \{ \triangle mu_i\ \triangle mv_i\ \triangle m\theta_i\ \triangle mu_j\ \triangle mv_j\ \triangle m\theta_j \}^T \quad \ldots\ldots (4)$$

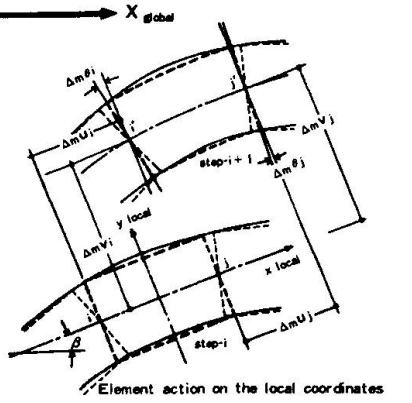

Fig. 2 Deformation & coordinates

d. The strain ($\triangle \epsilon_x$) in the element can be expressed by Eq. (5), taking a large deformation into consideration and using the assumption that its cross section remains plane after deformation;

$$\triangle \epsilon_x = \frac{d\triangle u}{dx} + \frac{1}{2}\left(\frac{d\triangle v}{dx}\right)^2 - \left(\frac{d^2\triangle v}{dx^2}\right) y \qquad \ldots\ldots (5)$$

Derivatives of $\frac{d\triangle u}{dx}$, $\frac{d\triangle v}{dx}$ and $\frac{d^2\triangle v}{dx^2}$ in Eq. (5) can be obtained by differentiating displacement function Eq. (1).

e. Following the assumptions c & d, only ϵ_x and σ_x are considered in each element, and yielding occurs according to their magnitude.

f. As for the stress-strain relation of material, a hysteresis loop which is shown in Fig. 3 is used, considering the strain-hardening and the Bauschinger-effect.

g. The distribution of stress intensity and strain in the cross section are considered by dividing the cross section into 20 layers as shown in Fig. 4, and the values of stress and strain in each layer are considered by the values at the each center of gravity.

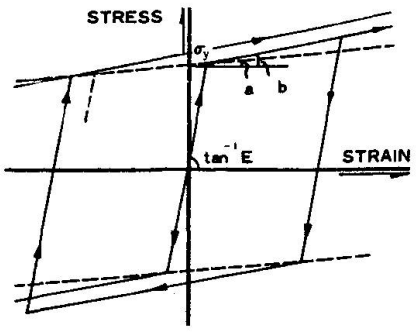

Fig. 3 Relation of stress-strain

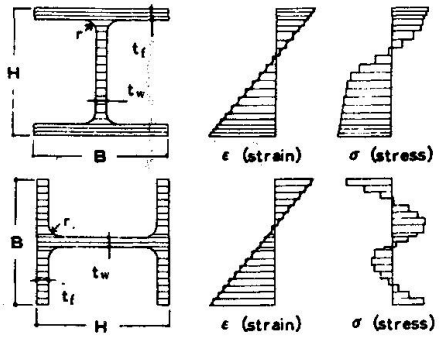

Fig. 4 Distribution of stress & strain

3. Nonlinear analysis based on the stationary principle of potential energy.

The strain energy $_mU$ which is stored in the element m by incremental displacements can be developed as follows,

$$ {}_mU = {}_mU_1 + {}_mU_2 \qquad \cdots\cdots\cdots\cdots\cdots (6) $$

where

$$ {}_mU_1 = \iiint_V \sigma_x \cdot \Delta\epsilon_x \, dx\,dy\,dz $$

$$ = \int_C \int_A \sigma_x \left\{ \frac{d\Delta u}{dx} + \frac{1}{2} \left(\frac{d\Delta v}{dx}\right)^2 - \frac{d^2\Delta v}{dx^2} y \right\} dA\,dx $$

$$ = {}_m\alpha^T \, {}_ma_1 + \frac{1}{2} {}_m\alpha^T {}_mA_1 \, {}_m\alpha - {}_m\alpha^T \, {}_ma_2 \qquad \cdots\cdots\cdots\cdots\cdots (7) $$

$$ {}_mU_2 = \iiint_V \frac{1}{2} E (\Delta\epsilon_x)^2 \, dx\,dy\,dz $$

$$ = \int_C \int_A \frac{1}{2} E \left\{ \frac{d\Delta u}{dx} - \frac{d^2\Delta v}{dx^2} \right\}^2 dA\,dx $$

$$ = \frac{1}{2} {}_m\alpha^T {}_mA_2 \, {}_m\alpha - \frac{1}{2} {}_m\alpha^T {}_mA_3 \, {}_m\alpha + \frac{1}{2} {}_m\alpha^T {}_mA_4 \, {}_m\alpha \qquad \cdots\cdots\cdots (8) $$

(herein, term $\frac{1}{2}\left(\frac{d\Delta v}{dx}\right)^2$ in $_mU_2$ is dropped because it is considered negligible.)

Symbols of $_ma_1$, $_ma_2$, and $_mA_1 \sim {}_mA_4$ in Eq. (7) and Eq. (8) are vectors and matrices given as follows;

$$ {}_ma_1 = \int_c \left(\int_A \sigma_x dA\right) \begin{Bmatrix} 0 \\ 1 \\ 0 \\ 0 \\ 0 \\ 0 \end{Bmatrix} dx \quad \cdots\cdots (9) \qquad {}_ma_2 = \int_c \left(\int_A \sigma_x \cdot y dA\right) \begin{Bmatrix} 0 \\ 0 \\ 0 \\ 0 \\ 2 \\ 6x \end{Bmatrix} dx \quad \cdots\cdots\cdots\cdots (10) $$

$$ {}_mA_1 = \int_c \left(\int_A \sigma_x dA\right) \begin{bmatrix} 0 & 0 & 0 & 0 & 0 & 0 \\ 0 & 0 & 0 & 0 & 0 & 0 \\ 0 & 0 & 0 & 0 & 0 & 0 \\ 0 & 0 & 0 & 1 & 2x & 3x^2 \\ 0 & 0 & 0 & 2x & 4x^2 & 6x^3 \\ 0 & 0 & 0 & 3x^2 & 6x^3 & 9x^4 \end{bmatrix} dx, \quad \cdots (11) $$

$$ {}_mA_2 = \int_c \left(\int_A E dA\right) \begin{bmatrix} 0 & 0 & 0 & 0 & 0 & 0 \\ 0 & 1 & 0 & 0 & 0 & 0 \\ 0 & 0 & 0 & 0 & 0 & 0 \\ 0 & 0 & 0 & 0 & 0 & 0 \\ 0 & 0 & 0 & 0 & 0 & 0 \\ 0 & 0 & 0 & 0 & 0 & 0 \end{bmatrix} dx \quad \cdots (12) $$

$$ {}_mA_3 = \int_c \left(\int_A E \cdot y dA\right) \begin{bmatrix} 0 & 0 & 0 & 0 & 0 & 0 \\ 0 & 0 & 0 & 0 & 2 & 6x \\ 0 & 0 & 0 & 0 & 0 & 0 \\ 0 & 0 & 0 & 0 & 0 & 0 \\ 0 & 2 & 0 & 0 & 0 & 0 \\ 0 & 6x & 0 & 0 & 0 & 0 \end{bmatrix} dx, \quad \cdots (13) $$

$$ {}_mA_4 = \int_c \left(\int_A E \cdot y^2 dA\right) \begin{bmatrix} 0 & 0 & 0 & 0 & 0 & 0 \\ 0 & 0 & 0 & 0 & 0 & 0 \\ 0 & 0 & 0 & 0 & 0 & 0 \\ 0 & 0 & 0 & 0 & 0 & 0 \\ 0 & 0 & 0 & 0 & 4 & 12x \\ 0 & 0 & 0 & 0 & 12x & 36x^2 \end{bmatrix} dx \quad \cdots (14) $$

Equations from (9) to (14) include $\int_A \sigma_x dA$, $\int \sigma_x \cdot y dA$, $\int E dA$, $\int E \cdot y dA$ and $\int E \cdot y^2 dA$ which are calculated on the both ends of divided elements according to the method which is described in the assumption (g) and are integrated inside of the elements assuming linear change in the respective axial directions of them. Here at the point situated in plastic region which σ_x is beyond the yield point, E is set as Est in the calculation.

After carrying out calculation mentioned above, the strain energy stored in an element due to incremental displacement is given in Eq. (15).

$$ {}_mU = {}_m\alpha^T ({}_ma_1 - {}_ma_2) + {}_m\alpha^T ({}_mA_1 + {}_mA_2 - {}_mA_3 + {}_mA_4) \, {}_m\alpha $$

$$ = \Delta {}_mu^T \, {}_mT^{-1T} ({}_ma_1 - {}_ma_2) + \Delta {}_mu^T \, {}_mT^{-1T} ({}_mA_1 + {}_mA_2 - {}_mA_3 + {}_mA_4) \, {}_mT^{-1} \Delta {}_mu $$

$$ = \Delta {}_mu^T \, {}_mf_{in} + \frac{1}{2} \Delta {}_mu^T \, {}_mK \Delta {}_mu \qquad \cdots\cdots\cdots\cdots\cdots\cdots\cdots\cdots\cdots\cdots\cdots\cdots\cdots (15) $$

The potential energy of Π_{i+1} for the whole structure in $(i+1)$ state is shown Eq. (17) by summing up strain energies of all elements and works done by external forces. The displacement components of all elements must be transformed into a global coordinate system using Eq. (16). (See Fig. 2)

$$\triangle m u_g = L \triangle m u \qquad \text{namely, } \triangle m u = L^{-1} \triangle m u_g \qquad \ldots\ldots (16)$$

where $\triangle m u_g$: incremental displacement vector of element m in global coordinate.

$$\Pi_{i+1} = \Pi_i + \frac{1}{2} \triangle u_g^T K \triangle u_g + \triangle u_g^T f_{in} - \triangle u_g^T f_{ex} \qquad \ldots\ldots (17)$$

where $K = \sum_m m L^{-1T}_m K_m L^{-1}$

$$f_{in} = \sum_m m L^{-1T}_m f_{in}$$

As the potential energy is stationary in the equilibrium condition, $\triangle u_g$ can be obtained by the variational principle. Namely, $\delta\Pi_{i+1}=0$ for any arbitrary $\delta\triangle u_g$ results in the following equation.

$$K \triangle u_g + f_{in} - f_{ex} = 0 \qquad \ldots\ldots (18)$$

Vector $\triangle u_g$ is obtained by solving the simultaneous equation given in Eq. (18). The coordinate of each joint-point can be adjusted using $\triangle u_g$.

The calculation of one step is completed when incremental strain $\triangle \epsilon_x$ is obtained by Eq. (5) and with it the strain and stress at both ends of each element are adjusted.

The planned analysis is made possible by accumulating the calculation described above by the step-by-step method and iterating technique.

The flow chart of this numerical analysis is shown in Fig. 5.

4. The elasto-plastic behavior of braced steel frames.

4-1) Objects of analysis.

The elasto-plastic behaviors of braced steel frames are analyzed numerically and compared with the experimental results, assuming the condition under which a K-type braced steel frame is subjected to repeated horizontal forces as shown in Fig. 9.

The divided state of elements is shown in Fig. 9, and it is taken into consideration such effects that a large deformation could occur and complicated distribution of deformation in plastic region could be followed.

Further, behaviors under repeated loading are studied by increasing or decreasing displacements of loading-point in a stepwise method to the ultimate state. In order to compare with the experimental results the following values of yield-stress of steel members are used for the calculation.

column and beam: (H-194x150x6x9) σ_y=3.04ton/cm^2
brace: (H-100x100x6x8) σ_y=2.86ton/cm^2

4-2) The results of the analysis and discussions.

Fig. 6 shows the relation between horizontal external force and horizontal deformation. This figure shows that the overall behavior agrees sufficiently well with the experimental result except scattered differences. As for the largest load the analytical result gives a little larger value than the experimental result. This is probably due to incompleteness of the test specimen, namely the influence of initial deformation and residual stress.

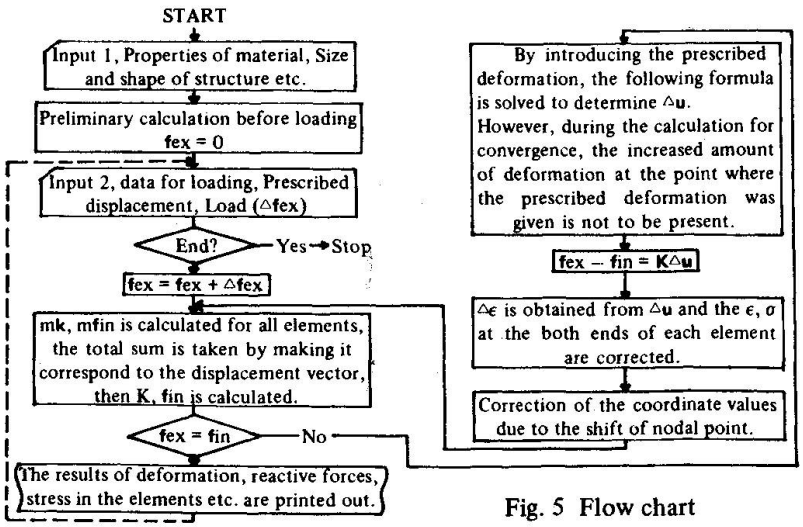

Fig. 5 Flow chart

The decrease of load after maximum loading (post-buckling of brace) is attained more suddenly in the analytical result than in the experimental result. The reason for this is that the analysis is made for the model which is replaced by beams with lengths which are spanning between nodal points, in other words, that some larger slenderness ratio is estimated in the analysis than in the test specimen.

Fig. 7 shows corresponding deformations to the state marked with heavy dots in Fig. 6. The scale of the deformation-figure is half of that of the model. The comparison of the final deformation form with Fig. 10 shows that they both are of very similar pattern. Fig. 8 shows the change of the yielded area until buckling is first observed on the brace of compressed side and also how yielded places occur as the deformation mode of braces changes.

5. Conclusion.

The numerical analysis of elasto-plastic behaviors of braced steel frames which are subjected to repeated horizontal forces and its comparison with experimental results has ascertained usefulness of this analytical method. It can be thought that this method of analysis generally makes it possible to analyze the elasto-plastic behaviors accompanied by instability phenomena, which hitherto was considered to be difficult, and also possible to acquire the distribution of stress inside of members, which is difficult to obtain from experiments.

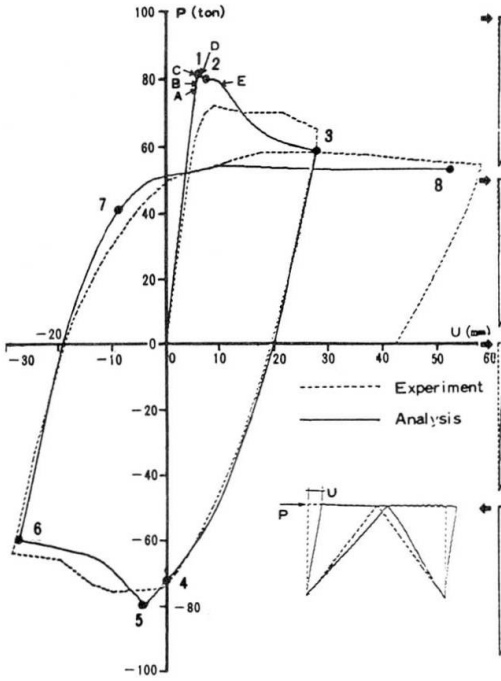

Fig. 6 Relation of load-deflection

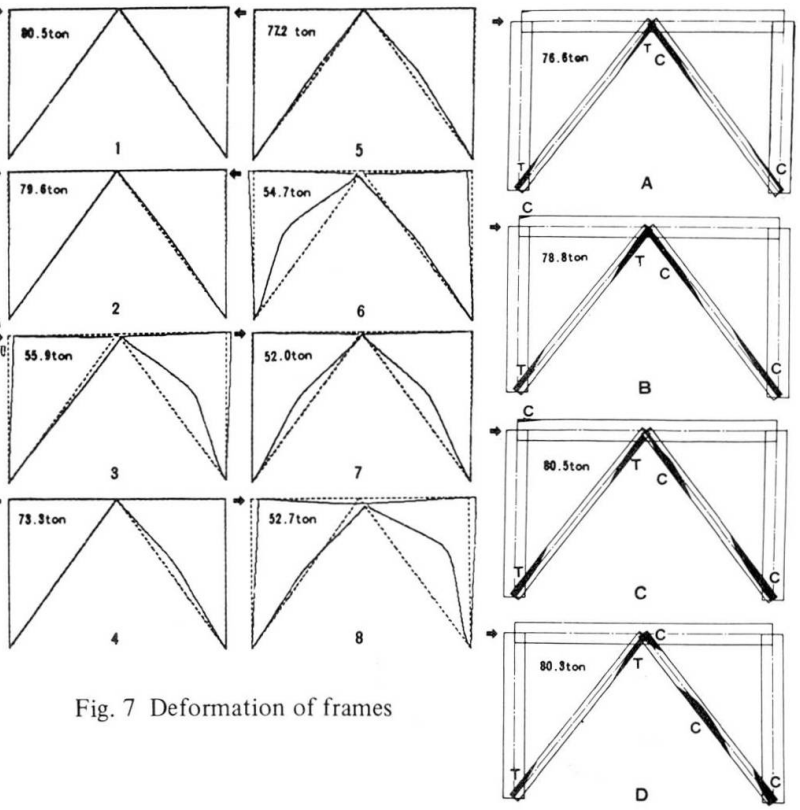

Fig. 7 Deformation of frames

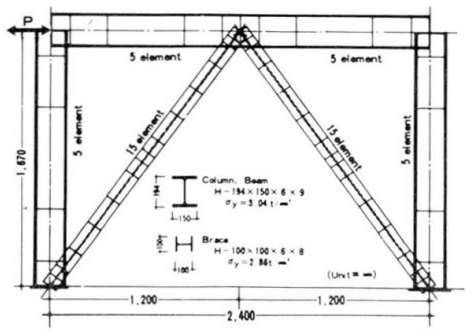

Fig. 9 Idealized model for the analysis

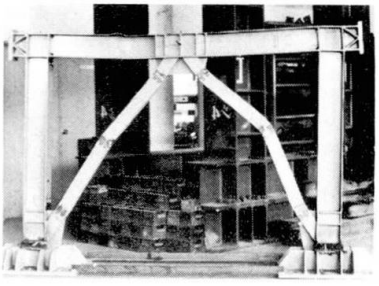

Fig. 10 Specimen after experiment

Fig. 8
Spread of pastic zones

6. Acknowledgement.

We would like to express our gratitude to Dr. Eng. H. HOKUGO and Mr. K. MORIYA of Nippon Telegraph and Telephone Public Corporation for providing with experimental data, enabling us to proceed in this study. We also wish to thank Mr. K. SHIRAKATA and Mr. R. KOSUGI, who were under graduate course of master of the Tokyo Institute of Technology when this research was being carried out.

7. Bibliography

a. "The Introductory Report of IABSE Symposium 1973" autumn, 1972.

b. Fujimoto, M., Hokugo, H., Hashimoto, A., Moriya, K.,: "Study on elasto-plastic behabior of braced rigid steel frame subjected to alternately repeated horizontal load. (No. 4) Trans. of Annual Meeting of A.I.J. Oct. 1972.

c. Igarashi, S., Inoue, K., Kibayashi, M., Asano, M.:"Hysteretic characteristics of steel braced frames", Trans. of A.I.J. June, 1972.

d. M.J. Turner, E.H. Dill, H.C. Martin, R.J. Melosh: "Large deflections of structures subjected to heating and external loads", A.I.A.A. Feb. 1960.

SUMMARY

This paper deals with a nonlinear analysis of K-type braced steel frames taking consideration of both the nonlinearity due to the yield of materials and the nonlinearity based on the finite deformation theory unable to be neglected in the analysis of instability problems.

RESUME

Ce rapport traite l'analyse élasto-plastique des cadres en acier avec contreventement en K en considérant la non-linéarité due au fluage du matériau et celle basée sur la théorie des déformations finies qui ne peut être négligée dans les problèmes d'instabilité.

ZUSAMMENFASSUNG

Dieser Bericht befasst sich mit einer numerischen Untersuchung des elasto-plastischen Knickproblems in der Fachwerkebene von K-Fachwerkständern aus Stahl unter der Einwirkung statisch wechselseitig wiederholter Horizontalkraft nach der Theorie endlich grosser Verschiebungen, nebst Vergleich mit den Versuchsergebnissen.

Traglasten von Stahlrahmen bei nicht-proportionaler Belastung

Ultimate Load of Steel Frames under Non-Proportional Loading

Charges limites des ossatures métalliques en cas de chargements non-proportionnels

K. BURTH
Dr.-Ing.
Ass.-Prof. an der

U. VOGEL
Dr.-Ing.
o. Prof. an der

Technischen Universität Berlin
BRD

Einleitung

Im Abschnitt 5.3 des Einführungsberichtes zum Thema I stellt R. PARK fest, daß bisher nur wenige Untersuchungen über das theoretisch zu erwartende Last-Verformungs-Verhalten von Stahlrahmen bei nicht-proportionaler Belastung vorliegen. Im folgenden wird versucht, einen Teil dieser Lücke zu schließen.

Bei den meisten bisher bekannten Näherungsverfahren und genaueren Methoden zur Berechnung der Traglasten von Stahlrahmen wird davon ausgegangen, daß diejenigen Lasten, die zu der für die Traglast ungünstigsten Lastkombinationen gehören, in einem festen Verhältnis zueinander gesteigert werden. Diese Voraussetzung wird auch dann beibehalten, wenn die Belastung des Tragwerkes aus mehreren Lasten verschiedenen Ursprungs besteht, obwohl sie in diesem Fall tatsächlich fast nie erfüllt wird. Um die tatsächlichen Verhältnisse besser kennenzulernen, wurde das Last-Verformungs-Verhalten von Stahlrahmen bei nicht-proportionaler, einsinniger Laststeigerung anhand von zwei Beispielen untersucht.

Ziel der Untersuchung

Es soll festgestellt werden, wie sich bei nicht-proportionaler Belastung die für die Bemessung verwendbaren charakteristischen Lasten und die Endverformungen des Tragwerks gegenüber den Werten bei proportionaler Belastung ändern. Diese charakteristischen Lasten sind

- die elastische Grenzlast (Fließbeginn, näherungsweise durch die Bildung des ersten Fließgelenks erfaßt)
- die Traglast (höchste bei stabilem Gleichgewicht gerade noch aufnehmbare Last) und die
- plastische Grenzlast (Last bei der Ausbildung des Fließgelenkmechanismus).

Entsprechend dem üblichen Vorgehen sollen auch bei der nicht-proportionalen Belastung die unabhängig voneinander aufgebrachten Lastanteile diejenigen Grenzen nicht überschreiten, die sich aus den Endwerten der Lastanteile beim Erreichen der Traglast unter proportionaler Belastung ergeben. Innerhalb dieser Schranken wird die Belastung in beliebiger Folge, aber einsinnig bis zum Erreichen der Traglast gesteigert, daß heißt, es wird keine Abminderung der unabhängigen Lastanteile zugelassen. Diese Voraussetzung ist natürlich nur dann von Bedeutung, wenn nicht-elastische Verformungen auftreten.

Für diese Untersuchung muß der Einfluß der Verformungen auf das Kräftegleichgewicht berücksichtigt werden (Theorie 2. Ordnung), denn ohne Berücksichtigung der Verformungen (Theorie 1. Ordnung) ist die Traglast immer identisch mit der plastischen Grenzlast und unabhängig von der Belastungsfolge.

Untersuchungsbeispiele und Berechnungsverfahren

Als Beispiele wurden zwei rechteckige Portalrahmen mit eingespannten Stielfüssen gewählt, die durch vertikale und horizontale Lasten verschiedenen Ursprungs beansprucht sind. Die Abmessungen und Belastungen der Rahmen sind aus den Bildern 1 und 3 ersichtlich, die Querschnittsabmessungen sind:

Stiele: $I = 1150\ cm^4$, $F = 43\ cm^2$; Riegel: $I = 5790\ cm^4$, $F = 46\ cm^2$.

Es wurde Baustahl St 37 mit der Streckgrenze $\sigma_F = 2{,}4\ Mp/cm^2$ zugrunde gelegt.

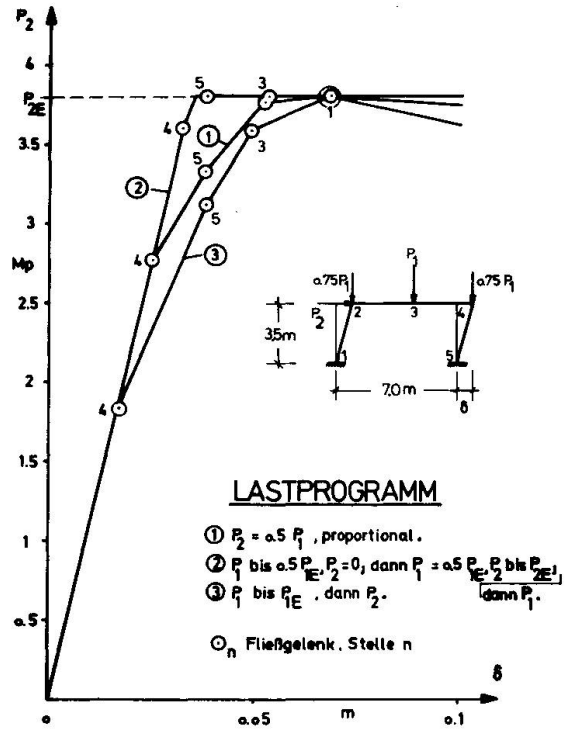

BILD 1: LAST-VERFORMUNGS-DIAGRAMM „STEIFER" RAHMEN 1

Der erste Rahmen (Bild 1) ist relativ "steif" (kurze Stiele, geringe Stiel-Normalkräfte) der zweite (Bild 3) relativ "weich" (lange Stiele, hohe Stiel-Normalkräfte). Das Last-Verformungs-Verhalten dieser Rahmen wurde für verschiedene Belastungsprogramme nach der Theorie 2. Ordnung unter Voraussetzung der Fließgelenkhypothese (elastisch-idealplastische Momenten-Krümmungs-Beziehung) mit einem Verfahren nach der Deformationsmethode berechnet. Hierbei wurden auch die Längenänderungen der Stiele und das Entlastungsgesetz bei Rückdrehung der Fließgelenke entgegen der ursprünglich vorhandenen Verdrehungsrichtung berücksichtigt. Das Berechnungsverfahren ist in [1], [2], das dazu gehörende Programmsystem in [2] im Einzelnen beschrieben.

Ergebnisse für proportionale Belastung

Die Ergebnisse werden einmal in der üblichen Form von Last-Verformungs-Linien dargestellt, zum anderen als Punkte und Linienzüge in der Lastebene ähnlich den bekannten Interaktionsdiagrammen für die Schnittlasten. Diese zweite Darstellung ist der Sonderfall n = 2 der Darstellung einer von n Parametern abhängigen Belastung im n-dimensionalen Lastraum. Jede Lastkombination wird in dieser Lastebene eindeutig als ein Punkt abgebildet, jedes Lastprogramm als ein Linienzug.

In den Bildern 2 und 4 sind zur Orientierung die Grenzlasten nach der Theorie 1. Ordnung gestrichelt eingetragen, soweit sie von den entsprechenden Lasten nach der Theorie 2. Ordnung (ausgezogene Linien) abweichen. Zusätzlich ist am Linienzug der plastischen Grenzlast der zu den einzelnen Abschnitten gehörige Mechanismus skizziert. Diese nach der Theorie 1. Ordnung ermittelten Linien begrenzen im Quadranten $P_1 \geq 0$, $P_2 \geq 0$ zwei Bereiche: Die äußere Linie der plastischen Grenzlast begrenzt nach dem Einzigkeitssatz der Traglasttheorie den Bereich, in dem überhaupt nur Gleichgewicht

möglich ist. Innerhalb dieses Bereiches begrenzt die Linie der elastischen Grenzlast (hier näherungsweise durch die Bildung des

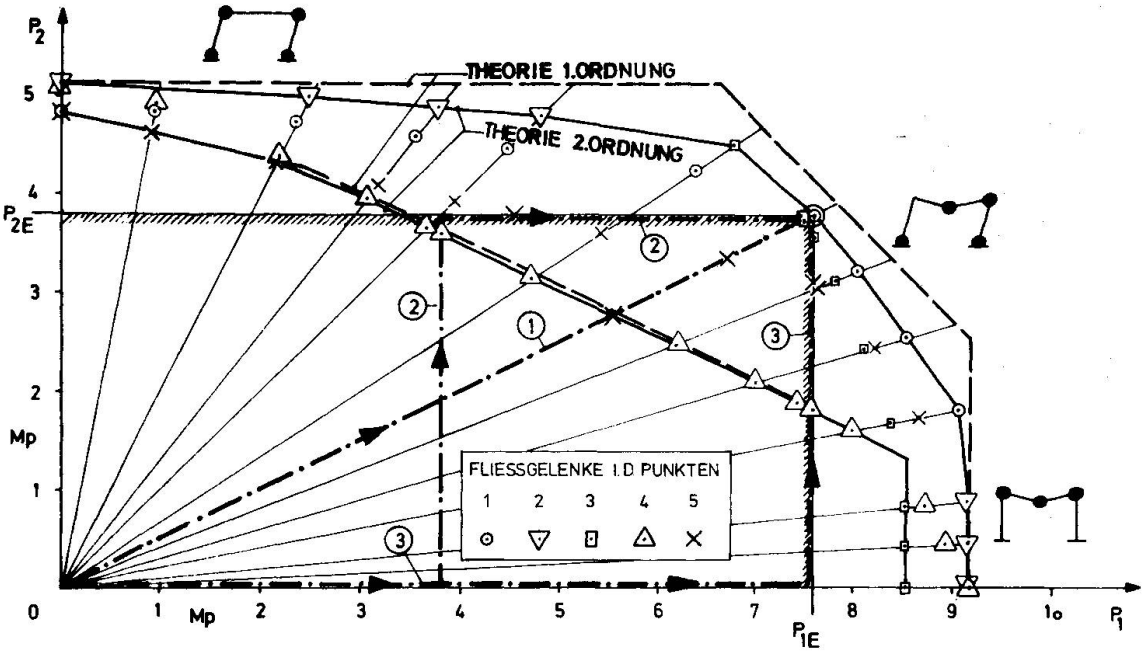

BILD 2: LASTWEGE UND GRENZLINIEN IN DER LASTEBENE, „STEIFER" RAHMEN 1

ersten Fließgelenks erfaßt) den Bereich, in dem bei der ersten Belastung nur elastische Verformungen auftreten. Bei Anwendung der Theorie 2. Ordnung ergeben sich zwei andere Linienzüge, die nur punktweise für verschiedene Lastverhältnisse bei proportionaler Belastung berechnet wurden. Der innere Linienzug der elastischen Grenzlast begrenzt wieder den Bereich, in dem bei der ersten Belastung nur elastische Verformungen auftreten. Für den vom äußeren Linienzug der Traglast begrenzten Bereich kann nur ausgesagt werden, daß er alle bei proportionaler Belastung erreichbaren stabilen Gleichgewichtszustände enthält.

Der Vergleich der Grenzlinien nach der Theorie 1. Ordnung und nach der Theorie 2. Ordnung zeigt in dieser Darstellungsweise deutlich, daß weniger die elastische Grenzlast, sondern vielmehr die plastische Grenzlast von den Verformungen des Systems beeinflußt wird. Weiterhin zeigt Bild 2, daß die nach Theorie 1. Ordnung ermittelten Mechanismen nicht immer mit den nach der Theorie 2. Ordnung bestimmten übereinstimmen. Die Auszählung der Fließgelenke in Bild 4 zeigt, daß die Tragfähigkeit des "weichen" Rahmens 2 bei Anwendung der Theorie 2. Ordnung weitgehend nicht mehr durch die Ausbildung eines Mechanismus, sondern durch Erreichen der Traglast begrenzt wird.

Ergebnisse für verschiedene Belastungsprogramme

Als Endwert für die Lasten P_1, P_2 wurden die bei einer bestimmten proportionalen Belastung und stabilem Gleichgewicht gerade noch aufnehmbaren Lasten gewählt. Bei dem "steifen" Rahmen 1 ist diese Lastgrenze z.B. für $P_2 = 0{,}5\ P_1$ die plastische Grenzlast, bei dem "weichen" Rahmen 2 z.B. für $P_2 = 0{,}3\ P_1$ die Traglast. Die Belastung wurde nun innerhalb der so festgelegten Lastgrenzen P_{1E},

P_{2E}, die in den Bildern 2 und 4 durch Schraffur hervorgehoben sind, auf verschiedenen Wegen gesteigert. Bleibende Verformungen der

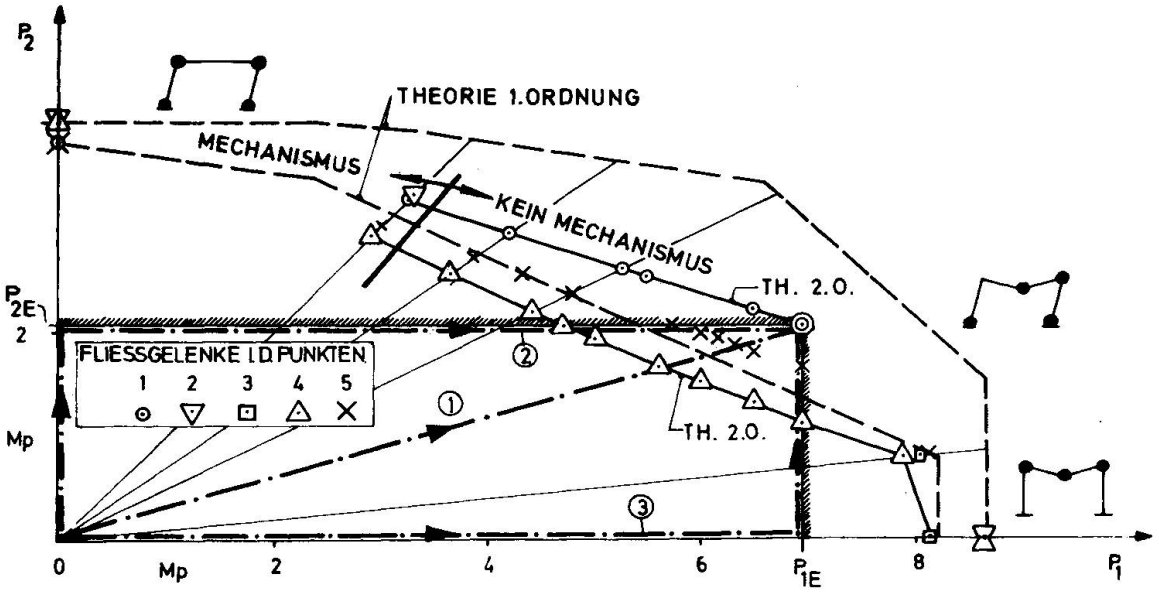

BILD 4: LASTWEGE UND GRENZLINIEN, „WEICHER" RAHMEN 2

Rahmen können nur in der rechten oberen Ecke des Bereichs, in dem durch die Linie der elastischen Grenzlast abgegrenzten Teilbereich auftreten. Für drei verschiedene, exemplarisch ausgewählte Lastwege ①, ②, ③ (strichpunktiert in den Bildern 2 und 4), die im wesentlichen die Grenzen des zugelassenen Lastbereichs erfassen, ergibt sich folgendes:

1. Bei einsinniger Laststeigerung bis zur Traglast sind keine Entlastungen aufgetreten.
2. Bei allen Belastungsprogrammen wird dieselbe Traglast erreicht (Bild 2, 4). Für den steifen Rahmen ist wegen der Voraussetzung der Fließgelenkhypothese die Traglast identisch mit der plastischen Grenzlast (Bild 1). Aus der Unabhängigkeit der Traglasten von der Belastungsfolge ist wegen der Beliebigkeit des gewählten Lastpunktes P_{1E}, P_{2E} zu schließen, daß die nur punktweise bei proportionaler Belastung berechnete Linie der Traglast in Bild 4 den Bereich der überhaupt möglichen Gleichgewichtslagen begrenzt. Sie entspricht insofern der Linie der plastischen Grenzlast nach der Theorie 1. Ordnung.

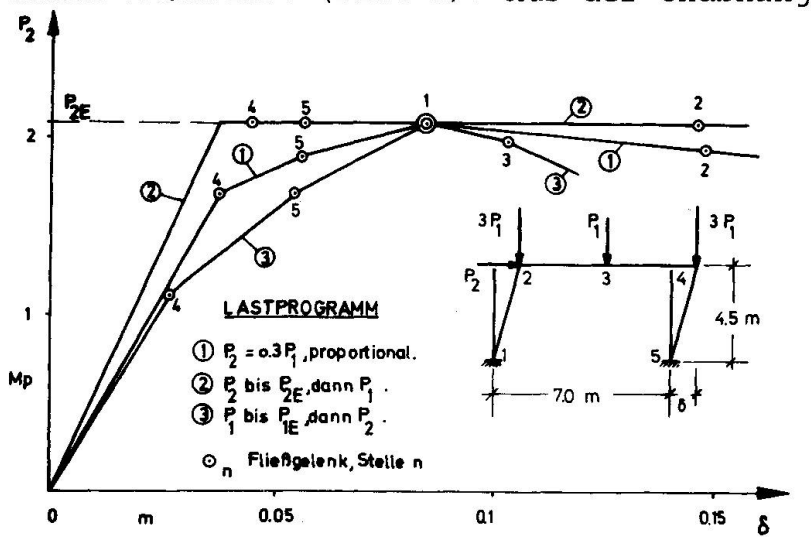

BILD 3: LAST-VERFORMUNGS-DIAGRAMM; „WEICHER" RAHMEN 2

3. Die zu den Traglasten gehörigen Verformungen sind ebenfalls unabhängig von der Belastungsfolge (Bilder 1, 3).
4. Die elastische Grenzlast ist diejenige Last, die von allen

charakteristischen Lasten am meisten vom Lastprogramm beeinflußt wird (Bilder 1, 3). Das erste Fließgelenk bildet sich bei den durchgerechneten Beispielen immer in der rechten oberen Rahmenecke. Auch alle folgende Fließgelenke bilden sich - innerhalb des durch die Schraffur begrenzten Bereiches - unabhängig vom Belastungsprogramm immer in derselben Reihenfolge (Bilder 2, 4).

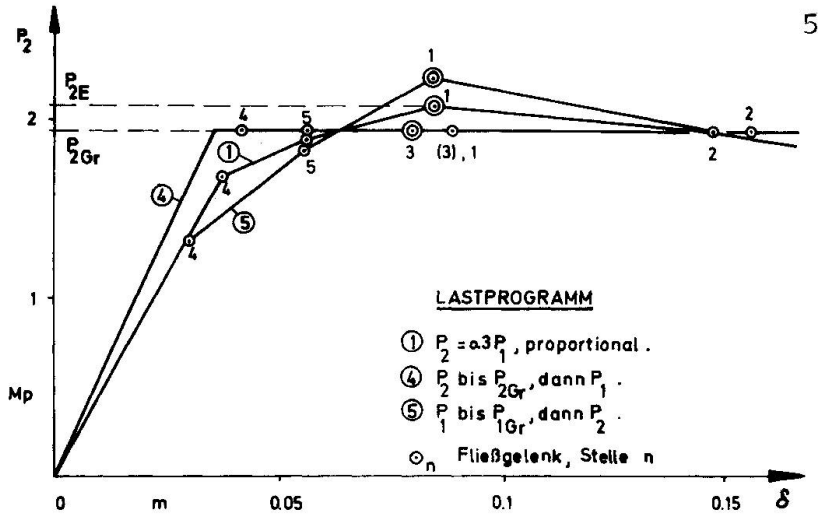

BILD 5: LAST-VERFORMUNGS-DIAGRAMM; „WEICHER" RAHMEN 2

5. Die plastische Grenzlast ist ebenso wie die zugehörige Endverformung nur dann von der Lastfolge unabhängig, wenn sie bei einsinniger Laststeigerung erreicht wird und deshalb wegen der Voraussetzung der Fließgelenkhypothese mit der Traglast zusammenfällt (Bild 1). Sie ist von der Lastfolge abhängig, wenn sie erst im instabilen Bereich auftritt (Bild 3), in dem Gleichgewichtszustände nur nach Abminderung der zur Traglast gehörenden Lastanteile möglich sind.

6. Wenn die plastische Grenzlast bei proportionaler Belastung erst im instabilen Bereich auftritt, liegt der zugehörige Punkt in der Lastebene im Innern des Bereichs stabiler Gleichgewichtszustände, der durch die Linien der Traglast begrenzt wird (siehe 2.). Es ist deshalb nicht möglich, bei einsinniger Belastung in vorgegebenen Grenzen die plastische Grenzlast auf irgendeinem Lastweg zu erreichen, ohne vorher die Traglast erreicht zu haben. Die Traglast liefert deshalb - im Rahmen der hier gemachten Voraussetzungen - eine sichere Angabe über die Tragfähigkeit. Zum Vergleich zeigt Bild 5 die Last-Verformungs-Linien für proportionale Belastung und zwei weitere Lastprogramme ④ und ⑤ , bei denen die Endlasten nicht mehr durch die vorgegebenen Lastschranken P_{1E}, P_{2E}, sondern durch die zur proportionalen Belastung gehörigen Lastanteile P_{1Gr}, P_{2Gr} der plastischen Grenzlast gegeben sind. In diesem Fall sind sowohl die Traglast als auch die zugehörigen Verformungen vom Lastweg abhängig. Für die plastische Grenzlast und die zugehörige Verformung trifft dies jedoch nur zu, wenn das Belastungsprogramm zu Entlastungen nach bereits erfolgter plastischer Deformation führt (Lastprogramm ④). Treten auch bis zum Erreichen der plastischen Grenzlast keine örtlichen Entlastungen (Rückdrehung von Fließgelenken) auf (Lastprogramm ① , ⑤), so sind die plastische Grenzlast und die zugehörige Verformung unabhängig vom Lastweg [3].

Schlußfolgerungen

In den durchgerechneten Beispielen sind, wenn von festen Lastschranken ausgegangen wird, die Traglasten und die zugehörigen Verformungen unabhängig von der Lastfolge und deshalb als Grundlage für die Bemessung geeignet. Die plastischen Grenzlasten, soweit sie

nicht mit den Traglasten zusammenfallen, und die zugehörigen Verformungen unterscheiden sich für verschiedene Lastfolgen. Auch die zugehörigen Mechanismen können sich unterscheiden. Es bleibt weiteren Arbeiten vorbehalten zu untersuchen, inwieweit diese Ergebnisse verallgemeinert werden können.

Literatur

[1] BURTH, K.
Zur Stabilität ebener Stabwerke mit elastisch-idealplastischen Schnittlast-Verformungs-Beziehungen
ZAMM 51, T 103 (1971)

[2] BURTH, K.
Traglasten und Stabilität ebener Rahmentragwerke bei Berücksichtigung von großen Verschiebungen und Schnittlastenumlagerungen
Dissertation, Technische Universität Berlin 1969

[3] VOGEL, U.
Über die Traglast biegesteifer Stahlstabwerke
Der Stahlbau 32 (1963), S. 106/113

ZUSAMMENFASSUNG

Es wird das Last-Verformungs-Verhalten von zwei rechteckigen Portalrahmen mit der Theorie 2. Ordnung numerisch untersucht. Es ergibt sich, dass bei einsinniger nicht-proportionaler Belastung die Traglast unabhängig von der Lastfolge ist, während die plastische Grenzlast von der Lastfolge abhängt, wenn sie nicht mit der Traglast zusammenfällt. Allein Traglast gibt deshalb eine sichere Schätzung der Tragfähigkeit der Rahmen.

SUMMARY

The load-deflection relationship of two rectangular portal frames is investigated numerically by second order elastic-plastic theory. It is found that under always increasing but non-proportional loading conditions, the ultimate load is independent of the load sequence, whereas the plastic limit load, if it does not coincide with the ultimate load, depends on the load sequence. Therefore only the ultimate load gives a reliable estimate of the load-carrying capacity of the structure.

RESUME

On examine numériquement le comportement charge-déformation de deux portiques rectangulaires simples en tenant compte des effets du second ordre. On constate que la charge limite est indépendante de la séquence de la mise en charge en cas des chargements indépendants toujours croissants, tandis que la charge de ruine plastique dépend de la séquence de la mise en charge dans les cas où elle ne coincïde pas avec la charge limite. C'est pourquoi, seulement la charge limite permettra une estimation sûre de la capacité portante de la structure.

Traglasten der Stahlstützen unter statischer und dynamischer Wirkung

Ultimate Loads of Steel Columns under Static and Dynamic Action

Charges ultimes des colonnes en acier soumis à des efforts statiques et dynamiques

Nikola S. DIMITROV P. GLASER
Prof. Dr.-Ing. Dipl.-Ing.
Institut für Tragkonstruktionen und konstruktives Entwerfen
Universität Stuttgart, BRD

Traglasten der Stahlstützen unter statischer und dynamischer Wirkung

Mit den Greenschen Funktionen $K(x,\xi)$ und $\Gamma(x,\xi)$ gemäß Fig. 1

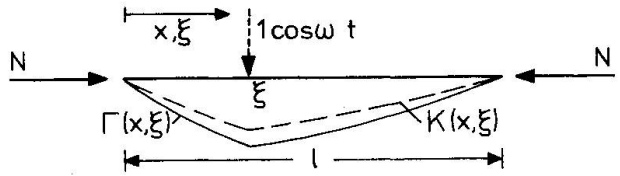

Fig. 1

lassen sich leicht die Biegemomente $M(x)$ und die Biegelinien $y(x)$ unter beliebiger Last $p(x)$ ermitteln:

Einfache Biegung:

$$M_0(x) = \int_0^l K(x,\xi)\, p(\xi)\, d\xi \tag{1}$$

Druckbiegung und harmonischer Schwingung:

$$M(x) = \int_0^l \Gamma(x,\xi) p(\xi)\, d\xi \tag{1a}$$

Allgemeine Biegelinie:

$$y(x) = \int_0^l \Gamma(x,\xi) \frac{M_0(\xi)}{EI}\, d\xi = \int_0^l K(x,\xi) \frac{M(\xi)}{EI} d\xi \tag{1b}$$

$$= \frac{M(x) - M_0(x)}{N} \tag{1c}$$

mit

$$\Gamma(x,\xi) = \begin{cases} x \leqq \xi: & l\left[\dfrac{\varphi_1^2}{\varphi_1^2+\varphi_2^2} \dfrac{\sin\varphi_1 x/l}{\varphi_1 \sin\varphi_1} \sin\varphi_1(1-\xi/l) + \right. \\ & \left. + \dfrac{\varphi_2^2}{\varphi_1^2+\varphi_2^2} \dfrac{\sinh\varphi_1 x/l}{\varphi_2 \sinh\varphi_2} \sinh\varphi_2(1-\xi/l)\right] \cos\omega t \\ x \geqq \xi: & x \text{ mit } \xi \text{ vertauschen} \end{cases} \tag{2}$$

$$\varphi_1 = l\sqrt{\mp\frac{N}{2EI} + \sqrt{\left(\frac{N}{2EI}\right)^2 + m\frac{\omega^2}{EI}}} \tag{2a}$$

$$\varphi_2 = l\sqrt{\mp\frac{N}{2EI} + \sqrt{\left(\frac{N}{2EI}\right)^2 + m\frac{\omega^2}{EI}}} \tag{2b}$$

Das obere Vorzeichen gilt für N als Druckkraft, das untere für Zugkraft.
Es bedeuten:

m - Masse je Längeneinheit
ω - Kreisfrequenz einer erzwungenen harmonischen Schwingung
EI - Biegesteifigkeit des Stabes.

Aus der Gl. (2) kann man im Sonderfall $N = 0$, $\omega = 0$ die einfache Kernfunktion $K(x\xi)$ bekommen.

Der kritische Fall $\varphi_1 = \pi$ gem. Gl. (2a), ergibt die allgemeine Euler-Last:

$$N_K = \frac{\pi^2 EI}{l^2}\left(1 - m\frac{\omega^2 l^4}{\pi^2 EI}\right) \tag{3}$$

$$= N_{Ko}\left(1 - \frac{\omega^2}{\omega_{Ko}^2}\right) \tag{3a}$$

oder nach ω_K (als Resonanzzahl)

$$\omega_K^2 = \frac{\pi^4 EI}{l^4 m}\left(1 - \frac{N}{N_{Ko}}\right) \tag{3b}$$

wenn

$$\omega_{Ko} = \frac{\pi^2}{l^2}\sqrt{\frac{EI}{m}} \tag{3c}$$

$$N_{Ko} = \frac{\pi^2 EI}{l^2} \qquad \text{(Euler - Last)} \tag{3d}$$

bedeuten.

Der Winkel φ_1 bleibt kleiner als π , wenn $N < N_K$ ist.

Es ist noch darauf hinzuweisen, daß bei rollender Einzellast mit einer Geschwindigkeit V_o und einer Einzelmasse m_ξ sowie unter harmonischer Schwingung als auch unter Normallast die Euler-Last noch weiter abgebaut wird, s. [4] :

$$N_{Kr} = N_{Ko}\left[1 - \frac{\omega^2}{\omega_{Ko}^2} - m\frac{V_o^2 l^2}{\pi^2 EI} - m_\xi\frac{V_o^2 l}{4EI} - m_\xi\frac{\omega^2 l^3}{4\pi^2 EI}\right] \tag{4}$$

Für die praktischen Berechnungen lassen sich leichte Näherungsformeln aus den Gl. (1 bis 1c) mit Hilfe der Reihenentwicklungen angeben.

So lautet ein einfacher Vergrößerungsfaktor:

$$f/f_o = \frac{1}{1 - (\omega/\omega_{Ko})^2 \mp N/N_{Ko}} \tag{5}$$

wenn f_o der Biegepfeil nach der linearen Theorie
und f die größte Amplitude bedeuten
Auch hier ist das obere Vorzeichnen für N als Druckkraft und das untere für Zugkraft.

Fig. 2 soll eine außermittig gedrückte Stütze bedeuten, die unter harmonischer Schwingung steht. Ihre Randmomente können im Sonderfall den Trapezverlauf annehmen.

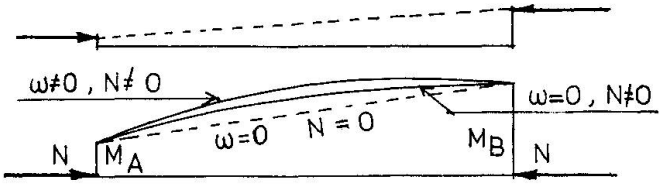

Fig. 2

Biegemomente beim gedrückten Stab

Der allgemeine Verlauf lautet, wenn $\cos \omega t = 1$ gesetzt wird :

$$M(x) = M_A\left[\frac{\varphi_1^2}{\varphi_1^2+\varphi_2^2}\,\frac{\sin\varphi_1(1-x/l)}{\sin\varphi_1} + \frac{\varphi_2^2}{\varphi_1^2+\varphi_2^2}\,\frac{\sinh\varphi_2(1-x/l)}{\sinh\varphi_2}\right] + M_B\left[\frac{\varphi_1^2}{\varphi_1^2+\varphi_2^2}\,\frac{\sin\varphi_1(1-x/l)}{\sin\varphi_1} + \frac{\varphi_2^2}{\varphi_1^2+\varphi_2^2}\,\frac{\sinh\varphi_2(1-x/l)}{\sinh\varphi_2}\right] \qquad (6)$$

Als Stützenquerschnitt wird ein Sandwich-Profil s. Fig.3, angenommen. Hierbei wird die Querschnittsfestigkeit im plastischen Zustand nicht beeinflußt. Um störende Einflüsse zu vermeiden, wird Biegung nur in einer Ebene angenommen sowie gleiche Randmomente $M_A = M_B = M$

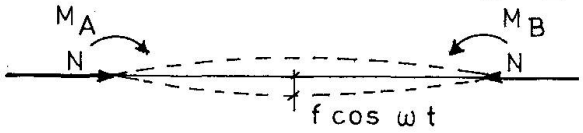

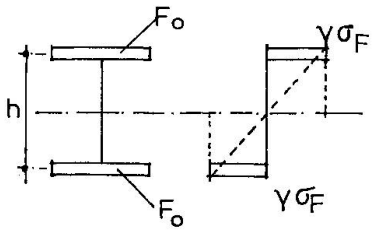

Sandwich-Profil Fig. 3

Unter Beachtung der Parameter

$$n_1 = \frac{N}{Nu} < 1 \quad ; \quad n_2 = \frac{\omega}{\omega_K} < 1 \; ; \; \mu = \frac{M}{M_U} < 1 \; ; \; \gamma = \frac{\sigma_W}{\sigma_F} < 1 \; ;$$

mit

$N_U = 2\,\sigma_F F_0$ (obere Schranke der Bruchlast)
$M_U = \gamma\,\sigma_F F_0 h$ (Tragmoment)
$\gamma < 1$ (Abminderungsfaktor der Baustoffestigkeit infolge Wechselwirkung als untere Schranke)

und der Querschnittswerte

$$F = 2\,F_o \quad ; \quad I = \frac{F_o\,h^2}{2}$$

sowie der Schlankkeitsgrad

$$\lambda = \frac{l}{\sqrt{I/F}} = \frac{2\,l}{h} \qquad (7)$$

kann die Tragfähigkeit der Stütze ermittelt werden. Sie ist gekennzeichnet durch die Grenzspannung $\gamma\,\sigma_F$ und durch die maximale Durchbiegung $f = y(l/2)$
Die Durchbiegung kann aus Gl. (1c) ermittelt werden:

$$N y(x) = M(x) - M_o(x)$$

wobei $M(x)$ nach Gl. (6) und

$$M_o(x) = M_A\,(1-x/l) + M_B\,x/l$$

Für $M_A = M_B = M$ hat man dann:

$$N \cdot y(x) = M\left[\frac{\varphi_1^2}{\varphi_1^2+\varphi_2^2}\,\frac{\sin\varphi_1(1-x/l) + \sin\varphi_1 x/l}{\sin\varphi_1} + \frac{\varphi_2^2}{\varphi_1^2+\varphi_2^2}\,\frac{\sinh\varphi_2(1-x/l) + \sinh\varphi_2 x/l}{\sinh\varphi_2} - 1\right] \qquad (8)$$

Für $x=l/2$ hat man für die größte Biegeordinate bezogen auf die Querschnittshöhe h die Beziehung:

$$\frac{f}{h} = \frac{\mu}{2\,n_1}\left[\frac{\varphi_1^2}{\varphi_1^2+\varphi_2^2}\,\frac{1}{\cos\varphi_1/2} + \frac{\varphi_2^2}{\varphi_1^2+\varphi_2^2}\,\frac{1}{\cosh\varphi_2/2} - 1\right] \tag{9}$$

Diese nichtlineare Funktion ist eine äußere Gleichgewichtsaussage.

Die Winkel φ_1 und φ_2 lauten für das obere Vorzeichnen der Gl. (2a) u. (2b) mit Einführung der Parameter n_1 und n_2

$$\varphi_1 = \lambda\sqrt{\frac{\sigma_F}{2E}}\,\sqrt{n_1+\sqrt{n_1^2+\frac{4\pi^4\,EI^2\,n_2^2}{l^4\gamma^2\,\sigma_F\,F^2}}}$$

$$\varphi_2 = \lambda\sqrt{\frac{\sigma_F}{2E}}\,\sqrt{-n_1+\sqrt{n_2^2+\frac{4\pi^4\,EI^2\,n_2^2}{l^4\gamma^2\,\sigma_F\,F^2}}} \tag{10}$$

In [1] ist der Sonderfall $n_2=0$, d.h. reine Knickbiegung bereits behandelt.

Der homogene Fall ($M_A = M_B = M = 0$) ergibt sich aus Gl. (3a) mit der abgeminderten kritischen Last

$$\frac{N_K}{N_U} = \frac{\pi^2\,E}{\sigma_F\,\lambda^2}\,(1-n_2^2) \tag{11}$$

Die innere Gleichgewichtsaussage $\bar{f}/h$ erhält man aus der Bemessung fur die Grenzspannung:

$$\frac{N}{F} + \frac{\bar{M}}{W} = \frac{N}{2F} + \frac{\bar{M}}{h\,F_o} = \gamma\,\sigma_F \;(\text{bzw.} = \sigma_F) \tag{12}$$

Das vorhandene innere Moment $M=\bar{M}$ bezogen auf das Tragmoment M_U lautet jetzt:

$$\frac{\bar{M}}{M_U} = \frac{1}{\dfrac{\varphi_1^2}{\varphi_1^2+\varphi_2^2}\,\dfrac{1}{\cos\varphi_1/2} + \dfrac{\varphi_2^2}{\varphi_1^2+\varphi_2^2}\,\dfrac{1}{\cosh\varphi_2/2}}\left(1-\frac{\sigma_n}{\sigma_F}\right)\frac{1}{\gamma} \tag{13}$$

In Gl. (9) eingesetzt erhält man entsprechend:

$$\frac{\bar{f}}{h} = \frac{1}{\dfrac{\varphi_1^2}{\varphi_1^2+\varphi_2^2}\,\dfrac{1}{\cos\varphi_1/2} + \dfrac{\varphi_2^2}{\varphi_1^2+\varphi_2^2}\,\dfrac{1}{\cosh\varphi/2}}\left[1-\frac{n}{\gamma}\right]\left(\frac{\varphi_1^2}{\varphi_1^2+\varphi_2^2}\,\frac{1}{\cos\varphi_1/2}+\frac{\varphi_2^2}{\varphi_1^2+\varphi_2^2}\,\frac{1}{\cosh\varphi_2/2}-1\right)\frac{1}{2n_1} \tag{14}$$

Diese Beziehung stellt in den Fig. 4 und 5 die Grenzkurven dar.

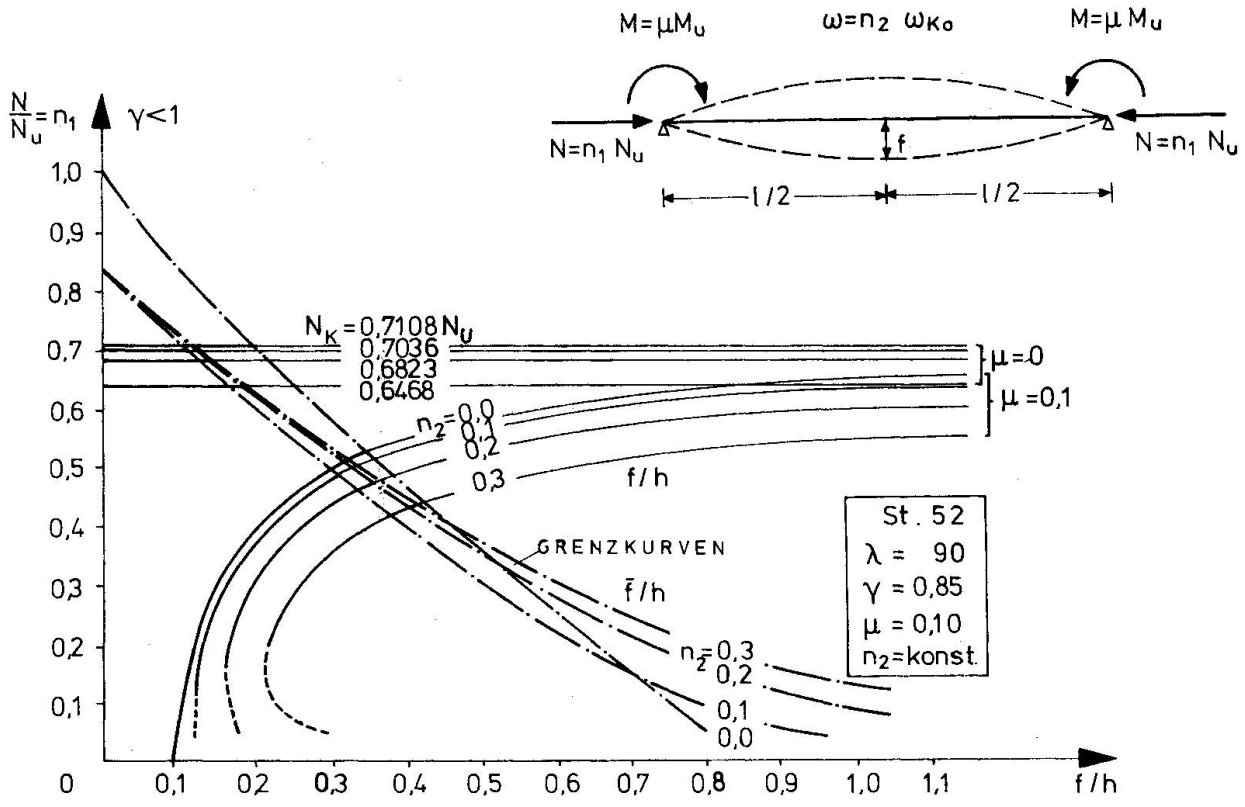

Traglastkurven für n_2 = konst. Fig. 4

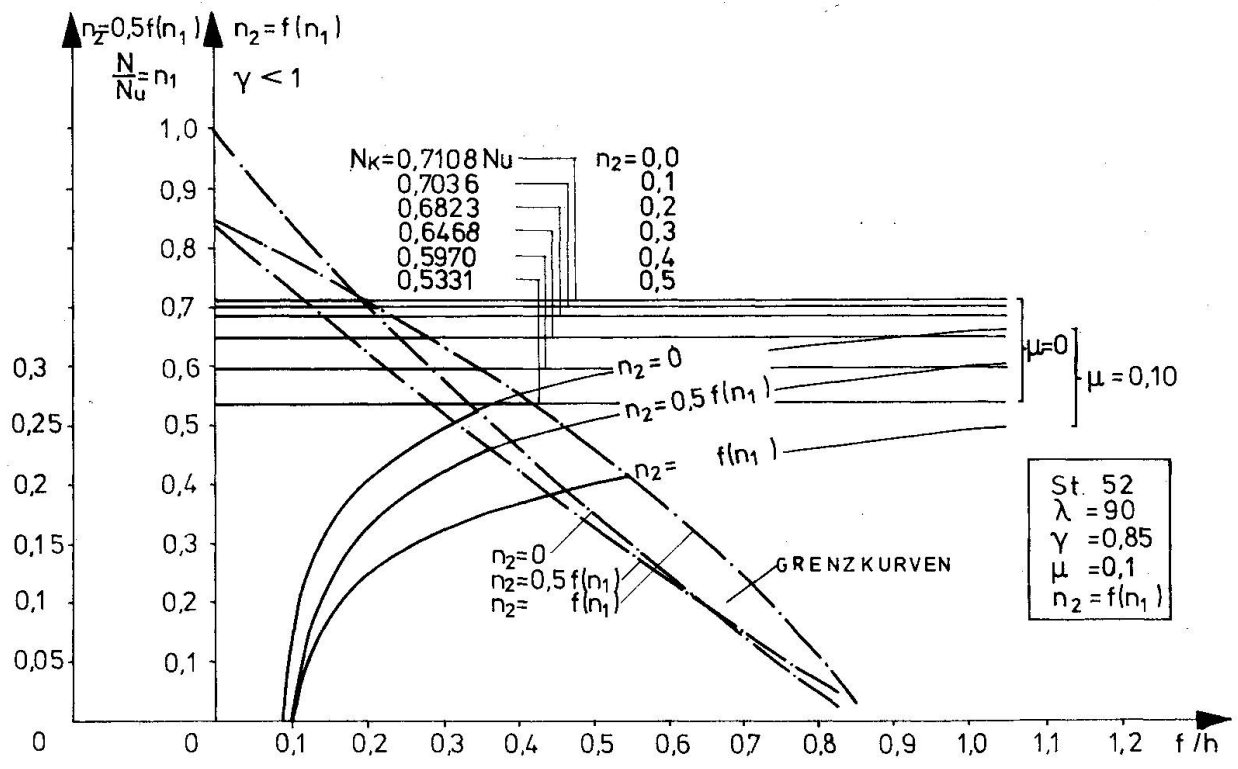

Traglastkurven für veränderliche $n_2 = f(n_1)$ Fig. 5

Schriftum

1 Dimitrov, N. und W. Herberg : Festigkeitslehre, Bd. 1, Sammlung Göschen Band 6144, Walter de Gruyter, Berlin-New York: 1971

2 Dimitrov, N. : Die Schnittkräfte des Balkens mit schwingender Querbelastung unter Berücksichtigung einer zusätzlichen Normalkraft. Der Stahlbau 26 (1956) Nr. 4 S. 107/111

3 Dimitrov, N. : Der Reduktionssatz und die Integralgleichung der Balkenbiegung. Der Bauingenieur 47 (1972) Nr. 5, S. 176/178, sowie Nr. 12

4 Dimitrov, N. : Berechnung der Stabwerke unter rollender Last und zusätzlicher Normalkraft. VDI-Z (1967) Nr. 2

5 Schuller, R. : Zum Stabilitätsproblem des querschwingenden Druckstabes mit konstanter Normalkraft auf der Grundlage der Elastizitätstheorie. Der Bauingenieur 48 (1973) Nr. 1, S. 16/22.

ZUSAMMENFASSUNG

Ganz allgemein wird gezeigt, dass mit Hilfe der Integralgleichungstheorie Traglasten bei Berücksichtigung verschiedenartiger Einflüsse berechnet werden können. Dies gilt auch für beliebige Systeme.

Die Berechnung wird an einer ausmittig beanspruchten Stahlstütze mit Sandwichquerschnitt vorgeführt. Es wird die Abminderung dieser Spannungen, wenn die Stütze unter harmonischen Schwingungen steht, gezeigt. Dabei sind zweierlei Einflüsse zu beachten:

1. geometrische: durch Zunahme der Verformung infolge Abnahme der kritischen Last bei Berücksichtigung von Schwingungen und Druckbiegung.

2. physikalische: durch Abnahme der Querschnittfestigkeit (Baustoffestigkeit) infolge Wechselwirkung als einfache Abminderung.

Die Kurven gem. Fig. 4 und 5 können einen Hinweis auf die Traglasten vermitteln, wobei viele störende Einflüsse wie Dämpfung, Torsion und Kippen vernachlässigt wurden.

SUMMARY

It is shown that by use of the theory of the integral equation one can compute the ultimate loads under consideration of various influences. This is valid for any system.

The computation is demonstrated on the example of a steel column with sandwich-cross-section under an excentric force. The reduction of these stresses are shown when the column is under harmonic vibration. Two influences are to be considered:

1. geometrical: by the increase of the deflection owing to the reduction of the critical load considering vibration and bending under compression.

2. physical: by the decrease of the strength of the cross-section (strength of material) owing to the alternating action as simple reduction.

The curves in Fig. 4 and 5 can give a hint of the ultimate load, whereby many influences of damping, torsion and buckling are neglected.

RESUME

On montre, de manière générale, le calcul des charges ultimes par la méthode des équations intégrales en tenant compte des différentes influences, ceci restant valable pour des systèmes quelconques.

On présente ensuite le calcul d'une colonne en acier à section en sandwich avec charge excentrique. On montre la diminution des tensions lorsque la colonne est soumise à des vibrations harmoniques. On soulignera deux sortes d'influences:

1. Influences géométriques: à cause de l'augmentation des déformations due à la diminution de la charge critique en tenant compte des vibrations et de la flexion due aux efforts de compression.

2. Influences physiques: à cause de la diminution de la résistance de la section (résistance du matériau) due aux charges alternées.

Les courbes des figures 4 et 5 donnent une idée des charges ultimes, bien que beaucoup d'influences gênantes, tel que l'amortissement, la torsion et le renversement aient été négligées.

Leere Seite
Blank page
Page vide

I

Cyclic Stress-Strain Response of 2024 Aluminium under Biaxial States of Stress

Courbe cyclique tension-déformation de l'aluminium 2024 dans un état de tension biaxiale

Zyklische Spannungs/Dehnungs-Reaktion von Aluminium 2024 unter zweiaxigem Spannungszustand

Fernand ELLYIN Kenneth W. NEALE
Professor Assistant Professor
Department of Civil Engineering
Université de Sherbrooke
Québec, Canada

INTRODUCTION

Although the stress-strain behaviour of metals under states of combined stress has been studied experimentally for monotonically-increasing loads, research into elastic-plastic material response for loadings of a repeated nature has been mainly concerned with uniaxial stress states [1,2]. Apart from a few recent investigations into low-endurance biaxial fatigue [3-5], there is very little test data for cyclic loading involving multiaxial stress states. Consequently, the major objective of the work initiated in this paper will be to determine cyclic stress-strain characteristics for metals under various states of biaxial stress in the plastic range. It is clear that such experimental work is essential to the formulation of adequate material models for the analysis of structural components subjected to complex, repeated loads [6,7].

In this preliminary investigation, cyclic biaxial response is determined for 2024-T351 aluminum by subjecting thin-walled cylinders to repeated axial loading combined with alternating torsion. Thus, the fundamental variables studied are axial stress σ, shear stress τ, axial strain ε and shear strain γ. For convenience, we introduce the quantities

$$\eta = \frac{\sigma}{\tau} \qquad \rho = \frac{\varepsilon}{\gamma} \tag{1}$$

which define a stress ratio and strain ratio, respectively. Furthermore, as a scalar measure of stress and strain under biaxial states, the following conventional definitions of "effective stress" $\bar{\sigma}$ and "effective strain" $\bar{\varepsilon}$ are adopted:

$$\bar{\sigma} = (\sigma^2 + 3\tau^2)^{\frac{1}{2}} \qquad \bar{\varepsilon} = \left(\frac{3\varepsilon^2 + \gamma^2}{3}\right)^{\frac{1}{2}} \tag{2}$$

In this paper, results are presented for a series of fully-reversed strain-controlled tests in which the amplitude of the effective strain, $\Delta\bar{\varepsilon}$, is the controlling parameter and a constant strain ratio ρ is maintained during a given test. Particular emphasis is given to the "steady-state" response of the material under cyclic biaxial loading.

EXPERIMENTAL INVESTIGATION

a) *Specimens and Apparatus*

The thin-walled tubular specimens employed in this investigation were machined from 1-$\frac{1}{2}$ in. (38 mm.) diameter solid bars of 2024-T351 aluminum to the dimensions shown in Fig. 1. The material was used as supplied and, after grinding, the internal and external surfaces of the cylinders were polished in order to prevent premature fatigue failures. A description of the pertinent mechanical properties of the aluminum alloy is given in Table 1.

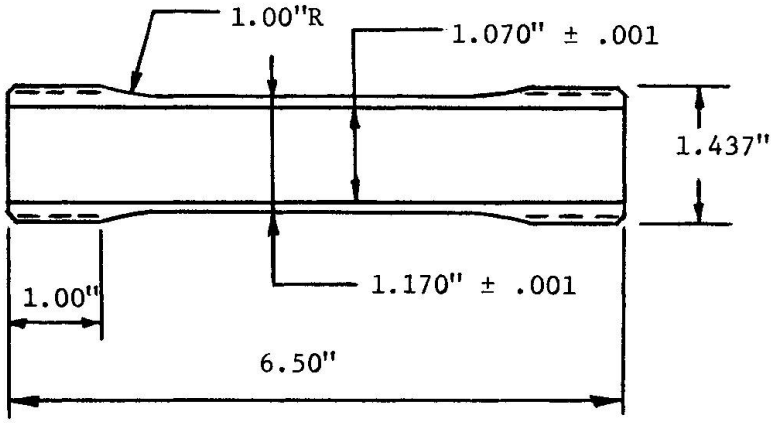

Fig. 1

TABLE 1

Tensile Properties

Modulus of Elasticity	Yield Strength	Ultimate Strength	% elongation
10,200 ksi	50.8 ksi	68.6 ksi	22
(717,000 kg/cm^2)	(3,570 kg/cm^2)	(4,820 kg/cm^2)	

All experiments were conducted using a specially-designed apparatus, which operates in a standard close-looped (MTS) servo-controlled electro-hydraulic testing system. This testing facility, which is described in detail elsewhere [8], permits simultaneous application of repeated axial loading and cyclic torsion to the tubular specimens. The axial load and torsion are controlled independently, and either the applied loading itself or the output (ε,γ) of the transducers measuring the strain may be selected as controlling parameters.

b) *Experimental Programme*

Due to possible frequency effects and the presence of "cyclic creep" under load-controlled conditions, a series of fully-reversed constant-amplitude strain-controlled tests was conducted. Cyclic stress-strain response was thus determined under biaxial stress states for the following prescribed strain ratios: $\rho=0,\frac{1}{2},1,2,\infty$; where $\rho=0,\infty$ correspond to pure torsion ($\sigma=0$) and axial stress ($\tau=0$), respectively.

For each predetermined value of ρ, two tests were performed: one for an

effective strain range $\Delta\bar{\varepsilon} = \pm 0.75\% = 1.5\%$, and a second test for which $\Delta\bar{\varepsilon} = \pm 1.0\% = 2.0\%$. All tests were run at a frequency of 0.1 cycles per second and during each test, axial load-deformation and torque-twist hysteresis loops were recorded periodically using X-Y plotters. Although the prime purpose of the experiments was to investigate material response prior to and including steady-state conditions, the cyclic loading programme in each case was applied until failure of the specimen occurred.

TEST RESULTS AND DISCUSSION

Results of a typical fully-reversed strain-controlled test are shown in Fig. 2 where hysteresis loops obtained for combined axial load and torsion ($\rho=1$) are reproduced for various cycles of deformation. For purposes of comparison, the monotonic stress-stress curve under axial tension is also included in this figure. As cycling proceeds a progressive increase in stress amplitude is evident, which indicates that this metal exhibits cyclic strain-hardening characteristics under biaxial loading. Furthermore, although the results for a given cycle show that the stress limits in torsion are essentially equal, one observes that the stress limit in compression for the axial stress σ becomes greater than the tensile limit during cycling. This behaviour, termed "mean stress relaxation", is apparently related to the "cyclic creep" phenomenon, which should occur in a corresponding load-controlled test [1,2].

In Fig. 3, the stress limits in torsion and axial stress are plotted against the number of cycles for the effective strain amplitudes $\Delta\bar{\varepsilon} = 1.5\%$, 2.0% and various strain ratios. These curves indicate that, during an initial transitory period of cyclic strain-hardening under combined stress, the stress-strain behaviour asymptotically approaches some limiting "steady-state" cyclic response. In addition, from the difference in stress limits for a particular cycle the amount of mean stress relaxation is readily obtained.

In order to characterize the material response under steady-state conditions, "steady-state yield-interaction" curves have been constructed (Fig. 4). Using the 0.2% proof stress as the definition of yielding, the yield stress components (σ_y, τ_y) obtained from the steady-state hysteresis loops are plotted and compared to the initial yield curve. From these results it appears that, in addition to the cyclic strain-hardening phenomenon mentioned above, another type of hardening accompanies cyclic deformation - a hardening which is manifested by an increase in yield stresses with increasing number of cycles. Yet, in contrast to cyclic strain-hardening (where the stress amplitude increases with increasing strain amplitude) the amount by which these steady-state yield stresses increase is less for the higher value of $\Delta\bar{\varepsilon}$. However, in view of the number of tests conducted in this preliminary investigation, and the particular definition of yield adopted (0.2% offset), more experimental data must be generated and the implication of other yield definitions examined [8] in order to confirm this trend. Further experiments are also required to determine "steady-state yield curves" for a variety of strain-controlled and load-controlled conditions and to assess whether interaction curves, such as those given in Fig. 4, provide useful information for the analysis and design of structural elements subjected to repeated loads.

In conclusion, the numbers of cycles to "failure" N_f are listed in the following table for the various applied strain amplitudes and prescribed strain ratios.

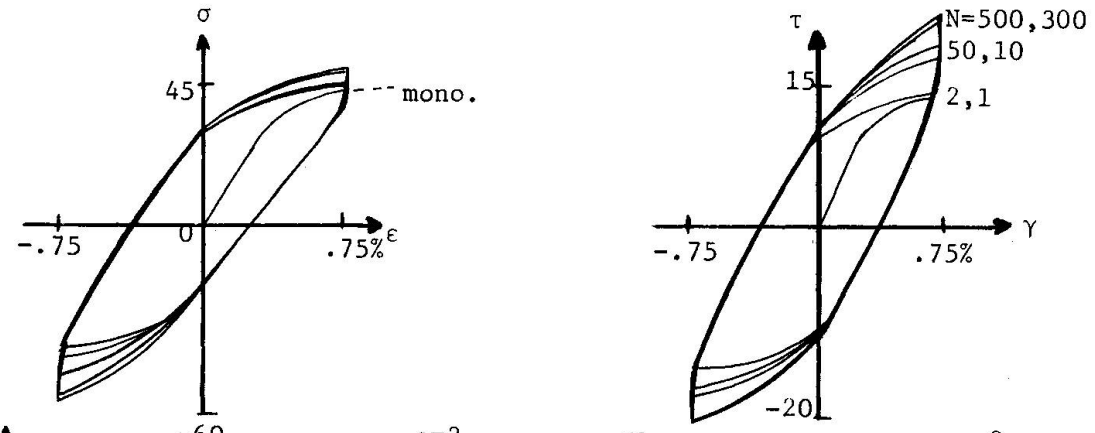

Fig. 2

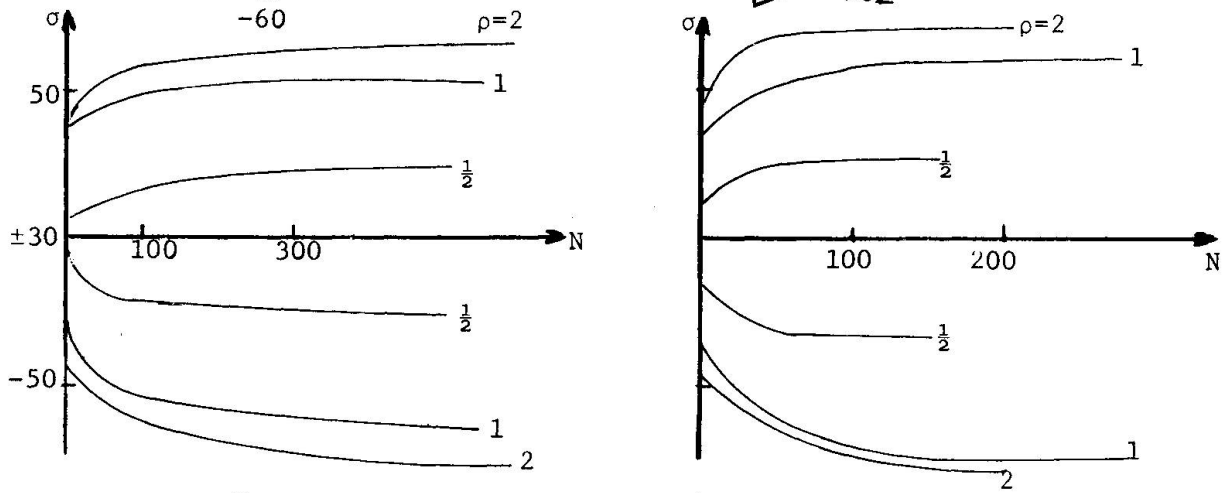

Fig. 3a

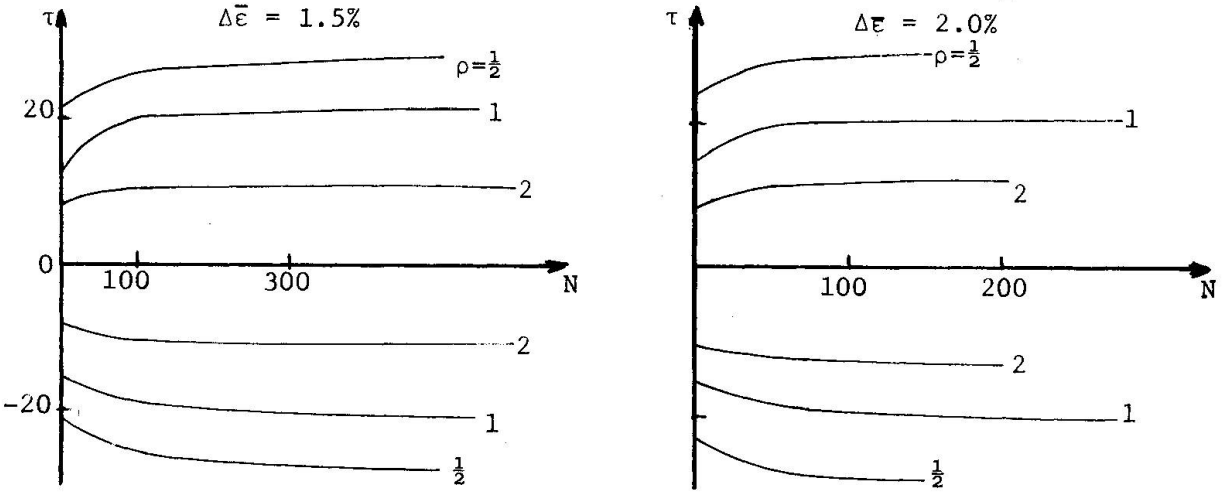

Fig. 3b

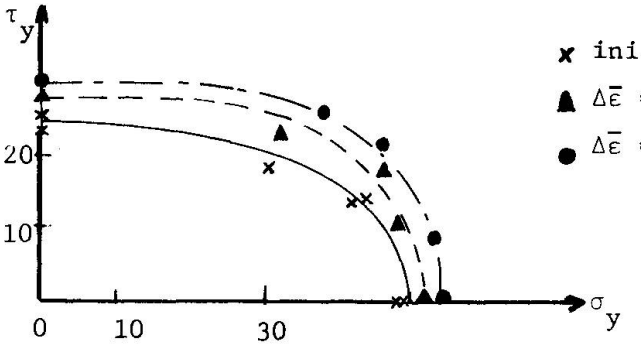

Fig. 4

TABLE 2

$\Delta\varepsilon$	$\Delta\gamma$	$\Delta\bar{\varepsilon}$	ρ	N_f
±1.00%	0%	2.0%	∞	197
±0.96	±0.48	2.0	2	219
±0.87	±0.87	2.0	1	299
±0.65	±1.31	2.0	$\frac{1}{2}$	166*
0	±1.73	2.0	0	43*
±0.75	0	1.5	∞	377
±0.72	±0.36	1.5	2	621
±0.65	±0.65	1.5	1	662
±0.49	±0.98	1.5	$\frac{1}{2}$	570
0	±1.30	1.5	0	324

* failed by buckling

It should be noted that, although most specimens exhibited fatigue failures, buckling occurred for the higher amplitudes of torsion. Certain aspects of this delayed-buckling phenomenon under cyclic torsion were briefly discussed in [9].

ACKNOWLEDGEMENTS

This work was supported in part by the National Research Council of Canada (Grants A-3803, A-8584), and le Ministère de l'Education du Gouvernement du Québec. The authors are also grateful to M. Bouveret for his help in carrying out the tests.

REFERENCES

[1] Dolan, T.J., "Nonlinear Response under Cyclic Loading Conditions", *Developments in Mechanics*, v. 3, p. 3 (1965).

[2] Topper, T.H., and Conle, A., "An Approach to the Analysis of the Nonlinear Deformation and Fatigue Response of Components Subjected to Complex Service Load Histories", *Proc. Int. Symposium on Experimental Mechanics*, University of Waterloo (1972).

[3] Crosby, J.R., Burns, D.J., and Benham, P.P., "Effect of Stress Biaxiality on the High-Strain Fatigue Behaviour of an Aluminum-copper Alloy", *Experimental Mechanics*, v. 9, p. 305 (1969).

[4] Havard, D.G., and Topper, T.H., "Biaxial Fatigue of 1018 Mild Steel at Low Endurance", *Proc. 1st Int. Conf. on Pressure Vessel Technology*, Delft, Part II, p. 1267 (1969).

[5] Rotvel, F., "Biaxial Fatigue Tests with Zero Mean Stresses Using Tubular Specimens", *Int. Jour. Mech. Sci.*, v. 12, p. 597 (1970).

[6] Mroz, Z., "On the Theory of Steady Plastic Cycles in Structures", *Proc. 1st Int. Conf. on Structural Mechanics in Reactor Technology*, Berlin (1971).

[7] Mroz, Z., and Lind, N.C., "On Simplified Theories of Cyclic Plasticity", *ASCE Annual and Environmental Engineering Meeting*, Houston, Texas (1972).

[8] Ellyin, F., and Grass, J.P., "Méthode expérimentale de détermination de surfaces d'écoulement plastique-application au titane 50A", *Rapport Technique No. FE-23-73*, Université de Sherbrooke, Sherbrooke, Québec (1973).
[9] Neale, K., and Schroeder, J., "Plastic Buckling of a Thin Tube under Cyclic Torsion", *Jour. Appl. Mech.*, v. 39, p. 847 (1972).

SUMMARY

The main objective of the work initiated in this paper is to determine stress-strain characteristics for metals under various states of repeated biaxial loading in the plastic range. In this particular investigation, the results of a series of constant-amplitude, fully reversed strain-controlled tests are reported for 2024-T351 aluminum under cyclic axial stress combined with alternating torsion. The observed cyclic strain-hardening and steady-state response are discussed, and the notion of a "steady-state yield-interaction" curve is introduced.

RESUME

L'objectif principal de l'analyse amorcée dans ce travail est de déterminer les caractéristiques tension-déformation des métaux soumis à différents états de charges répétées biaxiales dans le domaine plastique. Dans cette étude particulière, on présente les résultats d'une série d'essais sur l'aluminium 2024-T351 soumis à des tensions axiales variant cycliquement, combinées avec des efforts de torsion alternés, les déformations totalement inversées restant d'amplitude constante. On discute ensuite l'allure des courbes pour des déformations cycliques dans le domaine d'écrouissage et pour l'état stationnaire et on introduit la notion de courbe d'interaction des tensions de fluage à l'état stationnaire.

ZUSAMMENFASSUNG

Das Hauptziel der vorliegenden Arbeit ist die Bestimmung von Spannungs-Dehnungs-Charakteristiken für Metalle unter verschiedenen Zuständen wiederholter zweiachsiger Beanspruchung im plastischen Bereich. In dieser speziellen Untersuchung werden die Resultate einer Serie mit konstanter Amplitude und vollständig umgekehrter dehnungs-kontrollierter Versuche für Aluminium 2024-T351 unter zyklischer axialer Spannung kombiniert mit wechselseitiger Torsion, aufgezeigt. Die beobachtete zyklische Verfestigung und die Reaktion aus stetiger Belastung werden diskutiert und der Ausdruck einer "stetigen Belastung-Fliessen-Interaktion"eingeführt.

Time Effects in the Shakedown of Reinforced Concrete Beams

Effets du temps sur l'orientation de poutres en béton armé

Zeiteinwirkungen beim Sich-Einspielen von Stahlbetonträgern

G.S. McCLURE
Prof. of Architecture
Montana State University
Bozeman, Montana, USA

K.H. GERSTLE
Prof. of Civil Engineering
University of Colorado
Boulder, Colorado, USA

L.G. TULIN
Prof. and Chairman
Dept. of Civil and
Environmental Engineering
University of Colorado
Boulder, Colorado, USA

Introduction

The subject of shakedown on reinforced concrete beams, to which Professor Park's survey paper made reference, has been clouded by conflicting evidence; on one hand, early researchers (1) claimed that the elastic-perfectly plastic theory of incremental deformations was well able to predict the observed behavior of concrete beams under variable repeated loading. On the other hand, later work (2) indicated very little relationship between the predictions of the classical theory, and experimental results, and attributed this discrepancy variously to the effects of bond deterioration (3) and strain-hardening of the steel (4).

In a further effort to clarify the matter, we consider in this contribution the effect of concrete creep on the response of concrete beams subject to alternating repeated loads, and on the occurrence of shakedown. The approach consists of the following phases:

1. Development of a general analysis for concrete beams under arbitrary load histories, incorporating the effect of the time-dependent response of the concrete.
2. Verification of the analytical predictions by appropriate tests.
3. Use of the analysis to perform a study of the way in which creep affects the incremental deformations of concrete beams under cyclic loading.

The steps, and the resulting conclusions, will be discussed shortly in the following.

General Analysis for Arbitrary Load History

Following earlier work (5), time-dependent moment-curvature relations were established, based on classical concrete beam theory of plane sections and the actual properties of the constituent materials, of which steel was of the elastic-plastic-strain hardening type, and the concrete was of stress-strain-time relationships measured directly in the laboratory.

With moment-curvature-time relations known for all beam sections, any framed structure can be analyzed by adjusting the distribution of moments at any point in time so as to satisfy equilibrium and compatibility. Because of the non-linearity of the system, an interative solution scheme was used, which incorporates the necessary checks for elastic or inelastic loading, elastic unloading at any section, as well as attainment of the elastic limit which shifts in magnitude according to the maximum moment reached in prior load cycles (4). A computer program incorporating these features enables prediction of moments, curvatures, and deflections at any stage of arbitrary load histories applied to continuous beams. Effects of shear deformations or shear failure, or bond or anchorage deterioration, were not considered in the analysis.

Experimental Verification

It is obvious that an analysis as full of gross assumptions and simplifications as the one outlined must be checked by comparison of theoretical and experimental results. For this purpose, two-span continuous concrete beams were tested under a variety of load histories consisting of cyclic and sustained loading (6). The case presented here is typical of results obtained.

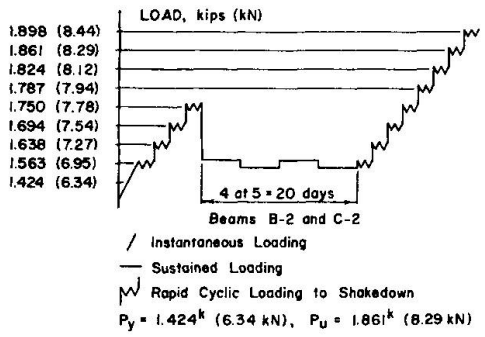

Figure 1

Fig. 1 shows the load history which consisted of a first stage of rapid cyclic variation of load at increasing levels, followed by a 20-day period of two load levels sustained alternately for five days each, and concluding with another sequence of cyclically varying loads to failure.

Figs. 2, 3, and 4 show the analytical and observed load-deflection curves for the rapidly-cycled loading stages, and the deflection-time-curves for the sustained loading stage. Good correlation is observed at all stages up to 98 per cent of the predicted plastic limit load for the two-span beam. By that time over 70 cycles of high loads had been applied, and some evidence of bond deterioration was apparent. Nevertheless, the observed deflections were less than those predicted up to failure, which occurred under a load slightly larger than the fully-plastic limit load.

It is concluded from this and other comparisons that the analysis is well capable of predicting the response of such beams to applied load histories.

Effect of Creep on Shakedown of Concrete Beams

Once the validity of the method of analysis of load history effects was confirmed experimentally, it was utilized with some confidence in a systematic exploration of the effects of creep on the incremental deformations of continuous concrete beams under repeated variable loading.

In tests, shakedown, or deflection stabilization of a structure is presumed to have occurred whenever the deformation increment between corresponding stages of two successive load cycles vanishes. Any change of displacement due to creep will give the

appearance of incremental deformations, unless considered in the theory, or eliminated by appropriately fast rates of load cycling

The previously established analysis was used to investigate the effect of creep on the displacements of a two-span continuous beam of the same properties as that of the previous analysis, under load cycles applied at various rates, and Fig. 5 summarizes the results. The applied load, of magnitude $P_{max}=0.92\ P_u$, is above the elastic-perfectly plastic shakedown load, and the dash-dotted line shows the linearly-increasing displacements predicted by classical theory of incremental deformations assuming perfect plasticity. Because of strain-hardening, the beam will actually shake down in the absence of creep, as shown by the curve labeled "No Creep." Intermediate curves indicate the predicted increase in deflections for different rates of load cycling, and demonstrate that the effect of creep will tend to give the appearance of perfectly-plastic incremental deformations.

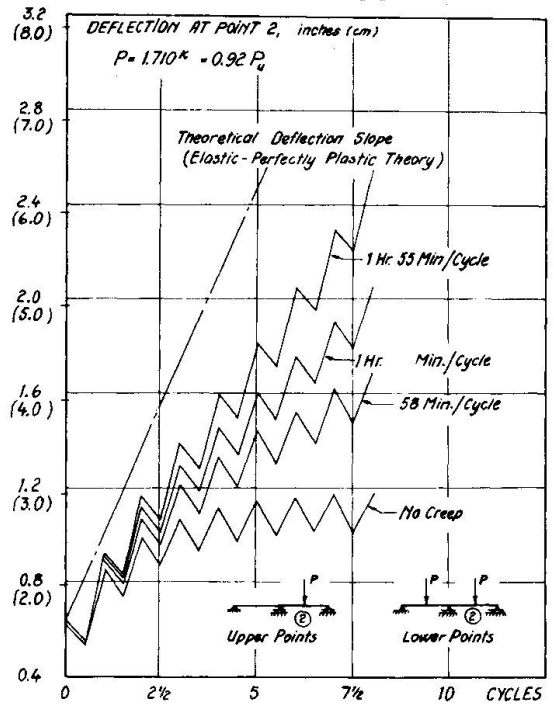

Figure 5. Theoretical Shakedown Including Creep

It may be concluded that both strain-hardening and creep should be included for a valid assessment of the occurrence of incremental deformations in concrete structures subject to cyclic overloads.

References

1. Rasmussen, B. H., "Incremental Collapse of Ordinary Reinforced Concrete Beams,"Publications of the International Association for Bridge and Structural Engineering, Vol. 16, 1965, pp. 439-456.
2. Gerstle, K. H., and Tulin, L. G.,"Shakedown of Continuous Concrete Beams, "International Symposium on the Effect of Repeated Loading of Materials and Structural Elements, Mexico City, 1966.
3. Ruiz, W. M., and Winter, G., "Reinforced Concrete Beams Under Repeated Loads, "Journal of the Structural Division. Proceedings of the American Society of Civil Engineers, Vol. 95, No. ST6, June 1969, pp. 1189-1211.
4. Gerstle, K. H. and Tulin, L. G., "Incremental Deformations of Reinforced Concrete Beams,"Magazine of Concrete Research No. 77, Dec. 1971.
5. Mozer, J. D.; Gerstle, K. H.; and Tulin, L. G., "The Time-Dependent Behavior of Concrete Beams,"Journal of the Structural Division. American Society of Civil Engineers, Vol. 96, No. ST3, March 1970, pp. 597-612.
6. McClure, G. S., Gerstle, K. H., Tulin, L. G., "Response of Concrete Beams to Sustained and Cyclic Loading,"Proc. A.S.C.E., Jnl. Struct. Div., Vol. 99, No. ST2, February 1973.

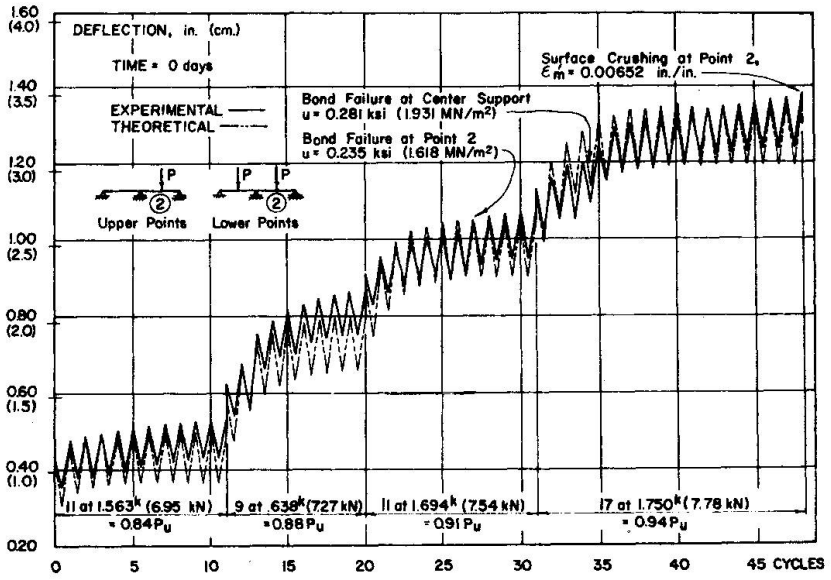

Figure 2

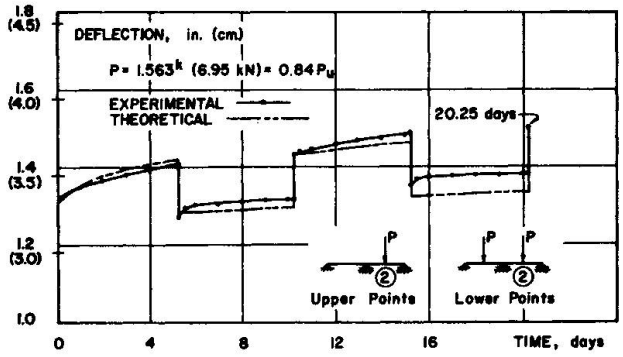

Figure 3

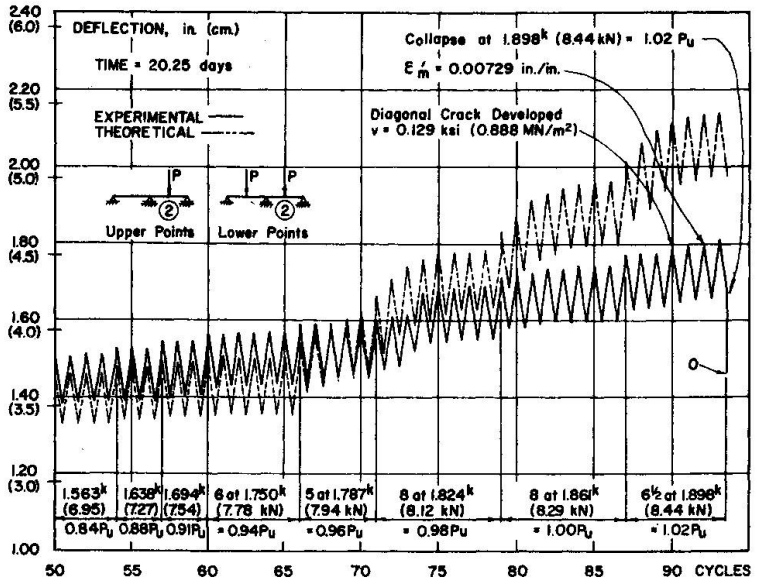

Figure 4

SUMMARY

A general analysis for the flexural response of reinforced concrete beams to arbitrary load and time histories is presented, and verified by comparison with experimental results. This analysis is then used to evaluate the effect of creep on the incremental deformations of concrete beams under variable repeated loading. It is concluded that creep should be considered for a valid assessment of theories of incremental deformation.

RESUME

Ce travail présente une méthode d'analyse générale pour l'étude du comportement de poutres en béton armé soumises à la flexion, à un instant arbitraire du processus de charge. Les résultats sont vérifiés par une série d'essais. Cette méthode est ensuite utilisée pour évaluer l'influence du fluage sur les déformations additionnelles de poutres en béton armé soumises à des charges répétées variables. Il en résulte que le fluage devrait être pris en considération pour une conception valable des théories sur les déformations additionnelles.

ZUSAMMENFASSUNG

Eine allgemeine Berechnungsmethode für das Biegeverhalten von Stahlbetonbalken unter beliebiger Last und zeitlichem Verlauf wird dargestellt und durch Vergleich mit experimentellen Resultaten bestätigt. Diese Methode wird dazu verwendet, den Effekt des Kriechens auf die zunehmenden Deformationen von Betonbalken unter variabler wiederholter Belastung zu ermitteln. Daraus wird gefolgert, dass das Kriechen beim brauchbaren Abschätzen der zunehmenden Deformationen berücksichtigt werden sollte.

Leere Seite
Blank page
Page vide

Shear Strength of Concrete Beams under Cyclic Loading – A Preliminary Study

Résistance au cisaillement de poutres en béton sous charges cycliques – Une étude préliminaire

Schubfestigkeit von Betonbalken unter zyklischer Belastung – Eine Vorstudie

H.N. SINGH
Engineer
Pennsylvania Department of Highways
Franklin, Pa., USA

K.H. GERSTLE
Prof. of Civil Engineering
University of Colorado
Boulder, Colorado, USA

L.G. TULIN
Prof. and Chairman
Dept. of Civil and
Environmental Engineering
University of Colorado
Boulder, Colorado, USA

Introduction

Numerous studies of the response of reinforced concrete members to cyclic loadings, many of which have been summarized at this meeting, have indicated that in general, the flexural strength of under-reinforced beams remains unimpaired under histories of loading consisting of a reasonable number of cycles. However, there is a body of evidence indicating that their shear strength may suffer under such loadings; a number of continuous beams (1), designed to fail in flexure under monotonically increasing loads, actually failed in a diagonal tension mode under cyclic loading which appeared to be triggered by bond cracking of the concrete at the level of the tensile steel.

An explanation of such premature shear failures may be found in the progressive deterioration of bond between reinforcing steel and concrete under cycles of high loads. Since the tensile crack pattern of concrete beams is closely associated with bond, it follows that any deterioration of the bond will affect the nature of the tensile cracks. Recently developed methods of analysis (2,3) can account for the effect of bond loss on the crack propagation within the concrete in a rational manner.

Following this line of thought, the pilot study discussed in this paper was divided in the following parts:

1. Experimental determination of the bond deterioration under repeated loading.
2. Development of a theory of shear strength of concrete beams which includes the effect of this bond deterioration.
3. Cyclic tests of concrete beams designed to fail in shear to check predictions.

While the investigation is at present incomplete, we feel that it is sufficiently important to focus attention on the importance of shear strength under cyclic loadings to warrant presentation of preliminary results.

Pullout Tests

A theory of bond behavior of pullout specimens, as shown in Fig. 1(a) under monotonic and cyclic loading is presented which may help explain the relation between bond deterioration and opening of tensile concrete cracks. Based on limited experimental evidence (4) it is assumed that each point along the embedment length of a bar has a fixed capacity to develop bond strength. When this capacity is reached, the strength begins to deteriorate. Bond failure of the specimen is possible only after all points along the embedment, one after the other, have achieved their full capacity. A plot of the peak strength of all points will be called the "envelope curve", and is shown in Fig. 1(b). Under applied tension force, bond stresses will develop, leading to a bond stress distribution as shown by Curve A-B-C in Fig. 1(b). The area under this curve between the loaded end and any point is proportional to the force transferred to the concrete, and the total area under the bond stress curve is proportional to the total applied load. Thus, the force in the tension bar at any point can be plotted as shown in Fig. 1(c). The area under this latter curve, in turn, is proportional to the elongation of the bar. As long as the free end of the bar is prevented from slipping, all of this elongation appears as slip of the loaded end.

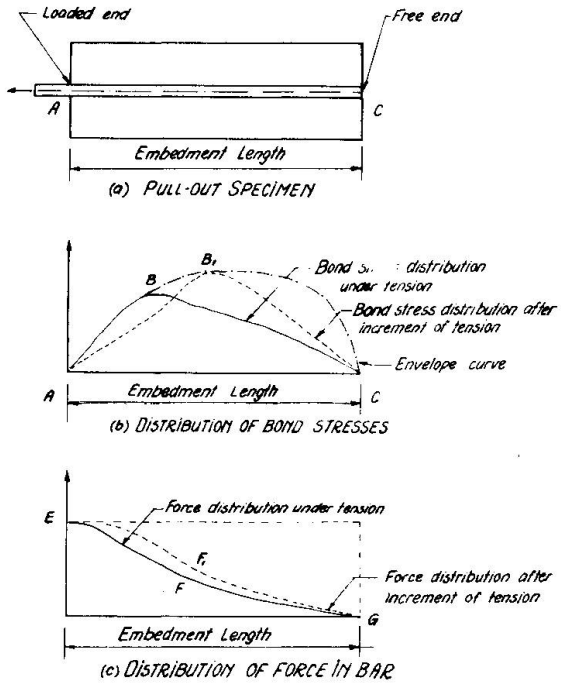

FIG. 1 - REPRESENTATION OF PULL-OUT SPECIMEN AND PERTINENT CHARACTERISTICS IN ANALYSIS

As the load on the bar is increased, the bond stress distribution changes, with those portions of the bar whose bond stress has attained the envelope value subject to bond deterioration, and others with ascending stresses, leading to a new bond stress distribution as shown by Curve A-B_1-C of Fig. 1(b). The difference between the area under the force diagram corresponding to this stress distribution, E-F_1-G in Fig. 1(c), and the previous one, E-F-G, is proportional to the increment of slip at the free end occurring due to the additional load. Under further increase of applied load, the area under the envelope curve is swept, with that bond stress distribution containing the largest area denoting the maximum bond strength.

These concepts can also be used to explain the action under cyclic loading. If the bar is subjected to repeated load of constant magnitude, some bond deterioration will occur with each cycle which will cause a redistribution of the bond stresses, shifting the bond stress curve toward the free end while maintaining its area constant. Thus, the area under the force diagram is increased, denoting increasing bar slippage. It can also be seen that this action may cause the envelope curve to be swept by successive bond stress distributions, leading to eventual bond failure under applied load smaller than one applied monotonically.

Pullout tests under monotonic and cyclic loadings were performed on 54 specimens in order to determine strength and slip

characteristics under both types of loading. The cyclic loads were initially applied at low load levels, repeated until the slip measurements showed stabilization, then increased by 1000 lb. increments and the process repeated to failure. The points on curves of cyclically applied load versus slip which indicate stabilization were connected by curves called "load-slip curves under cyclic loading". In Fig. 2 such curves are plotted for the case of specimens with 3 inch embedment length, and compared with similar load-slip curves for monotonic loading. These results are typical of many (5), and indicate increased slip and reduced strength due to cyclic loading, as predicted by the preceding theory.

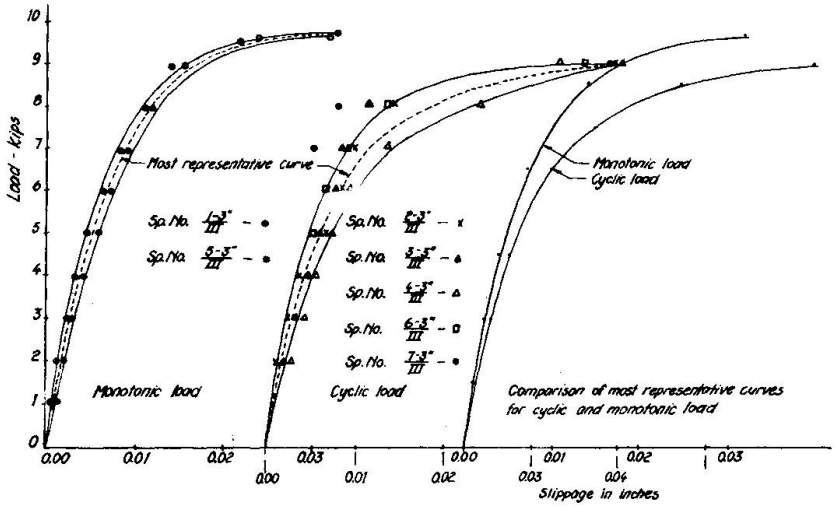

FIG. 2 - LOAD-LOADED END SLIPPAGE AND MOST REPRESENTATIVE CURVES FOR 3" EMBEDMENT LENGTH

Shear Strength of Beams under Cyclic Loading

Space limitations preclude adequate discussion of theories relating bond slip to shear failure of beams. Such theories have been based on technical beam theory (2) and on finite element analyses (3). The effect of bond deterioration which may result from repeated load histories may be summarized as follows:

1. Relative displacement of crack edges may lead to increased dowel forces which in turn may cause dowel cracking parallel to the tensile reinforcement.
2. Similarly, such widening of cracks may lead to aggregate interlock cracking, as explained by Fenwick (6).
3. Lastly, it has been shown by Krahl et. al. (2) that propagation of diagonal cracks into the compression zone may result from bond deterioration, leading to premature diagonal tension failure.

Beam Tests

To gain some insight into the shear strength of beams under cyclic loading, a series of ten simple beams, of concrete and reinforcement identical to that used in the pullout specimens, and designed to fail in shear, was tested. Most of the beams had two test sections at opposite ends of the span; one of these was tested monotonically, the other cyclically under 1000 lb. increments, loads at each level being applied repeatedly until stabilization of deflections. Instrumentation consisted of dial gages and gage plugs for the determination of concrete strains.

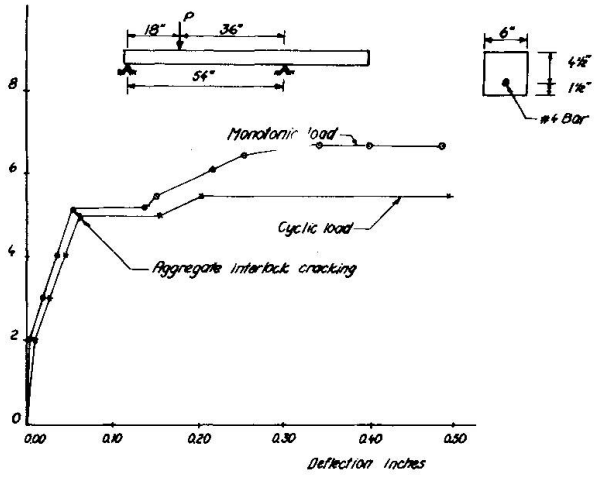

FIG. 3 - A TYPICAL LOAD-DEFLECTION CURVE FOR THE BEAMS

Fig. 3 shows a typical set of load-deflection curves for monotonically and cyclically applied loads, and Fig. 4 shows some of the beams after shear failure. A number of observations can be made on basis of these and similar results:

1. Shear failure under cyclic loading seems to occur as a consequence of aggregate interlock cracking; this occurs at a lower load applied cyclically than applied monotonically.

2. Aggregate interlock cracking seems to be somewhat more pronounced in cyclic than in monotonic loading. Prior to aggregate interlock cracking, load repetitions cause only minimal crack propagation and incremental deformations.

3. The effects of aggregate interlock cracking and dowel cracking are dominant in controlling the shear strength of beams under cyclic loading.

Conclusions

Present theories of flexural strength under cyclic load histories must be supplemented by means of predicting the cyclic shear strength under a variety of conditions. The tools for arriving at such predictions are available, but much more work is needed before the information can be applied to design of concrete structures.

References

1. Gerstle, K. H., and Tulin, L. G., "Shakedown of Continuous Concrete Beams", Proc. Int. Symp. on Repeated Loading, RILEM, Mexico City, 1966.
2. Krahl, N. W., Khachaturian, N., and Siess, C. P., "Stability of Tensile Cracks in Concrete Beams", Proc. A.S.C.E., Jnl. Struct. Div., Vol. 93, No. ST1, February 1967.
3. Nilson, A. H., "Nonlinear Analysis of Reinforced Concrete by Finite Element Method", Jnl. A.C.I., Vol. 65, No. 9, Sept. 1968.
4. Perry, E. S., and Thompson, J. N., "Bond Stress Distribution on Reinforcing Steel in Beams and Pull-out Specimens", Jnl. A.C.I., Vol. 63, No. 8, August 1966.
5. Singh, H. N., "Shear Strength of Reinforced Concrete Beams under Cyclic Loading", M.S. Thesis, University of Colorado, 1969.
6. Fenwick, R. C., and Paulay, T., "Mechanisms of Shear Resistance of Concrete Beams", Proc. A.S.C.E., Jnl. Struct. Div., Vol. 94, No. ST10, Oct. 1968.

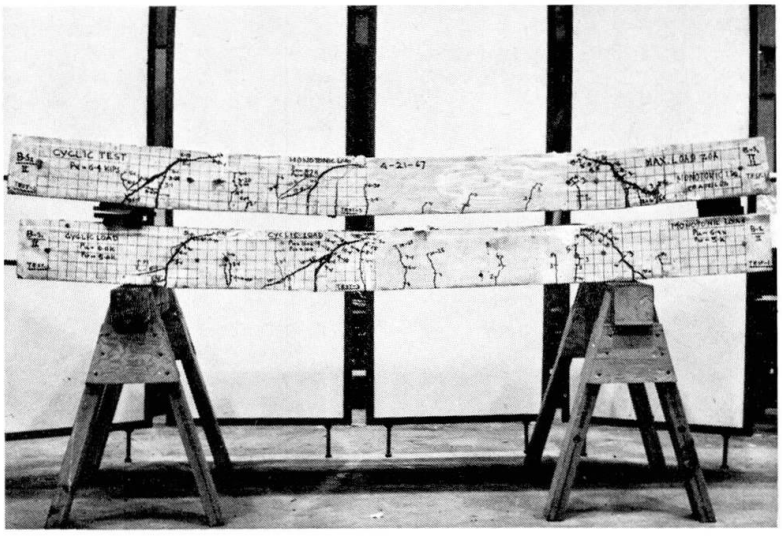

FIG. 4 - SHEAR FAILURE OF BEAMS

SUMMARY

The influence of bond deterioration on the shear strength of reinforced concrete beams under cyclic loadings has been discussed. It was shown that this bond deterioration may lead to aggregate interlock cracking, to dowel cracking, and to propagation of diagonal tensile cracks. A pilot series of beams was tested to obtain preliminary information about these effects.

RESUME

L'influence de détériorations dans l'assemblage sur la résistance au cisaillement de poutres en béton armé sous charge cyclique a été discutée. Il a été démontré que ces déteriorations peuvent donner lieu à une accumulation de fissures enchainantes, à la formation de fissures contigues et à la propagation de fissures de tension diagonales. Des essais ont été faits sur un certain nombre de poutres en vue d'obtenir des informations préliminaires sur ces effets.

ZUSAMMENFASSUNG

Der Einfluss von Schäden im Verband auf die Schubfestigkeit von Stahlbetonbalken unter zyklischer Belastung wurde diskutiert. Es wurde gezeigt, dass solche Verbandschäden zur Anhäufung ineinandergreifender Risse, zu zusammenhängender Rissbildung und zur Ausbildung diagonaler Streckrisse führen können. Eine Anzahl Balken wurde geprüft, um Vorinformationen über diese Einwirkungen zu erhalten.

Leere Seite
Blank page
Page vide

I

Analytical and Experimental Studies on the Deformation Evaluation of Reinforced Concrete Columns under Seismic Forces

Etudes analytiques et expérimentales sur l'évaluation de la déformation de colonnes en béton armé et précontraint soumises à des charges sismiques

Analytische und experimentelle Studie über die Deformationsabschätzung von Stahlbeton- und vorgespannten Stützen unter Erdbebenlasten

Hiroshi MUGURUMA
Professor of Architectural Engineering

Megumi TOMINAGA
Associate Professor of Architectural Engineering

Fumio WATANABE
Assistant Professor of Architectural Engineering

Japan

In the response analysis of middle or short height reinforced concrete structures, it is most important precisely to evaluate the stiffness degradation in the hysteresis loops because of their frequency sensitivity. It is supposed that these stiffness degradations are mainly caused by the shear deformation of reinforced concrete structural elements.

This study points out that the difficulties exists on the lack of the knowledges to estimate these shear deformations, such as the slippage of the reinforcing bars or shear cracks in the columns.

The authors proposed a research hypothesis that the deformation of the reinforced concrete columns under combined shear and flexure may be considered as the sum of individual deformation under the respective forces. The results of comprehensive experiments, including an elaborate measurement on the curvature distribution and the bond characteristics of reinforcing bars, gave a substantial support to this assumtion.

From the observed deformation mechanisms, a simple deformation model for the analytical purpose could be proposed. In this model the flexural deformation and the shear distortion may arise independently.

BASIC EXPERIMENTAL STUDY

Materials

River sand, synthetic lightweight coase aggregate (expanded shale) and portland cement were used. Mix proportion of concrete was 1:2.1:1.43 and water cement ratio, 51% by weight ratio respectively. Compressive strength of concrete at test was about 350 kg/cm^2 and the splitting tensile strength was about 19.7 kg/cm^2. Deformed bars of 19, 13, 10mm dia. (f_y = 4600 kg/cm^2) was used for longitudinal reinforcing steel and round bars of 6mm dia. (f_y = 2910 kg/cm^2) were used for the lateral reinforcing steel.

Specimens

Fig. 1 shows the details of test specimens. To obtain the

necessary informations the following widely ranged properties were given to the tested columns.

1. Shear span ratio (a/D); 1.0, 2.0 and 3.0.
2. Amount of longitudinal reinforcement P_t; 1.9, 2.54 and 3.8% in area ratio of gross steel.
3. Amount of lateral shear reinforcement P_v; 0, 0.25, 0.37, 0.75 1.50% in area ratio.

Each specimen had a rectangular section BxD = 15cm x 20cm. The number and the diameters of the longitudinal reinforcements were intentionally chosen so as to yield the same total perimeter ψ = 24cm in both compressive and tensile zones of the column respectively.

Test method

Monotonous loading tests were performed for all kinds of the specimens and reversed repeated loading tests with constant amplitude of the member rotation R = ± 0.01 rad. were performed only for the specimens of F-series with P_t = 3.8% in three kinds of shear span ratios. For comparison pure flexural tests were also performed. Fig. 2 shows the overall loading devices. Axial load was maintained so as to yield net concrete stress fc'/6 during the test.

The curvature distribution were measured by the dial gages attached to the 6mm dia. bolts buried in the specimen at intervals of 10cm. The relative displacements over the story height 2a between inner loading points were recorded as the story deflection δ or the member rotation. Also the strain distributions of the longitudinal reinforcements were measured by the electric resistance wire strain gages.

Test results

Fig. 3 shows the crack appearance of test specimens at the ultimate stage under monotonous loading, and Fig. 4 to 8 show the corresponding relationship between the shear force Q and the measured story deflection δ. Fig. 11 a), 12 a) and 13 a) show the Q-δ curves obtained from the reversed repeated loading tests for series F in which the constant amplitude of the member rotation R were ± 0.01 rad.

Observed deformation mechanisms

Flexural story deflection δ_{fl} may be obtained by the integration of the curvature distributions of the specimens measured by the attached dial gages. Shear story deflection δ_{sh} and shear strain $\gamma(Q)$ are defined by the following equations respectively.

$$\delta_{sh} = \delta - \delta_{fl}, \quad \text{and} \quad \gamma(Q) = \delta_{sh}/2a$$

In the case of the specimen with small shear span ratio, it was recognized that the experimental curves were well agreed with those calculated by the next equation before the diagonal cracks appeared.

$$(Q) = 8Q/7Bd \cdot G_c \qquad G_c = \frac{E_c}{2(1+\nu)}$$

Fig. 9 and 10 show the results of the separation between flexural and shear deformation for the specimens subjected to the monotonous loading. Also Fig. 11 c), 12 c) and 13 c) show the similar results for the specimens subjected to the reversed repeated loading.

Although the employed method of curvature measuring is not so correct, remainders from the flexural deformation are large in the case of specimens with small shear span ratios.

Fig. 14 a), 15 a) and 16 a) show the changes of strain distribution of longitudinal reinforcing steels for the F-series specimens, where the strains at the completion of axial load transferring are defined zero. Also Fig. 14 b), 15 b) and 16 b) show the changes of strain distribution of lateral shear reinforcements.

PROPOSED DEFORMATION MODEL FOR THE ANALYTICAL METHOD

This model shown in Fig. 17 represents the column deformation as the sum of the rigid body rotation for flexure and shear distortion respectively. It may be considered that the reinforced concrete prisms 2 d_c x B assumed in the compressive and tensile zones of the column may act the moment resisting role in flexure and have the simplified hysteresis rule between the axial force and the average strain as shown in Fig. 18.

Assuming that the distributions of the axial forces T_t and T_c acted to these prisms are linear and the plane section is remained plane after deformation, the concentrated displacements Δ_{top} and Δ_{bottom} may be obtained by the numerical integration of the strain distributions. Increases of the displacements due to the slippage of the longitudinal reinforcing bars are discarded in the present analysis but these may be taken into account for changing the assumption on the force distributions in the prisms.

Actual numerical computation may be carried out on the simplified model with the divided prism elements as shown in Fig. 19.

Therefore, the depth of rotation centers of the critical section in the n-th incremental stage of load may be expressed by the following equation.

$$Y^n = \left(\frac{\Delta^n_{top}}{\Delta^n_{top} - \Delta^n_{bottom}} \right)(D - 2\cdot d_c) + d_c \qquad (1)$$

Neglecting the tensile stress of concrete but considering all the compressive stress of the concrete above Y, the equivalence conditions about the axial force N and the moment M of the column are expressed as follos, referring to Fig. 19.

a) After crack development in the critical section

$$N^n = T^n_{u1} + \frac{1}{2}(y - d_c)\cdot B\cdot\sigma^n_t + T^n_{L1} \qquad (2)$$

$$M^n = (T^n_{u1} - T^n_{L1})\cdot\frac{D-2dc}{2} + \frac{1}{2}(y-dc)\cdot B\cdot\sigma^n_t\cdot\frac{(3D-10d_c-2y)}{6} \qquad (3)$$

b) Before crack development in the critical section.

$$N^n = T^n_{u1} + \frac{1}{2}(\sigma^n_t + \sigma^n_b)(D-4d_c)B + T^n_{L1} \qquad (2)'$$

$$M^n = (T^n_{u1} - T^n_{L1})\frac{D-2dc}{2} + \frac{1}{2}(\sigma^n_t - \sigma^n_b)(D-4d_c)\cdot B\cdot\frac{1}{6}(D-4d_c) \qquad (3)'$$

shear force equivalence is

$$Q^n = \frac{M^n}{a} = \tau n\cdot B\cdot y^n + \alpha\cdot\sum\sigma^n_{sv}\cdot A_v \qquad (4)$$

α : Effective coefficient of shear reinforcement

Any failure criterion of concrete under combined stress should be considered.

Total story deflection is as prescribed.

$$\delta^n = \delta^n_{fl} + \delta^n_{sh} = \left[\frac{\Delta^n_{top} - \Delta^n_{bottom}}{D - 2d_c} + \gamma^n(Q)\right]2a \qquad (5)$$

Succesive incremental calculation to the whole process produces the n+1 -th story deflection $\delta^{n+1} = \delta^n + \Delta\delta^n$.

CALCULATED RESULTS OF PRESTORING FORCE CHARACTERISTICS OF A REINFORCED CONCRETE COLUMN

For an example the specific details of the columns specimen F2 was given to the numeric calculation. The reinforced concrete prisms in the compressive and tensile zones of the column have the bredth B = 15cm and the depth $2d_c$ = 5.1cm. Both prisms are divided into four equal elements over the half distance of the story height. The reinforcing bars considered are 2-deformed bars of nominal diameter 19mm. The compressive strength f_c' and tensile one f_{sp} of concrete are 329 kg/cm^2 and 26.3kg/cm^2 respectively. The yield stress of the reinforcing bars is ± 4600 kg/cm^2. In present example the shear force effects for the column and the failure criterion of concrete under combined stress are dismissed but these factors may be easily considered in the analysis using the experimentally obtained results. Obtained hysteresis loop on the restoring force characteristics of reinforced concrete column is shown in Fig. 20. It is supposed that the difference between the experiment and analysis is caused by omitting the shear force effects.

SUMMARY

The deformations of the reinforced concrete columns under combined shear and flexure cannot be estimated only by flexural deformation. The correct solution to this problem may be achieved by taking account for the three deformation factors, i.e. conventional flexural deformation, the deformation due to the slippage of the longitudinal reinforcement and the shear distortion. This study shows an analytical method to estimate the column deformation, accompanying with the supporting experimental results.

RESUME

Les déformations des colonnes en béton armé soumises à des efforts combinés de cisaillement et de flexion ne peuvent pas être déterminées en ne tenant compte que des déformations dues à la flexion. La solution correcte de ce problème peut être obtenue en considérant les trois facteurs de déformation suivants: les déformations dues à la flexion, celles résultant du glissement des armatures longitudinales et celles dues au cisaillement. Cette étude présente une méthode analytique pour calculer les déformations de la colonne ainsi que les résultats d'essais.

ZUSAMMENFASSUNG

Die Deformation von Stahlbetonstützen unter kombiniertem Schub und Biegung kann nicht allein nur aus der Biegedeformation geschätzt werden. Die korrekte Lösung des Problems lässt sich durch Berücksichtigung der drei Deformationsfaktoren gewinnen: übliche Biege-Deformation, Deformation infolge Schlupf der Längseisen und infolge Schub. Diese Studie zeigt eine analytische Methode zur Abschätzung der Säulendeformation und die bestätigenden experimentellen Resultate.

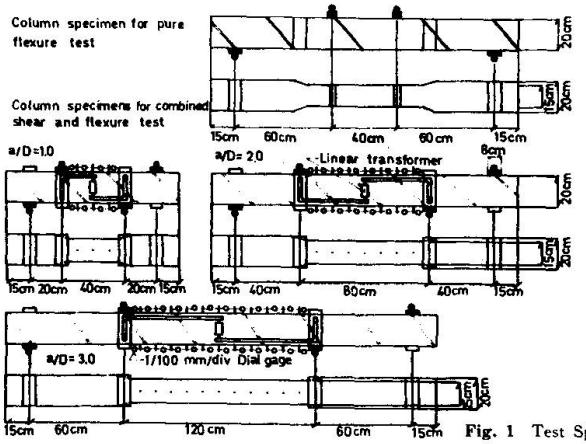

Fig. 1 Test Specimens

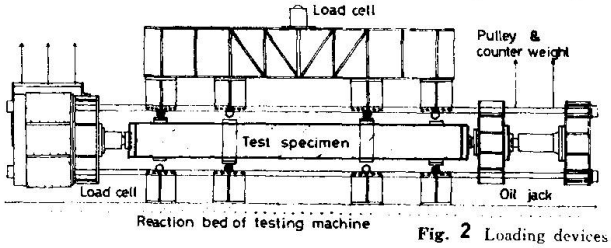

Fig. 2 Loading devices

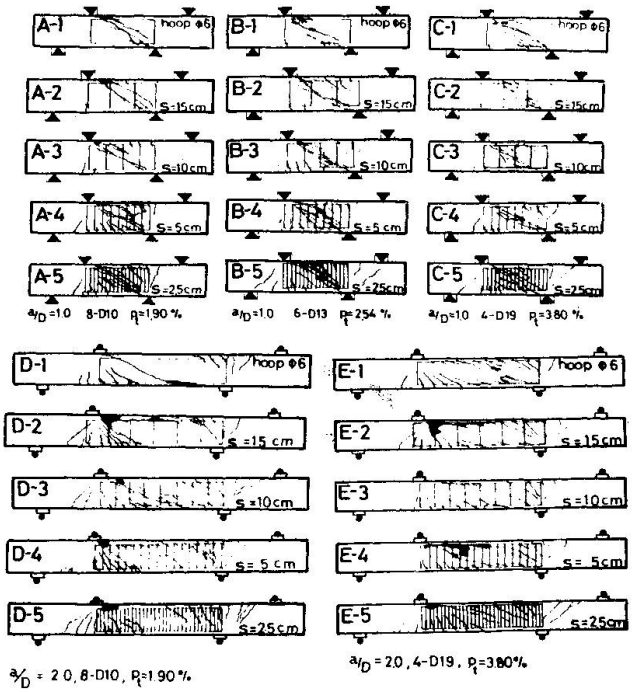

Fig. 3 Cracks of specimens at failure

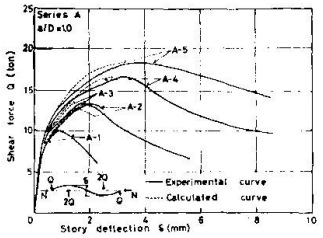

Fig. 4 Relationships between the shear force and the story deflection (a/D=1.0, p_t=1.90%)

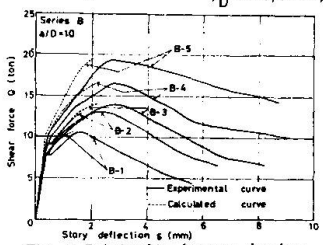

Fig. 5 Relationships between the shear force and the story deflection (a/D=1.0, p_t=2.54%)

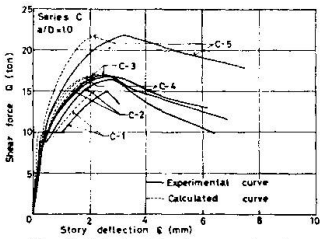

Fig. 6 Relationships between the shear force and the story deflection (a/D=1.0, p_t=3.80%)

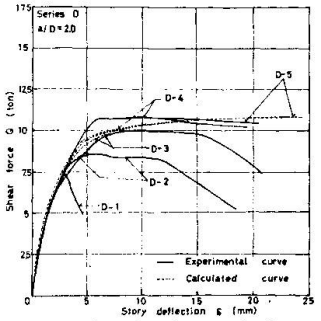

Fig. 7 Relationships between the shear force and the story deflection (a/D=2.0, p_t=1.90%)

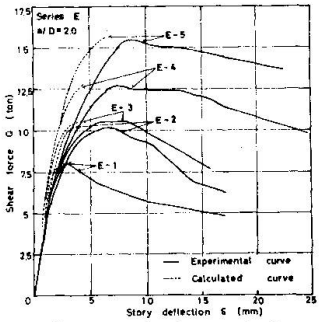

Fig. 8 Relationships between the shear force and the story deflection (a/D=2.0, p_t=3.80%)

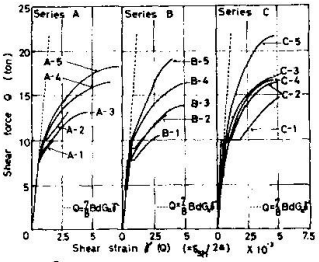

Fig. 9 Relationships between the shear force and the shear strain (a/D=1.0)

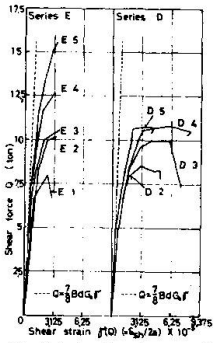

Fig. 10 Relationships between the shear force and the shear strain (a/D=2.0)

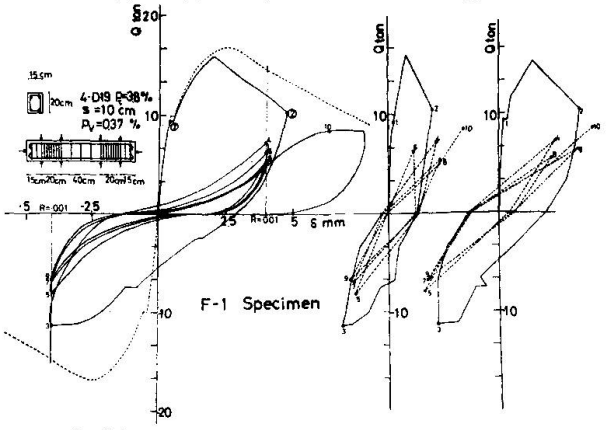

a) Q-δ curve b) Q-δ_{fl} curve c) Q-δ_{sh} curve

Fig. 11 Q-δ, Q-δ_{fl}, Q-δ_{sh} curves of F-1 specimen (a/D=1.0)

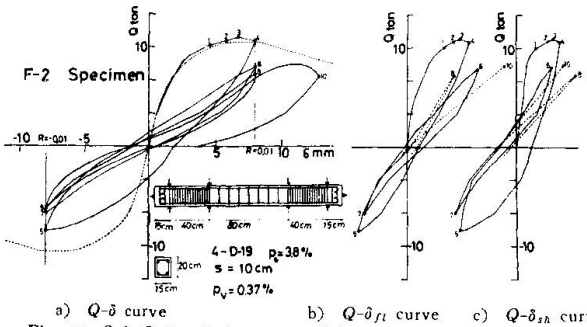

a) Q-δ curve b) Q-δ_{fl} curve c) Q-δ_{sh} curve

Fig. 12 Q-δ, Q-δ_{fl}, Q-δ_{sh} curves of F-2 specimen (a/D=2.0)

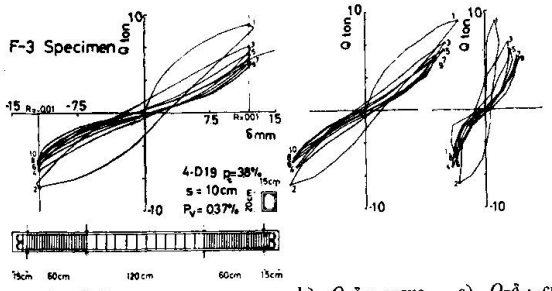

a) Q-δ curve b) Q-δ_{fl} curve c) Q-δ_{sh} curve

Fig. 13 Q-δ, Q-δ_{fl}, Q-δ_{sh} curves of F-3 specimen (a/D=3.0)

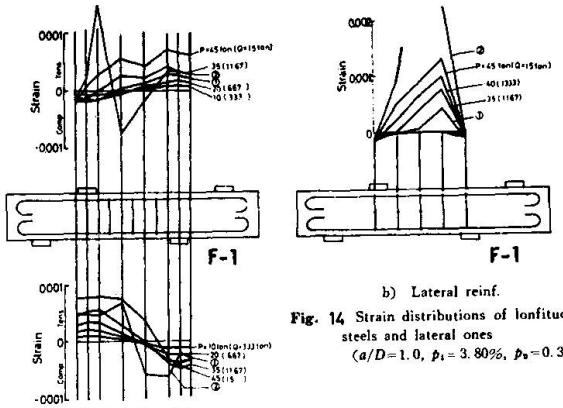

a) Longit. reinf. b) Lateral reinf.

Fig. 14 Strain distributions of lonfitudinal steels and lateral ones (a/D=1.0, p_t=3.80%, p_w=0.37%)

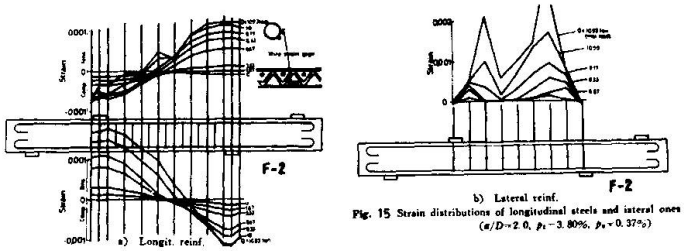

a) Longit. reinf. b) Lateral reinf.

Fig. 15 Strain distributions of longitudinal steels and lateral ones (a/D=2.0, p_t=3.80%, p_w=0.37%)

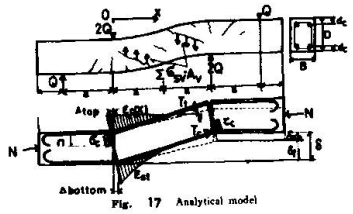

Fig. 17 Analytical model

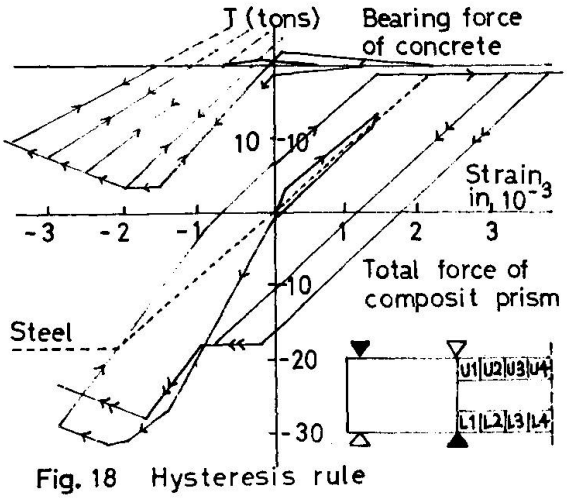

Fig. 18 Hysteresis rule

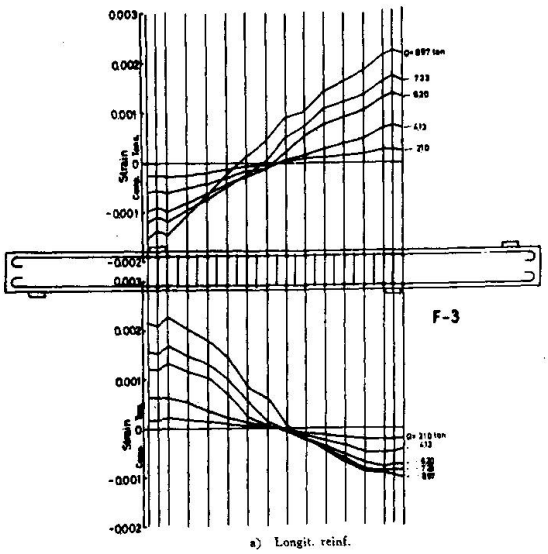

a) Longit. reinf.

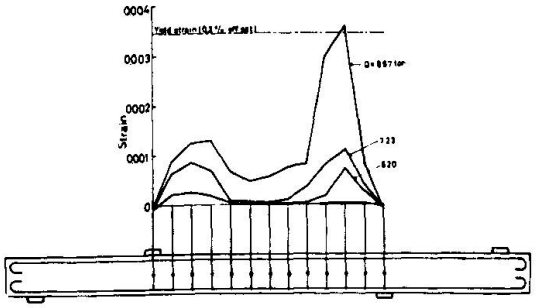

b) Lateral reinf.

Fig. 16 Strain distributions of longitudinal steels and lateral ones (a/D=3.0, p_t=3.80%, p_w=0.37%)

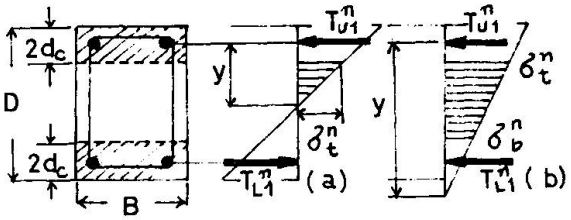

Fig. 19 Force equivalence of section

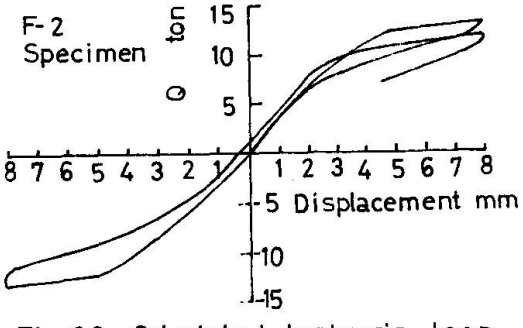

Fig. 20 Calculated hysteresis loop

An Overall Ductility Factor for Coupled Shear Walls

Un coefficient général de déformabilité pour les parois de cisaillement couplées

Ein globaler Duktilitätsfaktor für verbundene Schubwände

J. GLUCK
D.Sc. Senior Lecturer
Department of Structures
Faculty of Civil Engineering
Technion, Israel Institute of Technology
Haifa, Israel

Introduction

From studying the response of structures to strong earthquake motions it was concluded that the ability of the structure to dissipate energy by plastic deformations is very important, since an elastic analysis according to codes for earthquake resistant design is covering only moderate earthquake effects. To resist strong earthquakes the structure has to dissipate energy mainly by plastic deformations, since in modern structures the reserve of energy in non-structural elements is negligible. A common used characteristic to measure the ability of the structure to dissipate energy is the overall ductility factor, defined as the ratio between the maximum displacement at ultimate stage and the same displacement when at yield. In coupled shear walls the overall ductility factor is a direct function of the rotational ductility factor of the coupling beams defined as the ratio of the rotations at support section at ultimate, and yield. Current researches [1], [2] have shown that standard reinforced deep sprandels have a rotational ductility factor of 4 and with special diagonal reinforcing it may reach the value of 12.

For evaluation of the overall ductility factor the laminar method of analysis will be used. In this technique the coupling beams formed by vertically arranged uniform openings in a wall are replaced by infinitesimal elastic laminas of an equivalent stiffness. The displacement at yield will be involved with an elastic analysis of the coupled shear wall, a problem well covered in the literature [3], [4], while the displacementat ultimate stage requires an elasto-plastic analysis not yet completely solved. The first object of this paper is to present a solution for this problem. Approximative solutions for the elasto-plastic problem have been presented [5], [6] for the particular case where ultimate stage is reached when a collapse mechanism is formed by appearance of plastic hinges at both ends of all coupling beams and one plastic hinge develops at the base of each shear wall. In the most frequent cases the coupling beams may not supply the rotational ductility factor required by the above mentioned collapse mechanism. In this case ultimate stage is assumed to be reached when plastic hinges develop at ends of the coupling beams only over part of the height while in the remaining part they behave elastically. In the present paper this general case will be considered. Charts for evaluation of the overall ductility factor are presented for an upper triangle loading which is very often used to simulate the dynamic effect of earthquake motion.

Elastic Displacement

A prototype of a coupled shear wall is presented in Fig. 1 and its equivalent laminar model in Fig. 2. Consideration of equilibrium and compatibility condition yields the well-known differential equation of the elastic problem:

$$d^2Q/d\xi^2 - \beta^2 Q = \gamma H^2 M_o \tag{1}$$

where Q = unknown axial force function acting in the shear wall, M_o = cantilever moment produced by external load, and

$$\xi = x/H \tag{2}$$

$$\beta^2 = H^2 (\ell^2/I_o + 1/A_1 + 1/A_2) 12I^*/(hc^3) \tag{3}$$

$$\gamma = 12I^*/(hc^3 I_o) \tag{4}$$

in which H = height of the structure, ℓ = span between shear wall center lines, c = clear span of coupling beam, I^* = reduced moment of inertia of coupling beam allowing for shear distortion, I_o = sum of moments of inertia of shear wall 1 and 2, A_1, A_2 = cross setion areas of respectively shear wall 1 and 2, and h = height of story.

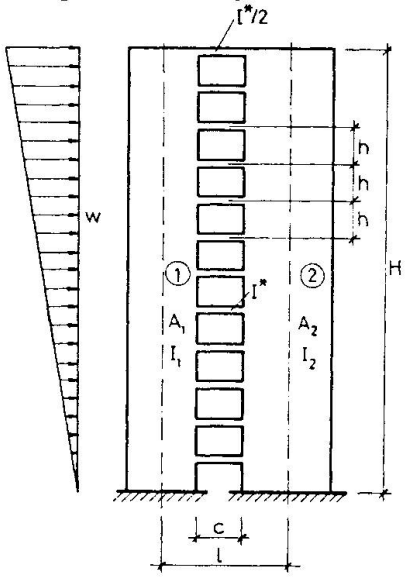

Fig. 1 Prototype of coupled shear wall.

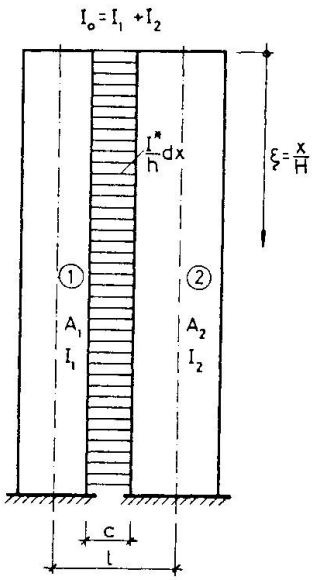

Fig. 2 Laminar model of coupled shear wall.

The solution of Eq. 1 for the normal force function Q for an upper triangle load pattern having the following moment variation

$$M_o = W H (\xi^2 - \xi^3/3) \tag{5}$$

where W = sum of lateral load, and satisfying the boundary conditions of the structure may be written in the form

$$Q = \gamma W H^3 \bar{Q}$$

where

$$\bar{Q} = C \operatorname{sh}\beta\xi + D \operatorname{ch}\beta\xi - [\xi^3/3 - \xi^2 + 2(\xi-1)/\beta^2]/\beta^2 \tag{6}$$

in which

$$C = [(2/\beta^2 - 1)/\operatorname{ch}\beta + 2(\operatorname{th}\beta)/\beta]/\beta^3 \tag{7}$$

$$D = -2/\beta^4 \tag{8}$$

The elastic displacement at the top of the wall is given by

$$EI_o y_{e\ max} = WH^3\left\{-1/15+\eta\{[C\ sh\beta+D(ch\beta-1)]+(1/5+2/\beta^2)/3\}/\beta^2-F\right\} \quad (9)$$

where

$$\eta = \gamma H^2 \ell \quad (10)$$

$$F = \eta[C\ ch\beta+D\ sh\beta+(1/\beta+1/4)/\beta]/\beta-1/4 \quad (11)$$

Elasto-Plastic Displacement

The general case where the rotational ductility factor of the laminas does not enable an ultimate stage with full laminar plastification is considered. In this case the ultimate stage will be reached when at the upper and lower zones or the lower zone only the laminas will behave elastically, while in the middle zone the laminas will have formed plastic hinges at their supports (see Fig. 3). To express equilibrium and continuity it is convenient to replace in the middle zone the fixed ends of the lamina supports by hinges acted by known external moments and shear forces representing the action of the ultimate laminar shear. The analytical scheme thus obtained will be treated as an elastic system acted by lateral load and distributed shear and moments at the hinged ends of the laminas of the middle zone, as shown in Fig. 4.

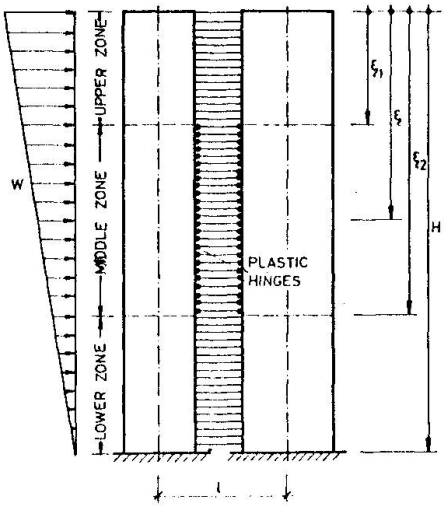

Fig. 3 Laminar model with plastified laminas in the middle zone.

The govering differential equation of the problem and boundary conditions will be obtained by applying the Principle of Least Work. The complementary energy will be expressed as function of the three unknown normal force functions acting along the center lines of the shear walls in the upper, middle and lower zones, denoted respectively by Q_s, Q_m and Q_i.

The complementary strain energy may be expressed in the form

$$\begin{aligned} 2EU = H\{&\int_o^{\xi_1}[hc^3(Q_s')^2/(12I^*)+(M_o-\ell Q_s)^2/I_o+(1/A_1+1/A_2)Q_s^2]d\xi + \\ &\int_{\xi_1}^{\xi_2}[hc^3(Q_m')^2/(12I^*)+(M_o-\ell Q_m)^2/I_o+(1/A_1+1/A_2)Q_m^2]d\xi + \\ &\int_{\xi_2}^{\xi_1}[hc^3(Q_i')^2/(12I^*)+(M_o-\ell Q_i)^2/I_o+(1/A_1+1/A_2)Q_i^2]d\xi\} \end{aligned} \quad (12)$$

The complementary energy as given in Eq. 12 is a function of , Q_s, Q_s', Q_m, Q_m', Q_i and Q_i'. According to the principle of Least Work the first variation of the complementary energy with respect to the functions Q_s, Q_s', Q_m, Q_m', Q_i and Q_i' must vanish. The ultimate laminar shear q_u being known, the axial force function in the middle zone may be expressed in the form

$$Q_m = Q_1+q_u H(\xi-\xi_1) \quad (13)$$

After variation of Eq. 12 and substituting in it Eq. 13 and effectuating the integration by part, results

$$\begin{aligned} &-\int_o^{\xi_1}(Q_s''-\beta^2 Q_s+\gamma H^2 M_o)\delta Q_s d\xi - H^2(Q_o'\delta Q_o-Q_1'\delta Q_1) \\ &+[\beta^2(\xi_2-\xi_1)(Q_1+q_u(\xi_2-\xi_1)/2)-\gamma WH^3((\xi_2^3-\xi_1^3)/3-(\xi_2^4-\xi_1^4)/12)]\delta Q_m - H^2 q_u(\delta Q_1-\delta Q_2) - \\ &-\int_{\xi_1}^{1}(Q_i''-\beta^2 Q_i+\gamma H^2 M_o)\delta Q_i d\xi - H^2 Q_H'\delta Q_H - H^2(Q_2'\delta Q_2-Q_H'\delta Q_H) = 0 \end{aligned} \quad (14)$$

where Q_o, Q_1 and Q_2, Q_H = the values of respectively Q_s and Q_i at ordinates $(0, \xi_1)$ and $(\xi_2, 1)$.

As the variations δQ_s, δQ_i and δQ_1 are arbitrary, Eq. 14 leads to the following Euler Differential equations expressing compatibility at the upper and lower zones.

$$Q_s''-\beta^2 Q_s+\gamma H^2 M_o = 0 \qquad (0 < \xi < \xi_1) \qquad (15)$$

$$Q_i''-\beta^2 Q_i+\gamma H^2 M_o = 0 \qquad (\xi_2 < \xi < 1) \qquad (16)$$

and the following algebraic equation expressing the compatibility condition for the middle zone:

$$\beta^2(\xi_2-\xi_1)(Q_1+q_u H(\xi_2-\xi_1)/2)-\gamma WH^3((\xi_2^3-\xi_1^3)/3 -(\xi_2^4-\xi_1^4)/12) = 0 \qquad (17)$$

The physical meaning of this condition is zero relative vertical gap between upper and lower limiting sections of the wall in the middle zone.

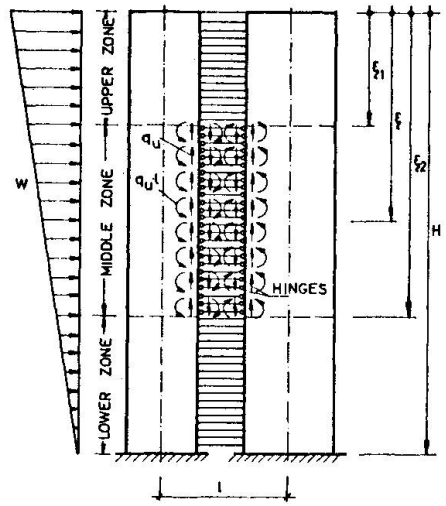

Fig. 4 Analytical model with applied loads.

Assuming a variation of the Q_s function so that $\delta Q_o=0$, and $\delta Q_1\neq 0$ and the variation of the Q_i function so that $\delta Q_2\neq 0$, and $\delta Q_H\neq 0$, the following boundary conditions result

$$Q_o = 0 \quad ; \quad Q_1' = 0 \qquad (18),(19)$$

$$Q_2' = 0 \quad ; \quad Q_H' = 0 \qquad (20),(21)$$

Eq. 17 together with the following equilibrium equation at limiting section between middle and lower zone

$$Q_2 = Q_1 + q_u H(\xi_2 - \xi_1) \qquad (22)$$

will serve to determine the limiting ordinates ξ_1 and ξ_2.

The solution for the upper zone represented by Eq. 15 satisfying the boundary conditions given by Eqs. 18 and 19, has the same form as that given by Eq. 6, where the coefficients C and D are replaced by C_s and D_s having the values:

$$C_s = [2(sh\beta\xi_1)/\beta^3+(\xi_1^2-2\xi_1+2/\beta^2)/\beta^2+\bar{q}_u]/(\beta ch\beta\xi_1) \qquad (23)$$

$$D_s = -2/\beta^4 \qquad (24)$$

where

$$\bar{q}_u = q_u/(\gamma WH^2) \qquad (25)$$

The normal forces in the middle zone are given by Eq. 13.

The solution for the lower zone represented by Eq. 16 satisfying the boundary conditions given by Eqs. 20 and 21 has as well the same form as that given by Eq.6, where the coefficients C and D are replaced by C_i and D_i having the values:

$$C_i=\{(2/\beta^2-1)/(\beta^2 ch\beta)-[(2/\beta^2-1)ch\beta\xi_2/(\beta^2 ch\beta)-(\xi_2^2-2\xi_2+2/\beta^2)/\beta^2 -\bar{q}_u]th\beta/(th\beta ch\beta\xi_2-sh\beta\xi_2)\}/\beta \qquad (26)$$

$$D_i=[(2/\beta^2-1)ch\beta\xi_2/(\beta^2 ch\beta)-(\xi_2^2-2\xi_2+2/\beta^2)-\bar{q}_u]/[\beta(th\beta ch\beta\xi_2-sh\beta\xi_2)] \qquad (27)$$

In the particular case when the plastification of the coupling beam ends extend until the top of the wall, there will be only two zones; a plastic one in the upper part and an elastic one in the lower part, with the limiting section having ordinate ξ_2. The axial force in the plastified zone will be given by

$$Q_m = q_u H\xi \qquad (28)$$

and that in the elastic zone will be the same as that of the lower zone, mentioned above.

The elasto-plastic displacement at the top of the wall is given by

$$y_{p\ max} = H\int_1^{\xi_2}\phi_s d\xi + H\int_{\xi_2}^{\xi_1}\phi_m d\xi + H\int_{\xi_1}^{1}\phi_i\, d\xi \qquad (29)$$

where

$$EI_o\phi_s = H\int(M_o - Q_s\ell)d\xi + F_s \tag{30}$$

$$EI_o\phi_m = H\int(M_o - Q_m\ell)d\xi + F_m \tag{31}$$

$$EI_o\phi_i = H\int(M_o - Q_i\ell)d\xi + F_i \tag{32}$$

in which F_s, F_m and F_i = constants of integration to be determined from the following boundary conditions:

1. Full restrain at support: $(\phi_i)_{\xi=1} = 0$ (33)

which leads to $F_i=\eta[(C_i ch\beta+D_i sh\beta)+(1/\beta^2+1/4)/\beta]/\beta-1/4$ (34)

2. Continuity of deflection line at $\xi=\xi_2$: $(\phi_i)_{\xi=\xi_2}=(\phi_m)_{\xi=\xi_2}$ (35)

which leads to $F_m=\eta\{\bar{Q}_1\xi_2+\bar{q}_u(\xi_2^2/2-\xi_1\xi_2)$

$$-(C_i ch\beta\xi_2+D_i sh\beta\xi_2)/\beta-[\xi_2^3/3-\xi_2^4/12-2(\xi_2^2-\xi_2)/\beta^2]/\beta^2\}+F_i \tag{36}$$

3. Continuity of deflection line at $\xi=\xi_1$: $(\phi_m)_{\xi=\xi_1}=(\phi_s)_{\xi=\xi_1}$ (37)

$$F_s=\eta\{(C_s ch\beta\xi_1+D_s sh\beta\xi_1)/\beta$$

$$+[\xi_1^3/3-\xi_1^4/12-2(\xi_1^2/2-\xi_1)/\beta^2]/\beta^2-\bar{Q}_1\xi_1+\bar{q}_u\xi_1^2/2\}+F_m \tag{38}$$

where

$$\bar{Q}_1 = Q_1/(\gamma WH^3) \tag{39}$$

Substituting the corresponding relations in Eq. 29 and integrating yields

$$EI_o y_{p\,max}=WH^3\{\eta\{[C_s sh\beta\xi_1+D_s(ch\beta\xi_1-1)+C_i(sh\beta-sh\beta\xi_2)+D_i(ch\beta-ch\beta\xi_2)$$

$$+(\xi_1^4-\xi_2^4)/12-(\xi_1^5-\xi_2^5)/60+1/15+(\xi_1^2-\xi_2^2-\xi_1^3/3+\xi_2^3/3+2/3)/\beta^2]/\beta^2-\bar{Q}_1(\xi_1^2-\xi_2^2)/2$$

$$-\bar{q}_u[(\xi_1^3-\xi_2^3)/6-{}_1(\xi_1^2-\xi_2^2)/2]\}-1/15-F_s\xi_1+F_m(\xi_1-\xi_2)+F_i(\xi_2-1)\} \tag{40}$$

The overall ductility factor of the coupled shear wall will be now

$$\mu_o = y_{p\,max}/y_{e\,max} \tag{41}$$

The graphs shown in Fig. 5 a,b,c,d may serve to establish the value of μ_o as

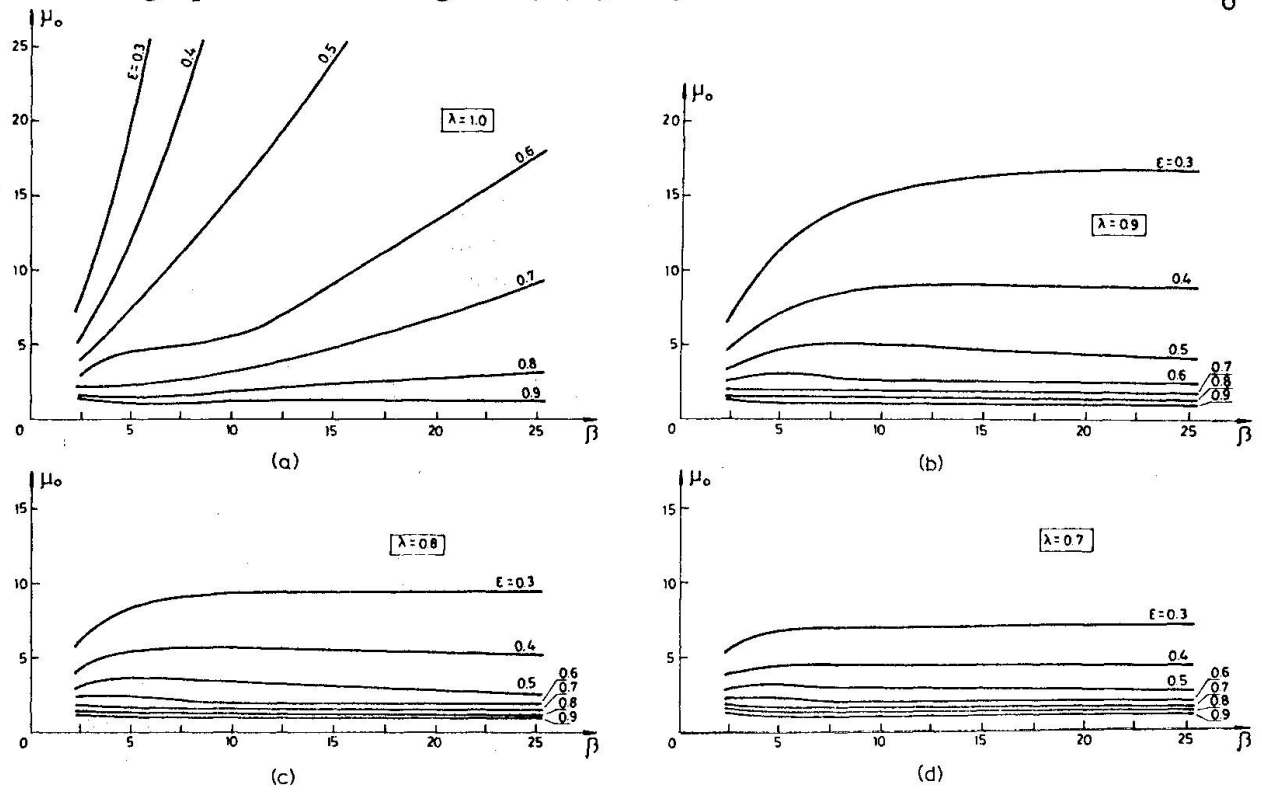

Fig. 5 Overall ductility factor.

function of β for various values of $\lambda=\eta/\beta^2$ and $\varepsilon=q_u/q_{max}$, where q_{max}= the maximum elastic laminar shear.

An important factor to be considered is the rotational ductility factor of the coupling beam end, which in fact limits the value of the ultimate laminar shear q_u to be taken in Eq. 40.

Considering the elastic wall rotations and extensional deformations it may be shown easily that the plastic laminar rotation at any height ξ as shown in Fig. 6 is given by:

$$\phi_p = \phi\ell/c - (d_1+d_2)/c - \phi_y \qquad (42)$$

where = the elastic rotation of the wall and ϕ_y = yield rotation of the coupling beam, which is related to the ultimate laminar shear as follows

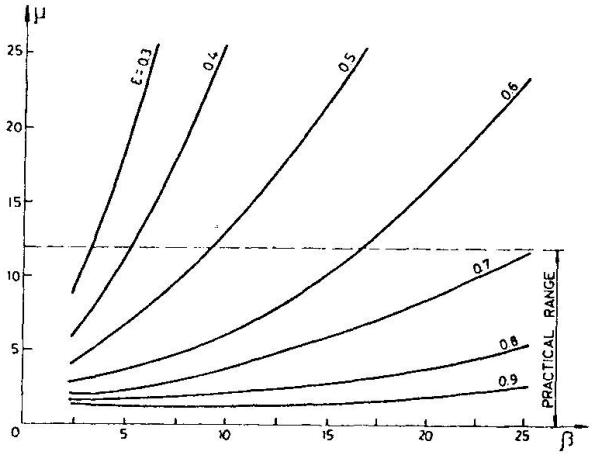

Fig. 7 Rotational ductility factor of coupling beam end.

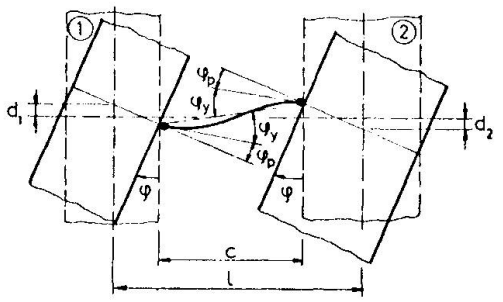

Fig. 6 Deformed position of shear wall and plastified lamina.

$$\phi_y = hc^2 q_u/(12(EI^*)) \qquad (43)$$

The rotational ductility factor at the support of the lamina will be

$$\mu = (\phi_{p\ max} + \phi_y)/\phi_y \qquad (44)$$

where $\phi_{p\ max}$= the maximum value of the plastic rotation.

The graphs given in Fig. 7 may serve to determine the rotational ductility factor as function of β for various values of q_u/q_{max}

References

1. Pauly, T., "Coupling Beams of Reinforced Concrete Shear Walls", J. of the Struc. Div., ASCE, Vol. 97, No.ST3, Proc. Paper 7984, March 1971, pp. 843-862.
2. Pauly, I., "Simulated Seismic Loading of Sprandel Beams", J. of the Struc. Div.,ASCE, Vol.97, No.ST9, Proc.Paper 8365, Sept.1971, pp. 2404-2419.
3. Beck, H., "Contribution to the Analysis of Coupled Shear Walls", ACI J., Proc. V. 59, August 1962, pp. 1055-1070.
4. Rosman, R., "Beitrag zur Statischen Berechnung Waagrecht Belasteter Querwaende bei Hochbauten", Der Bauingenieur, V. 35, No. 4, April 1960, S. 133-136.
5. Pauly, T., "Elasto-Plastic Analysis of Coupled Shear Walls", ACI J., Proc. V. 67, Nov. 1970, pp. 915-922.
6. Winokur, A. and Gluck, J., "Ultimate Strength Analysis of Coupled Shear Walls", ACI J., Proc. V. 65, Dec. 1968, pp. 1029-1036.

SUMMARY

An analytical procedure for establishing the overall ductility factor for coupled shear walls is presented. The continuum approach was applied by assuming an upper triangle lateral load pattern, very often used to simulate earthquake motion effect. Plastification of the coupling beam ends may be on part or over the whole height. The graphs presented may be used for direct evaluation of the overall ductility factor and associated with it the rotational ductility of the coupling beam end.

RESUME

Ce travail présente une méthode analytique pour déterminer le coefficient général de déformabilité des parois de cisaillement couplées. On utilise un processus d'approximation en admettant un modèle de charge latérale en triangle au sommet de la paroi, modèle qui est souvent utilisé pour simuler les effets des mouvements sismiques. La plastification des extrémités des barres de liaison peut être admise sur une partie ou sur toute la hauteur. Les diagrammes présentés peuvent être utilisés pour l'évaluation directe du coefficient général de déformabilité et, associée à ce dernier, pour la détermination de la déformabilité rotationnelle de l'extrémité de la barre de liaison.

ZUSAMMENFASSUNG

Es wird eine analytische Methode zur Bestimmung eines globalen Duktilitäts-faktors für verbundene Schubwände vorgelegt. Die Kontinuums-Näherung wurde unter Annahme einer nach oben zunehmenden dreieckigen horizontalen Last-Verteilung angewendet, die sehr oft zum Simulieren von Erdbebeneffekten verwendet wird. Plastifizierung der verbindenden Stabenden kann über einen Teil oder über die ganze Höhe auftreten. Die angegebenen graphischen Darstellungen können zur direkten Ermittlung des globalen Duktilitätsfaktors und mit ihm die Rotationsduktilität der verbindenden Stabenden verwendet werden.

Leere Seite
Blank page
Page vide

Cyclic Load-deflection Curves of Multi-storey Strain-hardening Frames Subjected to Dead and Repeated Alternating Lateral Loadings

Courbes cycliques charge-déformation de cadres à plusieurs étages soumis à des charges latérales dynamiques alternées

Zyklische Lastausbiegungs-Kurven von mehrstöckigen aussteifenden Rahmen unter Eigengewicht und wiederholter, wechselnder horizontaler Last

Yoshitsura YOKOO Prof. Dr. Eng.
Tsuneyoshi NAKAMURA Assoc. Prof., Ph.D.Dr. Eng.
Department of Architecture
Kyoto University

Shuzo ISHIDA Assoc. Prof.
Takashi NAKAMURA
Department of Architecture
Kyoto Technical University

Kyoto, Japan

1. INTRODUCTION

A rational theoretical investigation of the nonlinear behavior of a framed structure subjected to complicated alternating repeated loads must be based upon (1) an accurate stress-strain relation of the constituent structural material and the corresponding accurate cross-sectional force-generalized strain relations and (2) an accrate numerical method of analysis which is able to incorporate therein the complicated constitutive equations of the material and of the members. So far as the overall nonlinear behavior of a frame is to be investigated theoretically, any approximate formulation for the problem (1) must always be made, with the aim of and in a form convenient for, generating an accurate member-or element-stiffness or flexibility matrix which can be used on a computer currently available. While some complicated equations may be indispensable for describing complex nonlinear behaviors of a member with a considerable accuracy, it will be necessary to introduce some approximation in accordance with its aim.

The present contribution to the prepared discussion describes first an efficient computational method of analyzing nonlinear static and dynamic behaviors of multi-story plane steel frames. The method takes into account the gravity effect due to large deflection, incorporates the bilinear or nonlinear hysteretic stress-strain relation for a structural steel and is able to trace gradual spreading or diminishing of strain-hardening regions along member axes. Since the general idea of the authors' (Nakamura and Ishida) method has been presented in [1], the details of the procedure of generating an elastic-plastic member-stiffness matrix applicable to incremental large deflection analysis are described here. It is at this stage that the appropriateness of an approximate formulation of the stress-strain relation and of the corresponding axial force-moment-curvature relation is assessed with respect to its applicability to an overall frame. Although the numerical results in this prepared discussion are based upon the bilinear hysteretic stress-strain relation, the proposed method is of such a formulation that is able to incorporate a nonlinear hysteretic stress-strain rela-

tion. The senior authors' (Yokoo and Nakamura) contribution to the prepared discussion on Theme III presents a nonstationary hysteretic stress-strain relation and an approximate formulation of the moment-curvature relation under the presence of an axial force with the intention of incorporating them in the present method of generating the member-stiffness matrix. Some numerical results of the static load-deflection analysis of multi-story frames subjected to dead and alternating repeated lateral loads and of the dynamic analsis of the frames subjected to an amplified earthquake disturbance of a recorded wave form are presented in order to illustrate the efficiency of the method and to clarify the gravity effect and the effect of strain-hardening.

2. ELASTIC-PLASTIC MEMBER-STIFFNESS MATRIX FOR INCREMENTAL LARGE DEFLECTION ANALYSIS

Each member having an idealized sandwich section is treated as one element for its elastic response and then subdivided automatically in the program into as many elements as are necessary as the strain-hardening regions spread thereover. For the purpose of generating an accurate member-stiffness matrix, the transfer matrix technique in a form extended so as to incorporate the effect of accumulated large deflection, is applied to the member as a subsystem consisting of one-dimensionally connected elements. The essential steps of generating a member-stiffness matrix are as follows:(1) Derivation of an element-stiffness matrix [1] for a cantilever element as shown in Fig.1 in a local coordinate system, in a form excluding the rigid-body displacements; (2) Transformation of the cantilever element-stiffness matrix into an expanded form with respect to a global coordinate system of the member so as to incorporate the rigid-body displacements; (3) Sequential interconnection of the expanded element-stiffness matrices by the transfer matrix technique; (4) Transformation of the contracted transfer matrix into the member-stiffness matrix with respect to the member end forces and displacements. For the convenience of and in view of the accuracy consistent with the numerical integration with respect to time, the rate of a field variable is directly approximated by a finite increment and the problem for any incremental step is linearized without iteration for the nonlinear effect within the step.

2.1 TRANSFORMATION OF INCREMENTAL ELEMENT-NODAL DISPLACEMENT VECTOR

The nodal displacement vector $\{d_a\}=\{u_a,\ v_a,\ \theta_a\}^T$ for a cantilever element shown in Figs.1 and 2 in the local coordinates is transformed into the vector $\{D\}=\{U_a,\ V_a,\ \Theta_a,\ U_b,\ V_b,\ \Theta_b\}^T$ in the global coordinates by

$$\{d_a\}=[[T_R]^T\,|\,-[T_R]^T]\{D\}+[T_R]^T\{1,\ 0,\ 0\}^T-\{1,\ 0,\ 0\}^T, \tag{1}$$

where all the displacement components have been nondimensionalized with respect to l, the length of the undeformed element and where

$$[T_R]=\begin{bmatrix} c & -s & 0 \\ s & c & 0 \\ 0 & 0 & 1 \end{bmatrix}, \quad c=\cos\Theta_b \text{ and } s=\sin\Theta_b \tag{2}$$

The linear incremental transformation equation may be written as

$$\{\Delta d_a\}=[[T_R]^T\,|\,-[T_R]^T]\{\Delta D\}+[[\Delta T_R]^T\,|\,-[\Delta T_R]^T]\{D\}+[\Delta T_R]^T\{1\ 0\ 0\}^T,$$

where

$$[\Delta T_R]=\begin{bmatrix} -s & -c & 0 \\ c & -s & 0 \\ 0 & 0 & 0 \end{bmatrix}\Delta\Theta_b=\begin{bmatrix} -s & -c & 0 \\ c & -s & 0 \\ 0 & 0 & 0 \end{bmatrix}[0\ 0\ 0\ 0\ 0\ 1]\{D\}. \tag{3}$$

$$\tag{4}$$

In view of Eq.(4), Eq.(3) may be reduced to the form

$$\{\Delta d_a\}=[T]\{\Delta D\}, \tag{5}$$

where

$$[T]=\begin{bmatrix} [T_R] \\ \hline -[T_R][H] \end{bmatrix}^T \quad \text{and} \quad [H]=\begin{bmatrix} 1 & 0 & 0 \\ 0 & 1 & 0 \\ -v_a & 1+u_a & 1 \end{bmatrix}. \tag{6a,b}$$

2.2 TRANSFORMATION OF INCREMENTAL ELEMENT-NODAL FORCE VECTOR

The transformation law between the nondimensionalized nodal force vector $\{p_a\}=\{p_a \ q_a \ r_a\}^T$ for the cantilever element in the local coordinates and the vector $\{P\}=\{P_a \ Q_a \ R_a \ P_b \ Q_b \ R_b\}^T$ in the global coordinates may be written, directly from the contragradient law, as

$$\{P\}=[T]^T\{p_a\}. \tag{7}$$

Eq.(7) can of course be derived directly by writing equilibrium equations. The linear incremental transformation equation may be written as

$$\{\Delta P\}=[T]^T\{\Delta p_a\}+[\Delta T]^T\{p_a\} \tag{8}$$

The second term of the right hand side of Eq.(8) may be transformed into the expression in terms of $\{\Delta D\}$, i.e.

$$\{\Delta T\}^T\{p_a\}=[P_a]\{\Delta D\} \tag{9}$$

where

$$[P_a]=\begin{bmatrix} [0] & \{F_a\} \\ \hline \{F_a\}^T & M_a \end{bmatrix}, \qquad \{F_a\}^T=\{-Q_a \ P_a \ 0 \ Q_a \ -P_a\} \tag{10a-c}$$

$$M_a = -q_a v_a - P_a(1+u_a)$$

2.3 EXPANDED ELEMENT-STIFFNESS MATRIX

Let $[\kappa]$ denote the 3×3 element-stiffness matrix in the local coordinates, as has been derived in [1]. The stiffness equation

$$\{\Delta p_a\}=[\kappa]\{\Delta d_a\}. \tag{11}$$

incorporates not only the effect of large deflection but also the strain-hardening effect. Substitution of Eqs.(9), (11) and (5) into Eq.(8) provides

$$\{\Delta P\}=[\kappa_G]\{\Delta D\}, \tag{12}$$

where

$$[\kappa_G]=[[T]^T[\kappa][T]+[P_a]] \tag{13}$$

is the desired expanded element-stiffness matrix in the global coordinates.

2.4 INCREMENTAL MEMBER-STIFFNESS EQUATION

Eq.(12) may further be rewritten in terms of the state vectors to define the field transfer matrix for the element. By applying the standard procedure of the transfer matrix method to a member j consisting of several elements, the field transfer matrix in terms of the state vectors at the left and right ends of the member can be derived. The resulting state equation may readily be reconverted into the desired incremental member-stiffness equation.

3. COMPUTATIONAL METHOD

The displacement increment method developed by the present authors (Nakamura and Ishida [2,3]) in 1969 for the second-order analysis of elastic-perfectly plastic frames, has been applied to obtain load-displacement curves of the strain-hardening frames subjected to piecewise proportional loading. The method is simply to convert the ordinary system stiffness equation

$$[K]\{\Delta u\}=\Delta\lambda\{f\} \tag{14}$$

in terms of the nodal displacement vector $\{\Delta u\}$ and the nodal force

vector $\Delta\lambda\{f\}$ prescribed by the load factor $\Delta\lambda$, into the form

$$[K^*]\{\Delta u^*\}=-\Delta u_i\{k_i\} \tag{15}$$

where

$$[K^*]=[\{k_1\}\{k_2\}\cdots\cdots\{k_{i-1}\}\{f\}\{k_{i+1}\}\cdots\cdots\{k_n\}], \tag{16a}$$

$$\{\Delta u^*\}=\{\Delta u_1\ \Delta u_2\cdots\cdots\Delta u_{i-1}\ -\Delta\lambda\ \Delta u_{i+1}\cdots\cdots\Delta u_n\}^T, \tag{16b}$$

and to solve Eq.(15) for a prescribed increment Δu_i of a representative displacement u_i. This method enables one to trace load-displacement curves beyond their elastic-plastic limit points at which [k] becomes "singular" or computationally "nearly singular". For dynamic analysis, Wilson-Clough's method of numerical integration with respect to time has been utilized.

4. NUMERICAL RESULTS

4.1 VERIFICATION OF THE ACCURACY OF THE MEMBER-STIFFNESS MATRIX

Fig.4 shows the load-deflection curve of a cantilever column (shown in Fig.3) subjected to a constant axial force and a repeated alternating lateral load. The numerical result agrees almost precisely with the analytical result due to Nakamura [4]. Fig.6 shows the load-deflection curve for a roller-supported beam (Fig.5) subjected to a constant axial force and a repeated alternating lateral load. The result appears to exhibit a fairly good numerical simulation of the actual behavior shown in Fig.7 which was obtained experimentally by the senior authors [5]. While the value 0.01E of the linear strain-hardening coefficient has not been derived by any approximation theory for equivalence and while the accuracy of simulation of the behavior near the shoulder portions can not be said to be good, yet the result seems to promise the effect of refinement by incorporating the nonlinear hysteretic stress-strain relations for the flanges of equivalent sandwich sections.

4.2 NUMERICAL INVESTIGATION OF THE LARGE-DEFLECTION ELASTIC-PLASTIC BEHAVIORS OF LINEAR STRAIN-HARDENING MULTI-STORY FRAMES OF ONE-BAY

Fig.8 shows the dimensions of the model frame. Three frames have been designed for the base shear coefficient values S_B=0.05, 0.10 and 0.15. The method of minimum weight design [6] was applied in a modified form to the frames with the assumed inverted triangular lateral force distribution and with an *a priori* estimate of the PΔ-effect based upon a linear sidesway mode. The numbers in the round bracket in Fig.8 denote the cross-sectional areas of the members of the frame designed for S_B=0.10. Fig.9 shows the load-top displacement curves of the three frames under uniformly distributed one-way lateral loads. Fig.10 shows the *overall* force-displacement curves [3] of the same result. Fig.11 and 12 show respectively the load-top displacement curves and the corresponding *overall* force-displacement curves of the three frames under uniformly distributed alternating lateral loads repeated with a constant top-displacement amplitude. It can readily be observed that the first maximum loads are almost proportional to S_B and that the load-displacement curves for a frame designed for a smaller S_B exhibit more deterioration. The hysteresis loop for S_B=0.15 has converged more rapidly to a steady-state loop, whereas the loop for S_B=0.05 exhibits a gradual cyclic deterioration.

The numerical experiments for the effect of member stiffness distribution on the hysteresis loops have also been carried out but no significant effect has been found. Incidentally, the computation time for one incremental step was about 1~2 sec. on a FACOM 230-60 computer.

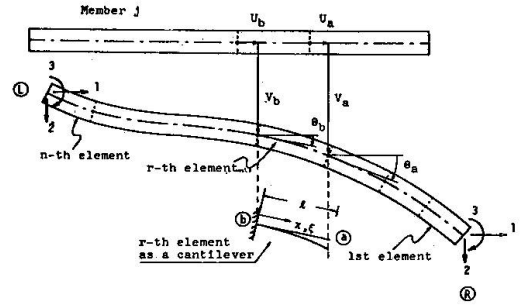

Fig.1 COORDINATES FOR A MEMBER AND FOR AN ELEMENT

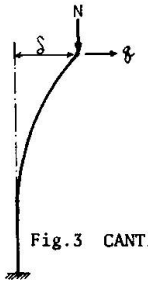

S_{MAX} = CONST

N/N_p = 0.3

E'/E = 0.01

Fig.3 CANTILEVER SPECIMEN

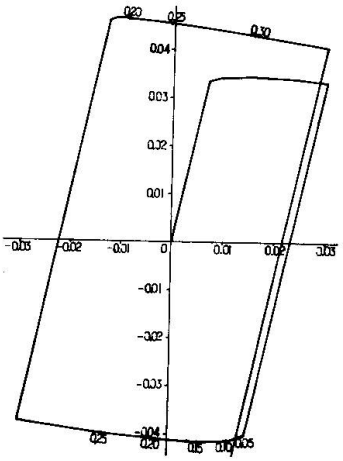

Fig.4
LOAD-DEFLECTION CURVE
FOR CANTILEVER

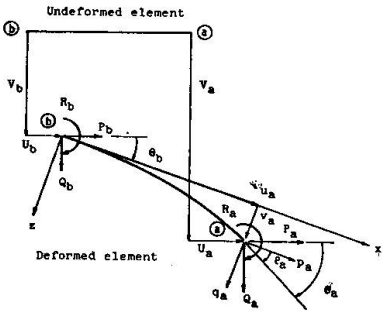

Fig.2 LOCAL AND GLOBAL COORDINATES FOR AN ELEMENT

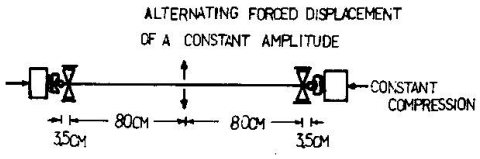

SPECIMEN DIMENSION	
AREA	23.6 cm^2
SECTIONAL MOMENT OF INERTIA	376 cm^4
HALF SPAN LENGTH	80 cm
COMPRESSIVE YIELD STRESS	3.02 t/cm^2
TEST CONDITION	
AXIAL FORCE RATIO	0.567
FORCED DEFLECTION AMPLITUDE	14.8 cm

Fig.5 SIMPLE BEAM SPECIMEN

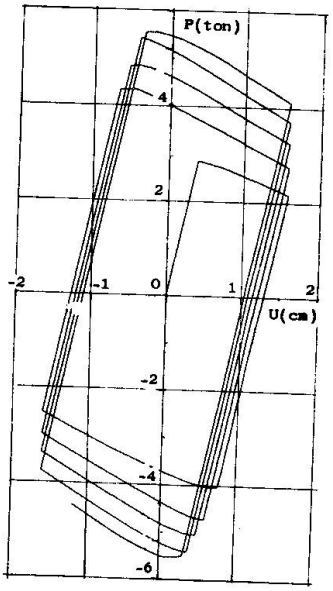

Fig.6 COMPUTED LOAD-DEFLECTION CURVE FOR SIMPLE BEAM SPECIMEN

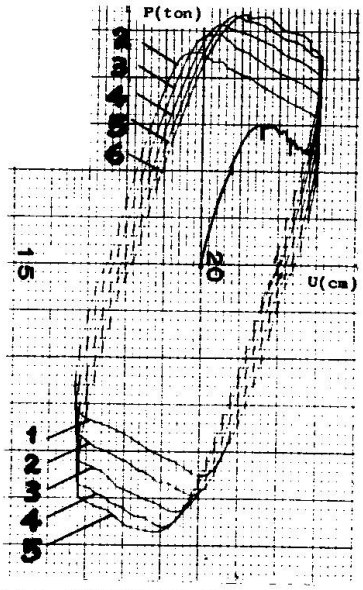

Fig.7 EXPERIMENTAL LOAD-DEFLECTION CURVE FOR SIMPLE BEAM SPECIMEN

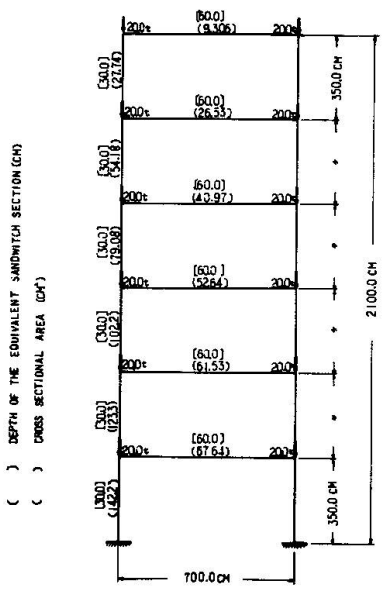

Fig.8 FRAME DIMENSION

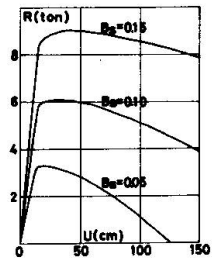

Fig.9 ONE WAY
LOAD-DEFLECTION CURVES

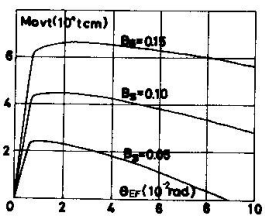

Fig.10 ONE WAY OVERALL
FORCE-DEFLECTION CURVES

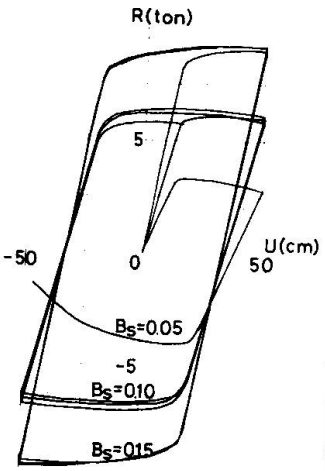

Fig.11
CYCLIC LOAD-DEFLECTION
CURVES

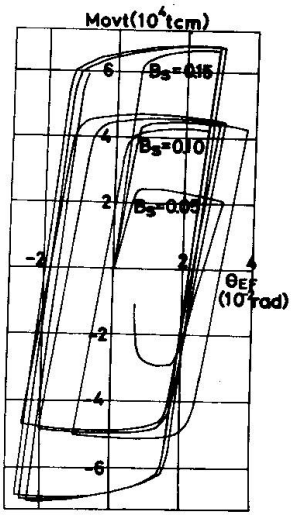

Fig.12 CYCLIC OVERALL
FORCE-DEFLECTION CURVES

4.3 RESPONSE ANALYSIS OF FRAMES SUBJECTED TO A STRONG-MOTION EARTHQUAKE DISTURBANCE

The three frames with the dimensions shown in Fig.8 and described in 4.2 have been subjected to the amplified earthquake excitation of 1.0g with the wave patterns of VERNON S82°E. The stiffnesses of the springs shown in Fig.13 representing the foundation stiffnesses were determined by Barkan's method. The internal damping coefficients for the members and the foundation springs were assumed to be 0.01 and 0.20, respectively. As an example of the numerical results, the story shear-relative story displacement diagram for S_B=0.05 has been shown in Fig.14.

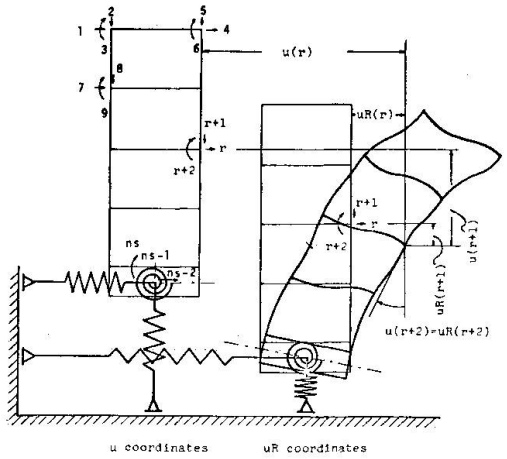

Fig.13 IDEALIZED FRAME AND COORDINATE SYSTEM

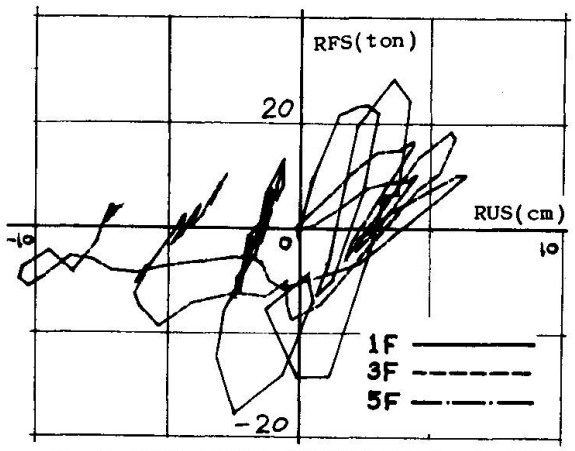

Fig.14 STORY SHEAR-STORY DISPLACEMENT DIAGRAM FOR VERNON(S82°E) EXCITATION

REFERENCES

[1] Ryo Tanabashi, Tsuneyoshi Nakamura and Shuzo Ishida, "Gravity Effect on the Catastrophic Dynamic Response of Strain-hardening Multi-story Frames," 5th World Conf. Earthquake Engng., to be presented in June 25-29, 1973.

[2] Ryo Tanabashi, Kiyoshi Kaneta, Tsuneyoshi Nakamura and Shuzo Ishida, "To the Final State of Rectangular Frames", Proc. 4th World Conference on Earthquake Engineering, Chile, pp. A 4-179-194, 1969.

[3] Ryo Tanabashi, Tsuneyoshi Nakamura and Shuzo Ishida, "Overall Force-displacement Characteristics of Multi-story Frames", Proc. Symposium on Ultimate Strength of Structures and Structural Elements, 1969.12, pp. 87-100.

[4] Tsuneyoshi Nakamura, "Elastic-plastic behavior of a Linear Strain-hardening Sandwich Column Subjected to an Alternating Lateral Force," Summaries of Technical Papers of Annual Meeting of A.I.J.Kinki Branch, 1967, pp117-120.

[5] Ryo Tanabashi, Yoshitsura Yokoo, Minoru Wakabayashi, Tsuneyoshi Nakamura and Haruo Kunieda, "Deformation History Dependent Inelastic Stability of Columns Subjected to Combined Alternating Loading", Proc. 1971 RILEM International Symposium on Experimental Analysis of Instability Problems on Reduced and Full-scale Models, Buenos Aires, Sept. 1971, Vol. III, pp. 275-295.

[6] Ryo Tanabashi and Tsuneyoshi Nakamura, "The Minimum Weight Design of a Class of Tall Multi-story Frames Subjected to Large Lateral Forces, I, II", Trans. A.I.J., No. 118 (Dec. 1965), pp. 10-18, and No. 119 (Jan. 1966), pp. 37-44. Also Proc. 15th Japan National Congress of Applied Mechanics, pp. 72-81, 1966.

SUMMARY

An efficient computational method of static and dynamic large-deflection analysis of strain hardening plane frames has been outlined. The load-displacement curves of a cantilever, a beam-column and three six-story frames of one-bay subjected to alternating repeated loads have been presented and the effect of cyclic alternating plastic deformation on the load-carrying behaviour of frames has been investigated. The effect of gravity and of strain-hardening upon the response of frames to an amplified earthquake disturbance has been clarified to some extent through the numerical examples.

RESUME

On esquisse dans cette étude une méthode d'analyse numérique pour le calcul des cadres plans dont certaines sections travaillent dans le domaine d'écrouissage, en considérant les grandes déformations statiques et dynamiques. On présente les courbes charge-déplacement pour une poutre en porte à faux, une colonne et trois portiques multiples à six étages et une travée, soumis à des charges alternantes répétées. On étudie l'effet des déformations plastiques alternées sur le comportement des portiques chargés. L'influence de la pesanteur et de l'écrouissage sur le comportement des portiques soumis à une perturbation sismique amplifiée a été analysée jusqu'à un certain degré dans les exemples numériques.

ZUSAMMENFASSUNG

Es wird eine leistungsfähige Computer-Methode zur Berechnung statisch und dynamisch grosser Auslenkungen von versteifenden ebenen Rahmen vorgeführt. Die Last-Ausbiegungskurven eines Kragarms, einer Stütze und dreier zweistieliger sechsstöckiger Rahmen unter wechselseitiger zyklischer Belastung werden gezeigt und der Effekt von zyklischer wechselseitiger plastischer Deformation auf das Tragverhalten der Rahmen untersucht. Die Wirkung der Gravitation und der Verfestigung auf die Reaktion der Rahmen auf eine verstärkte Erdbebenstörung wird zum Teil an numerischen Beispielen erklärt.

Leere Seite
Blank page
Page vide